THE APPLICATION OF SIZE-RESOLVED HYGROSCOPICITY MEASUREMENTS TO UNDERSTANDING THE PHYSICAL AND CHEMICAL PROPERTIES OF AMBIENT AEROSOL

A Dissertation

by

JOSHUA L. SANTARPIA

Submitted to the Office of Graduate Studies of
Texas A&M University
in partial fulfillment of the requirements for the degree of

DOCTOR OF PHILOSOPHY

May 2005

Major Subject: Atmospheric Sciences

THE APPLICATION OF SIZE-RESOLVED HYGROSCOPICITY MEASUREMENTS TO UNDERSTANDING THE PHYSICAL AND CHEMICAL PROPERTIES OF AMBIENT AEROSOL

A Dissertation

by

JOSHUA L. SANTARPIA

Submitted to the Office of Graduate Studies of
Texas A&M University
in partial fulfillment of the requirements for the degree of

DOCTOR OF PHILOSOPHY

Approved as to style and content by:

Don R. Collins (Chair of Committee)	R. Lee Panetta (Member)
Ping Yang (Member)	William H. Marlow (Member)
Richard E. Orville (Head of Department)	

May 2005

Major Subject: Atmospheric Sciences

ABSTRACT

The Application of Size-Resolved Hygroscopicity Measurements to Understanding the Physical and Chemical Properties of Ambient Aerosol. (May 2005)

Joshua L. Santarpia, B.S., The New Mexico Institute of Mining and Technology; M.S., Texas A&M University

Chair of Advisory Committee: Dr. Don R. Collins

During the summer of 2002, a modified tandem differential mobility analyzer (TDMA) was used to examine the size-resolved hydration state of the ambient aerosol in Southeast Texas. Although there were slight variations in the measured properties over the course of the study, the deliquescent particles observed were almost always present as metastable aqueous solutions. A relative humidity (RH) scanning TDMA system was used to measure the deliquescence/crystallization properties of ambient aerosol populations in the same region. During August, sampling was conducted at a rural site in College Station, and in September at an urban site near the Houston ship channel. Measurements from both sites indicate cyclical changes in the composition of the soluble fraction of the aerosol, which are not strongly linked to the local aerosol source. The observations show that as temperature increases and RH decreases, the hysteresis loop describing the RH-dependence of aerosol hygroscopic growth collapses. It is proposed that this collapse is due to a decrease in the ammonium to sulfate ratio in the aerosol particles, which coincides with increasing temperature and decreasing RH. This cyclical change in aerosol acidity may influence secondary organic aerosol (SOA) production and may exaggerate the impact of the aerosol on human health. The compositional changes

also result in a daily cycle in crystallization RH that is in phase with that of the ambient RH, which reduces the probability that hygroscopic particles will crystallize in the afternoon when the ambient RH is a minimum. During June and July of 2004 airborne measurements of size-resolved aerosol hygroscopic properties were made near Monterey, California. These were used to examine the change in soluble mass after the aerosol had been processed by cloud. The calculated change in soluble mass after cloud-processing ranged from 0.66 $\mu g\ m^{-3}$ to 1.40 $\mu g\ m^{-3}$. Model calculations showed these values to be within the theoretical bounds for the aerosols measured. Mass light-scattering efficiencies were calculated from both an averaged aerosol size distribution and from distributions modified to reflect the effects of cloud. These calculations show that the increase in mass light-scattering efficiency should be between 6% and 14%.

This work is dedicated to my wife Amy and our three children: Christian, Emi, and George. Without all of their patience, I would never have finished.

ACKNOWLEDGEMENTS

The completion of a dissertation can rarely if ever be attributed to a single person. In fact, besides the immediate assistance that I have received from my advisor, committee and colleagues, the education I obtained throughout my lifetime, and those people responsible for it, have contributed more than they suspect to the work that I present here. First and foremost, I would like to thank my parents, Peggy and Craig Santarpia. My parents have encouraged me to study math and science for as long as I can remember and they have provided me with immeasurable support and encouragement to continue my education. Their generosity and support have been literally bottomless throughout my education. Next, I would like to thank my high school physics teacher, David Brink. Although I had been interested in physics since childhood, he gave me my first real understanding of physical concepts and a real appreciation for physics in the real world. Dr. Brad Baker, my undergraduate advisor at New Mexico Tech, helped to appreciate simplicity in both theory and instrumentation. You often achieve the best understanding of a difficult concept by examining its most basic properties. My master's advisor, Dr. Michael Biggerstaff, taught me independence and gave me my first real taste of field work. Dr. Gerald North has been an excellent friend and mentor to me for many years now and has many times lent me the wisdom of his experiences. My doctoral advisor, Dr. Don Collins, has seen me through the past few years of study with unfailing support and help. My research has not been easy nor, at times, straightforward; my efforts have not always been rewarded with success, but Dr. Collins has guided me through both the science and the style of research and publication. The guidance of my committee members, Dr. Lee Panetta, Dr. Ping Yang and Dr. William Marlow is also greatly

appreciated. Dr. Runjun Li is responsible for the construction of several of the instruments used in my research. I would also like to thank Roberto Gasparini, Chance Spencer and other members of the aerosol research group for assistance in collecting data and writing papers. Finally, I would like to thank my wife and children: Amy, Christian, Emi and George. They have worked for this as much as I have.

TABLE OF CONTENTS

LIST OF FIGURES

FIGURE Page

LIST OF TABLES

CHAPTER I

INTRODUCTION

Atmospheric aerosol may influence a wide range of atmospheric phenomena. The absorptive properties and the ubiquitous nature of elemental carbon may impact global climate (Sato et al., 2003), while acidic aerosol has been linked to epidemiological effects in some population centers (Gwynn et al., 2000). Through careful observation of the physical and chemical properties of aerosol, it has become possible to incorporate the effects of aerosol into the framework of these phenomena; however, large uncertainties still remain. Despite our general understanding of the effects and feedbacks of specific types of aerosols, the net effect of aerosols on climate cannot yet be determined. One of the largest uncertainties in determining the effects of aerosol on climate is the interaction of aerosols with clouds to modify climate, or the aerosol indirect effect (Twomey, 1974). This refers to the increase in cloud droplet number, and the subsequent increase in cloud albedo, that would result from an increase in cloud condensation nuclei (CCN). As reported by the Inter-governmental Panel on Climate Change in 2001, no estimate of the indirect effects of aerosol climate can be made, although it is possible that these cooling effects may be almost equal in magnitude to the warming effects of greenhouse gasses.

The tools available to study aerosols in the atmosphere are almost as varied as the effects of the aerosol themselves. Aerosol particles may be studied remotely from satellite instruments that can measure aerosol optical depth. These observations can be

---

This dissertation follows the style and format of the *Journal of Geophysical Research*.

useful in determining the large scale transport of aerosol. Other ground based remote sensors, such as sun and sky scanning photometers and laser induced detection and ranging (LIDAR), measure aerosol optical depth from fixed locations. Networks of these instruments such as AERONET can offer globally distributed information on aerosol properties. In addition to remote sensing, aerosol properties may be measured in situ using a wide variety of sampling methods. The most straightforward of these methods is the collection of aerosol on filters (e.g. Hegg and Hobbs, 1982), which may be done from aircraft or land based sites. These samples may be analyzed to determine chemical composition. In situ measurement of aerosol scattering properties may also be measured by nephelometers (e.g. Rood et al., 1985). These measurements can be used to estimate aerosol composition or hydration state among other properties. Aerosol mass-spectrometry may also be used to directly measure the composition of individual aerosol particles or of bulk samples.

It is often of interest to examine the distribution of aerosol and their size-resolved properties. This can be done according to the aerodynamic size by impactors (e.g. Laj et al., 1997) or with an aerodynamic particle sizer (APS). The former separates particles by impaction using the inertia of the particle to determine its size, while that latter relies on the time of flight of the aerosol between sequential optical detectors. Aerosols may also be optically sized by optical particle counters (OPC) which use the scattering properties of individual aerosol particles to determine their size.

In addition, the size of an aerosol may be determined by the electrical mobility of aerosol with a known charge. The relationship between particle diameter (d) and

electrical mobility (Z), the mobility of a charged particle in an electrical field, is given by:

$$Z=\frac{neC_c}{3\pi\eta d}$$

where e is the elementary charge, n is the number of charges, C_c is the slip correction factor and η is the viscosity of the medium. The velocity of a particle in a uniform electric field (V_E) of strength E can then be written as:

$$V_E=ZE$$

A differential mobility analyzer (DMA) capitalizes on the electrical mobility of aerosol with a known charge distribution to separate it according to size. The DMA consists of two concentric cylinders; the inner maintained at a high voltage, typically between 0.1 and 10 kV, while the outer is grounded. A polydisperse aerosol that has been neutralized, so that the charge distribution of the aerosol is known, is introduced between the cylinders close to the outer wall. As each particle follows the parabolic flow between the cylinders it migrates across the gap between the cylinders at a rate determined by its electrical mobility. Larger particles move slower than smaller particles. The voltage of the inner cylinder is adjusted so that particles in a narrow size range are removed from the flow through a slit near the bottom of the inner cylinder. The width of the distribution of particles that are removed is controlled by the ratio of the clean air flow and the sample aerosol flow; higher ratios yielding smaller widths. If the voltage is held constant, a single aerosol size may be selected. If the voltage is scanned during

measurement, the size distribution of particles may be determined within the range of the instrument (typically 0.01μm to 1μm).

Tandem differential mobililty analyzers (TDMA; Liu et al., 1978) employ the use of two DMAs, the first selecting aerosol of a specific size and the second examining the distribution of those particles after they have been exposed to conditions that would cause a change in size of some of the particles (e.g. high relative humidity or heat). In this manner, the size-resolved properties of the aerosol can be determined.

Aerosol hygroscopicity and hygroscopic behavior are directly measurable using a TDMA, by exposing the aerosol to controlled changes in relative humidity (RH) between the DMAs, and can illuminate an aerosol population's relative importance to many phenomena. Directly, aerosol hygroscopicity controls the size of an aerosol at a given RH below 100%. This change in size with relative humidity impacts the scattering efficiency of an aerosol population which can affect both radiation budgets and local visibility. The existence of an aqueous phase within the aerosol can facilitate multiphase reactions (Dentener and Crutzen, 1993) and the corresponding increase in surface area due to condensational growth can enhance other heterogeneous reactions that are independent of surface composition. Gas and aerosol partitioning has also been shown to be influenced by an aqueous phase (Anasari and Pandis, 2000). In addition, the hygroscopic behavior of an aerosol can be an indicator of general composition.

Many aerosols types exhibit hysteresis in their sub-saturated, hygroscopic growth. This hysteresis can be generally characterized by little to no growth of the aerosol at low relative humidity, where it exists as a crystalline particle. At the point when it reaches its

deliquescence relative humidity (DRH), it takes on water and becomes aqueous and continues to grow with increasing relative humidity. As the aqueous aerosol is taken from high relative humidity to lower relative humidity it will shrink by releasing water, but will remain aqueous to a lower relative humidity than the DRH. When it reaches its crystallization relative humidity (CRH) it will release all remaining water and return to a crystalline state.

Using knowledge of the hygroscopic growth behavior many aerosol properties may be resolved. It is possible to determine whether the aerosol is in a metastable or a crystalline state. It is possible to determine the fraction of that aerosol which is soluble in water if something is known about the bulk composition of the aerosol. These properties may additionally be used to quantify changes that occur to the aerosol.

The analyses presented in the following pages employ measurements of size-resolved aerosol hygroscopic behavior to examine the aerosol's physical and chemical properties and changes in those properties using TDMA analysis. Several experiments were performed in: College Station, Texas; Houston, Texas; and in the coastal Pacific near Monterey, California. These experiments examined the ambient hydration state of the aerosol, the diurnal cycles in the hygroscopic growth hysteresis of the ambient aerosol of southeast Texas, and the production of sulfate through in-cloud reactions.

CHAPTER II

DIRECT MEASUREMENTS OF THE HYDRATION STATE OF AMBIENT AEROSOL POPULATIONS[*]

1. Introduction

It has become increasingly apparent that understanding the hygroscopic properties of atmospheric aerosols is critical to understanding many aspects of atmospheric physics and chemistry. The efficiency with which aerosol populations scatter light controls their impact on regional and global radiation budgets, and on local visibility. The dependence of that scattering efficiency on particle size distributions translates into a dependence on hygroscopicity in humid environments. The presence of an aqueous phase within an aerosol facilitates many multiphase reactions (Dentener and Crutzen, 1993), while the increased surface area that accompanies hygroscopic growth may enhance even those heterogeneous reactions that are insensitive to surface composition. Partitioning of many semi-volatile compounds between the gas and aerosol phase is also influenced by the presence and amount of liquid water in the aerosol (Ansari and Pandis, 2000). Although prediction of the hygroscopic behavior of an aerosol is not trivial, it can be estimated based on a description of the size-resolved particle composition. Unfortunately, knowledge of the hygroscopic behavior of an aerosol is not always sufficient to predict whether it is hydrated since, for many particle types, there can exist two stable states at a

---

[*] Reproduced by permission of American Geophysical Union. Santarpia, Joshua L., Runjun Li and Don R. Collins, Direct measurements of the hydration state of ambient aerosol populations, *Journal of Geophysical Research*, 109, D18209, doi: 10.1029/2004JD004653, 2004. Copyright [2004] American Geophysical Union.

given relative humidity (RH). This complexity results from the hysteresis behavior observed for a range of compounds in which the transition from a crystalline to aqueous state (deliquescence) occurs at a higher relative humidity than for the aqueous to crystalline transition (crystallization or efflorescence). Between these RH extremes, an aqueous particle exists in a metastable state, where it can remain for an indefinite period of time (Tang and Munkelwitz, 1984). Since almost all aerosol properties are at least somewhat dependent upon water content, any modeling effort designed to predict those properties when the relative humidity is between that of crystallization and deliquescence must include an assumption of the ambient state of the aerosol. The importance of this assumption for modeling the radiative impact of aerosols was demonstrated by Martin et al. (2003a), who showed that the difference between the top-of-atmosphere radiative forcing calculated assuming particles reside on the upper leg of the hysteresis loop was 24% greater than that calculated assuming they reside on the lower leg. Unfortunately, lack of information concerning the current particle composition distribution, the evolution of that composition over the lifetime of each of the particles, and the relative humidity history each particle is exposed to during that evolution often precludes anything beyond a guess of the true hydration state.

The hygroscopic growth hysteresis behavior of a variety of individual chemical species, as well as multicomponent mixtures of several species, has been investigated both theoretically and experimentally (see Martin, 2000, Table 3 for a comprehensive summary). Since ambient particles are rarely composed of only one compound, the multicomponent studies are of most direct relevance for comparison with, or

interpretation of, field measurements. Laboratory studies have shown that particles composed of mixtures of salts exhibit complex growth and evaporation behavior with multiple deliquescence and crystallization points (Tang and Munkelwitz, 1993). Wexler and Seinfeld (1991) showed that in a multicomponent aqueous droplet the deliquescence point for each component is at a lower relative humidity than if it were in a single component solution, which results in a decreased RH range over which particles may exist as metastable solutions. Whereas thermodynamic equilibrium models can be applied to predict the deliquescence RH of aqueous mixtures (i.e., Wexler and Clegg, 2002), no comparable models exist for prediction of crystallization RH, and instead parameterizations based on laboratory data have been used (Martin et al., 2003b). Further complicating the prediction of crystallization RH is the observation that it increases when particles contain solid inclusions composed of substances such as mineral dust components (Martin et al., 2001), and organic compounds (Lightstone et al., 2000).

The repeated demonstration that common aerosol types exhibit hygroscopic growth hysteresis, coupled with evidence that metastable aqueous solutions may exist for extended periods of time without undergoing crystallization, suggests that metastable ambient particles should be abundant. Although this is a logical conclusion, it has not been extensively tested. Furthermore, the compositional complexity of atmospheric particles may not be reflected in the laboratory aerosols studied. Observations of the ambient state of hygroscopic aerosol populations have suggested that a significant fraction of the particles do in fact reside on the metastable leg of the hysteresis loop.

Rood et al. (1989) used a temperature scanning nephelometer to show that the water associated with metastable aqueous particles was often sufficient to cause a detectable change in light scattering. However, determination of the partitioning of particles between the crystalline and aqueous states is difficult based only on integrated measurements of light scattering when the ratio of the concentration within the two populations is very different.

Unlike instruments such as nephelometers that provide a measure of the overall properties of an aerosol population, tandem differential mobility analyzers (TDMA; Liu et al., 1978) permit size-resolved characterization of aerosol properties such as hygroscopicity. The response of particles to a prescribed increase in RH has been examined in a number of urban environments (McMurry and Stolzenburg, 1989; Cocker et al., 2001) rural locations such as National Parks (Zhang et al., 1993; Dick et al., 2000), and in the marine atmosphere (Berg et al., 1998; Swietlicki et al., 2000). For most measurements made using a TDMA, the aerosol is dried prior to initial size classification. Even if the RH of the sample stream is not intentionally altered, any difference in temperature between the ambient environment and the room or other enclosure in which the instrument is operated will alter the RH, which may cause particles to move from one leg of a hysteresis loop to the other. Here we describe data collected using a modified TDMA to examine size-resolved ambient aerosol hydration state. Unlike previous investigations of ambient aerosol populations, this approach benefits from the ability to detect the presence of both particle populations simultaneously, even if the overwhelming majority of particles reside on one leg of the hysteresis loop. To assist in

the interpretation of these data, a second, RH-scanning, TDMA was concurrently operated to directly characterize the deliquescence and crystallization properties of the aerosol.

2. Methodology

Sampling was conducted in College Station, TX between Aug 9 and Aug 12, 2002. The two TDMAs used in this study were operated from within, or immediately outside of, a room on the roof above the 12th story of the Eller Oceanography and Meteorology Building on the campus of Texas A&M University. The height of this sampling location minimized influence from local sources. Because most of the components within the two TDMA systems used in this study were the same, a single schematic for both is shown in Figure 1. The subtle differences between the two systems are identified in the figure. Three identical Permapure PD-070-18T-24SS Nafion tube bundles were used within each of the TDMAs to create the desired RH profiles. High Flow DMAs designed by Aerosol Dynamics, Inc. (Stolzenburg et al., 1998) were employed in both of the instruments. Aerosol size distributions were also measured with a differential mobility analyzer (DMA).

2.1. Measurement of Ambient State

For the system used to characterize the ambient hydration state (here referred to as the AS-TDMA), DMA 1 was positioned outside, under an overhang that shielded it from the sun until mid-afternoon. Prior to entering this upstream DMA, the sample flow passed through a bipolar neutralizer to bring the aerosol to a predictable charge state. Since the sample was not heated or cooled prior to entering the DMA, the particles

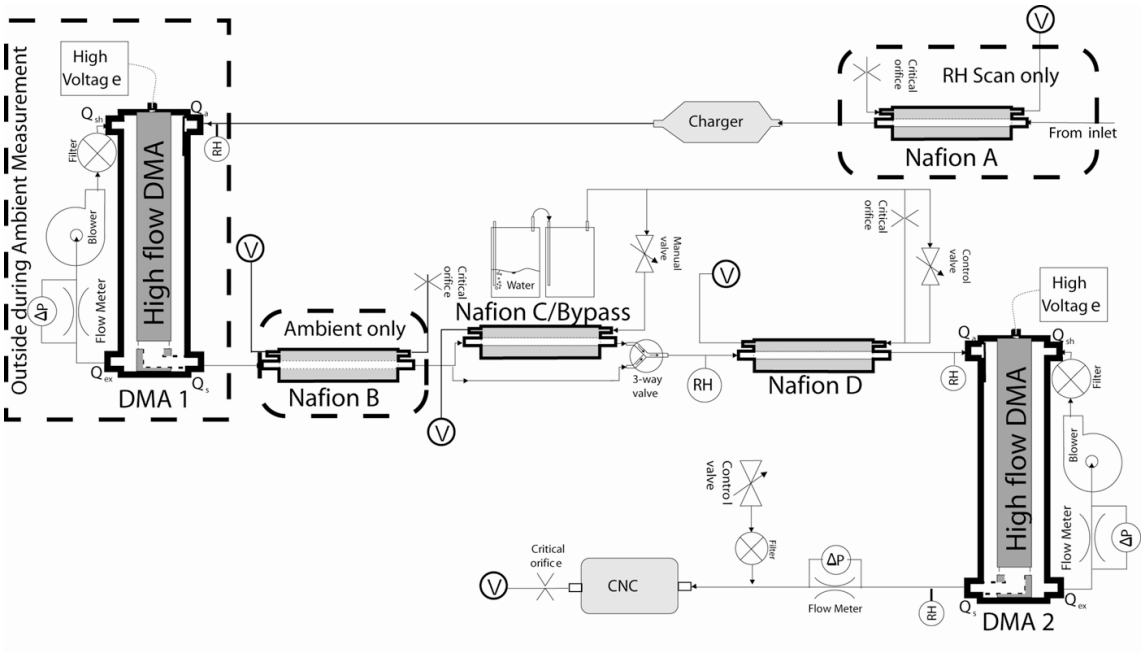

Figure 1. Schematic of both the ambient state and RH-scanning TDMAs. Circled V indicates connection to vacuum, and circled RH indicates the location of an RH probe.

remained in their ambient state. Although it was not directly measured, the temperature within the DMA is expected to be very close to ambient as well. The only potential heating source is the regenerative blower, which has been found to have a minimal impact on temperature in the configuration used. To examine any possible size dependence of the particle hydration state, this upstream DMA sequentially classified 160 and 320 nm diameter particles. A relative humidity sensor was located outside, adjacent to the upstream DMA.

Following classification at ambient RH by the upstream DMA, the initially monodisperse aerosol was dried within Nafion B to below 20% RH, which is below the crystallization point of most common salts. The dried aerosol alternately passed through, or bypassed, Nafion C, which raised the sample RH to between 85 and 90%. Following this intermittent humidification, the sample RH was controlled to the simultaneously measured ambient RH by varying the water vapor pressure within the purge flow of Nafion D. This control technique has been used extensively to maintain a constant RH between the two DMAs of a conventional TDMA, but this was the first application with a varying setpoint. Although deviations from ambient RH were generally less than 4%, about half of the distributions were not considered in this analysis because the deviation exceeded 8% for a significant time during the measurement. Figure 2 shows the ambient (DMA 1) and controlled (DMA 2) RH during the sampling period on August 10.

The downstream DMA (DMA 2) in the AS-TDMA continuously scanned through particle size with a scan time of 120 s. During previous studies at this location, it was observed that the growth factor (hydrated diameter / dry diameter) of the more

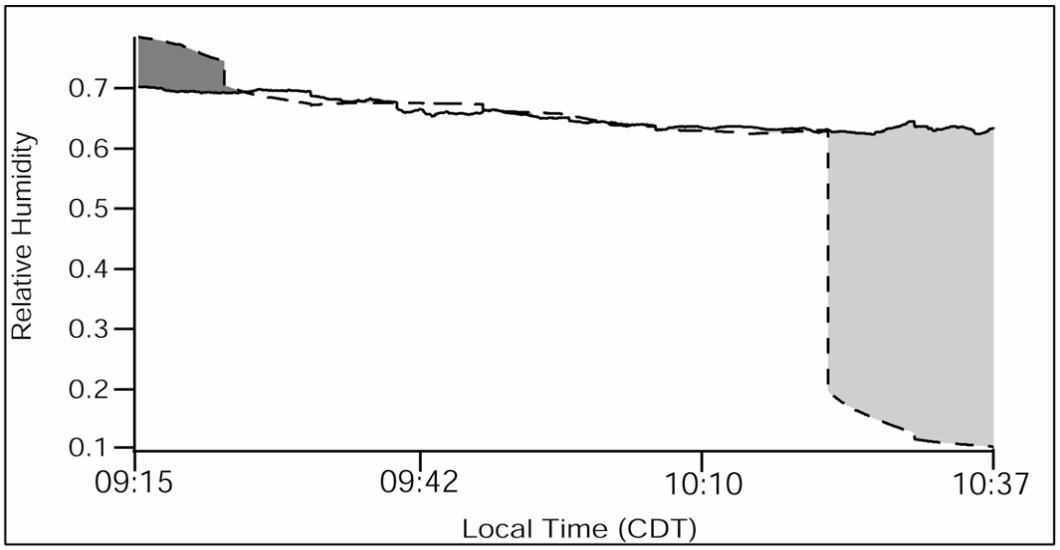

Figure 2. Example of the accuracy with which the RH was controlled within the AS-TDMA (dashed line) to match the simultaneously measured ambient RH (solid line). The dark shaded region at the beginning of the scan indicates a time period during which the deviation between ambient and instrument RH was excessive and the data were not considered. The drop in instrument RH at the end of the sampling interval (lightly shaded region) corresponds to the dry scan (AS3 in the table on p. 20) measurement.

hygroscopic fraction of the aerosol is typically less than that of pure ammonium sulfate. This, coupled with the fact that even pure ammonium sulfate has a growth factor of only 1.27 when in a metastable hydrated state at the typical measurement RH of 60%, resulted in relatively small changes in particle size. To help discern the resulting shift in the measured distributions, the DMA resolution was increased by operating at a sheath to aerosol flow ratio of 13, rather than the more conventional ratio of 10.

To understand the effect the RH path within the AS-TDMA has on particle size, it is instructive to consider Figure 3, which shows the hygroscopic growth hysteresis of ammonium sulfate based on empirical fits of solution activity and density from Tang and Munkelwitz (1994). For those measurements in which Nafion C is bypassed, a hygroscopic (but not necessarily hydrated) particle is pushed from ambient RH (RH_{amb}) to a low RH (RH_{low}), and back to RH_{amb}. Aqueous particles that reside on the metastable leg of the hysteresis loop (D_m) will crystallize after exposure to RH_{low}, but will not return to their hydrated state when the RH is brought back to RH_{amb}. These particles will have a final size that is D_s / D_m (< 1) of their initial size. Particles that are not hydrated (either hydrophobic or hygroscopic but crystalline), and those that do not exhibit deliquescence / crystallization behavior will remain the same size. For those measurements in which the sample is humidified in Nafion C, all hygroscopic particles are hydrated upon reaching RH_{high}. Particles that are initially crystalline will remain hydrated after the RH returns to RH_{amb}, and will therefore be larger than when they were initially classified in the upstream DMA. The size of metastable or thermodynamically stable aqueous particles, and of non-hygroscopic particles, will be unchanged following the

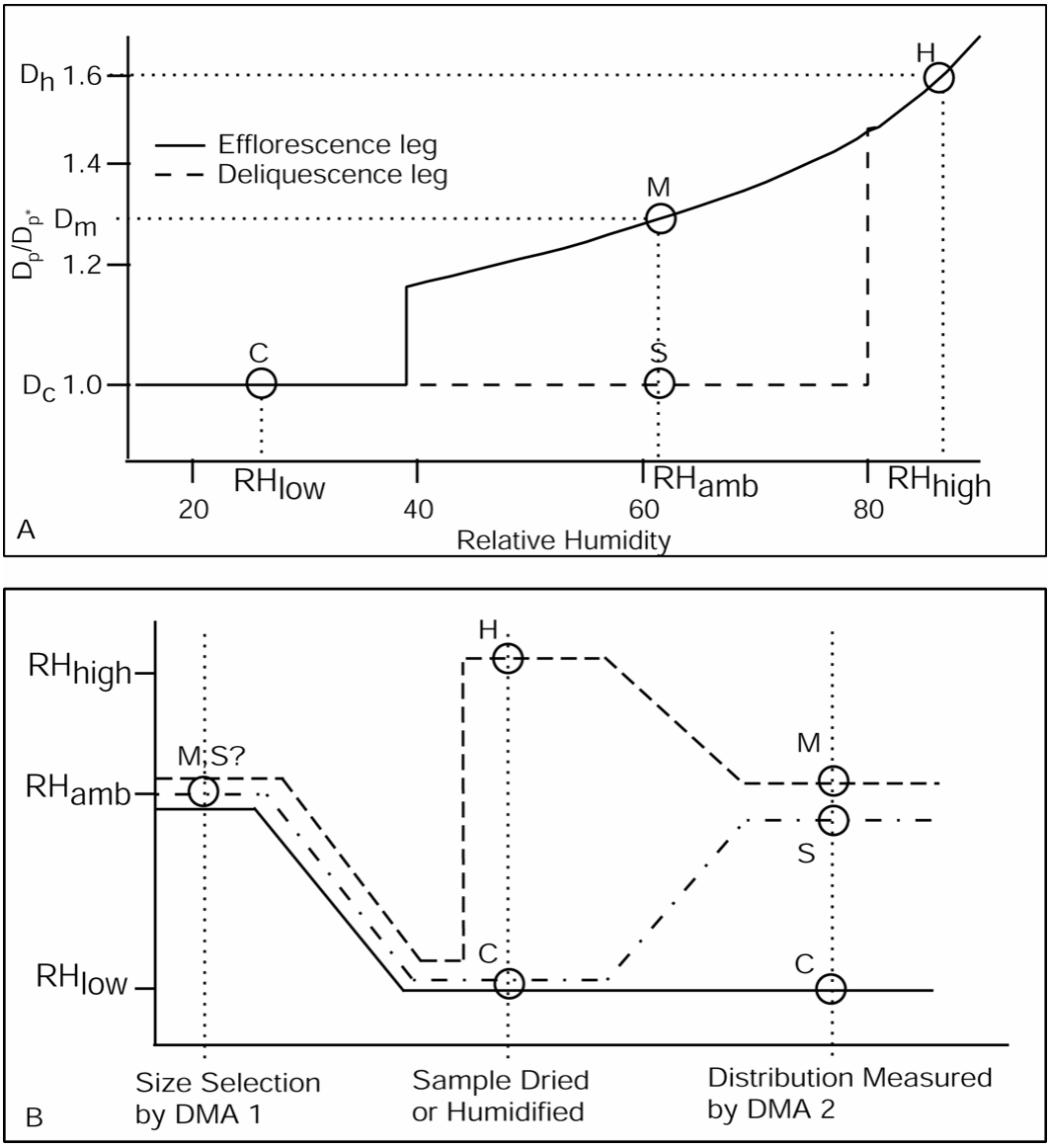

Figure 3. Part A: Theoretical deliquescence and crystallization behavior of ammonium sulfate particles. Point C represents a dry, crystalline particle while H represents a hydrated solution droplet. Points M (metastable) and S (stable) represent the two possible states of a particle at RH_{amb}. Part B shows the relative humidity experienced by an individual particle as it travels through the AS-TDMA. The particle state at three points along its path is indicated by labels that correspond to part A.

conditioning. On all but the first sampling day, additional measurements were intermittently made in which, following classification by the upstream DMA, the aerosol was dried in Nafion B, but not returned to ambient RH prior to entering the downstream DMA. The difference between the concentration of particles with no detectable change in size measured during these so-called dry scans, and that measured during the normal scans when Nafion C was bypassed, represents the concentration of hygroscopic, but non-deliquescent, particles.

2.2. Measurement of Deliquescence / Crystallization Behavior

To complement the ambient state measurements, a humidity-scanning TDMA (HS-TDMA) was also operated throughout the study period. Unlike the AS-TDMA, the entire HS-TDMA was located inside, and the aerosol sample was dried in Nafion A prior to classification by the upstream DMA. Following a single measurement at a fixed RH of 85%, the relative humidity between the two DMAs in this instrument slowly decreases from about 85% to 30%, and then slowly increases back to 85%, while the growth factor distributions of either 160 nm or 320 nm dry diameter particles are continuously measured. Nafion C is bypassed during the decreasing RH measurements, and, as a result, the aerosol is exposed to the maximum RH it experiences within the instrument just as it enters the downstream DMA. If the sampled aerosol exhibits hysteresis, the growth factors measured during this portion of the RH scan describe the lower leg of the loop. During the increasing RH measurements, the aerosol classified by the upstream DMA is exposed to a high (>85%) RH within Nafion C and then returned to a lower RH in Nafion D before entering the downstream DMA. This RH conditioning

ensures that all hygroscopic particles are initially hydrated so that the growth factors measured describe the crystallization (or upper) leg of any hysteresis loop. Figure 4 shows an example of a calibration of this HS-TDMA for which pure sodium chloride particles were sampled. The dashed line in the figure represents the predicted growth factors based on data from Tang et al. (1997). The agreement between these published data and the calibration results is quite good.

Combined, the data collected using the AS-TDMA and HS-TDMA indicate i) whether all or some of the hygroscopic particles exhibited hysteresis, and ii) what fraction of those deliquescent particles remained in a metastable aqueous state when the ambient RH was intermediate of the crystallization and deliquescence RH. A summary of the relative humidity profiles within the two TDMAs during the different measurements is provided in Table 1.

The growth factor distributions measured by both TDMAs were parameterized by fitting them with one or more log-normal distributions as shown in Figure 5. This was essential since the resolution of the DMA was often not sufficient to separate the different particle types into discrete growth factor modes. Distributions measured during AS2 and AS3 (from Table 1) scans typically had the appearance of a single, asymmetric, mode with a tail on the side of the smaller, secondary mode. Bimodal fits generally reproduced these features extremely well, while single mode fits often sufficed for the AS1 measurements. These parameterizations also provided a direct means for comparison of the distributions measured using the AS-TDMA and the HS-

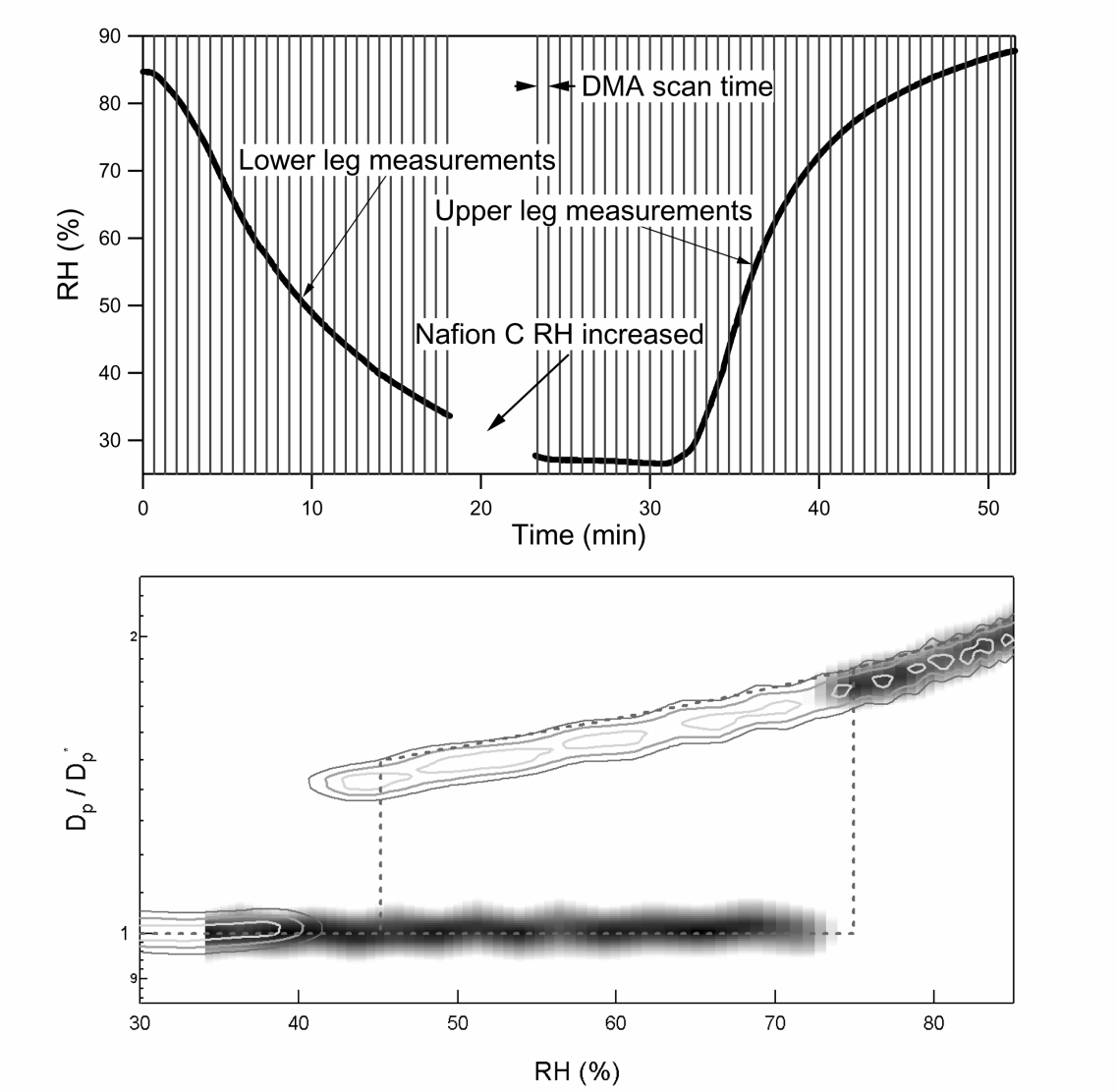

Figure 4. An example of a calibration of the HS-TDMA for which pure sodium chloride was analyzed. The top plot shows the recorded RH during the approximately one hour measurement. The spacing between the vertical lines represents the DMA scan time. In the lower plot, distributions measured when Nafion C was bypassed are presented as an intensity plot, while those measured when it was not bypassed are presented as a contour plot. The dashed line represents the expected growth for sodium chloride based on empirical fits of solution activity and density provided in Tang (1997).

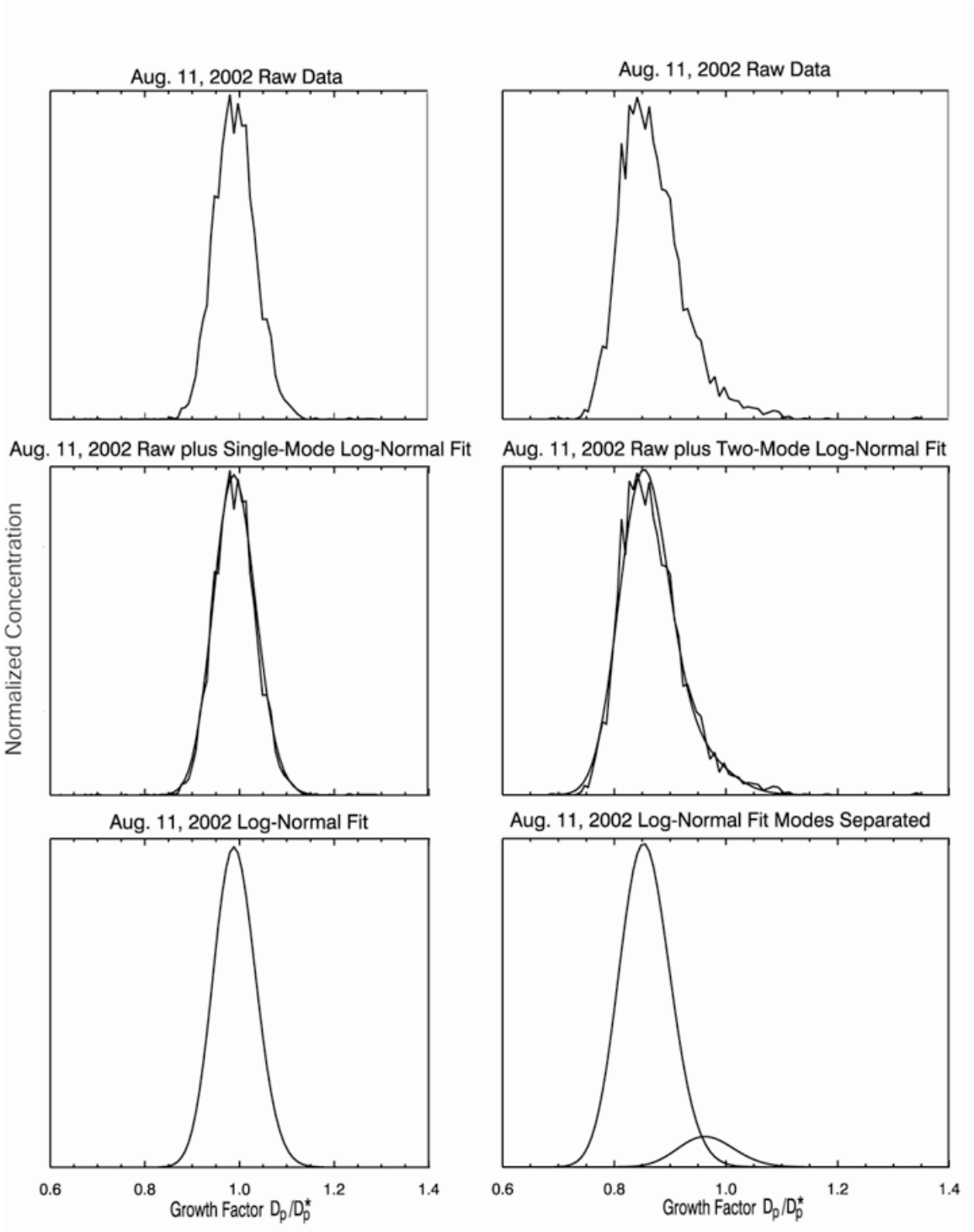

Figure 5. Examples of mathematical fits of AS-TDMA distributions. The raw data shown in the top graphs from August 11 were fit with the log-normal distributions shown in the bottom graphs.

Table 1. Summary of the RH within the AS-TDMA and the HS-TDMA for each of the measurements made.

	Nafion A	DMA 1	Nafion B	Nafion C	Nafion D/DMA 2	Primary Quantity Measured
				AS-TDMA		
AS1	N/A	ambient	≤20%	≥85%	ambient	concentration of deliquescent particles on the lower leg (stable) of the hysteresis loop
AS2	N/A	ambient	≤20%	≤20%	ambient	concentration of deliquescent particles on the upper leg (metastable) of the hysteresis loop
AS3	N/A	ambient	≤20%	≤20%	≤20%	concentration of nonhygroscopic particles
				HS-TDMA		
HS1	≤20%	≤20%	N/A	≤20%	85 → 30%	growth factor along the lower leg (stable) of the hysteresis loop
HS2	≤20%	≤20%	N/A	≥85%	30 → 85%	growth factor along the upper leg (metastable) of the hysteresis loop
HS3	≤20%	≤20%	N/A	≤20%	85%	growth factor at fixed RH

[a]The locations of the Nafion tube bundles are shown in Figure 1.

TDMA.

3. Source Regions and RH History of the Sampled Aerosol

The AS-TDMA and HS-TDMA were operated in the morning and early afternoon between August 9 and August 12, 2002. As is typical for Southeast Texas during the summer, winds were generally from the south. Thirty-six hour back-trajectories calculated using NOAA HYSPLIT (Draxler, 1988) with the Eta Data Assimilation System (EDAS) meteorological dataset are shown in Figure 6. These trajectories were calculated for an arrival time of 12:00 CDT and a final height of 50 m. Based on these trajectories, the air sampled on Aug 9, 10, and 12 had traveled from the Gulf of Mexico over the Houston area, while that on Aug 11 crossed much of Louisiana and remained to the north of Houston. The shading of these trajectories is used to represent the modeled RH history of the sampled air. This predicted RH history, coupled with National Weather Service measurements at Easterwood Airport (CLL) shown in Figure 7, suggest that the aerosol sampled on each of these days had been exposed to a relative humidity greater than 80% before or soon after sunrise. By 11:53 CDT (hourly reporting time for CLL), the RH at CLL had decreased to 61% on Aug 10, and to 55% on Aug 9, 11, and 12. Hence, the elevated RH the aerosol had been exposed to should have hydrated any hygroscopic particles, while the ambient RH during the sampling periods was below the deliquescence RH of common aerosol types such as ammonium sulfate (80%), letovicite (69%), ammonium nitrate (62%), and sodium chloride (75%).

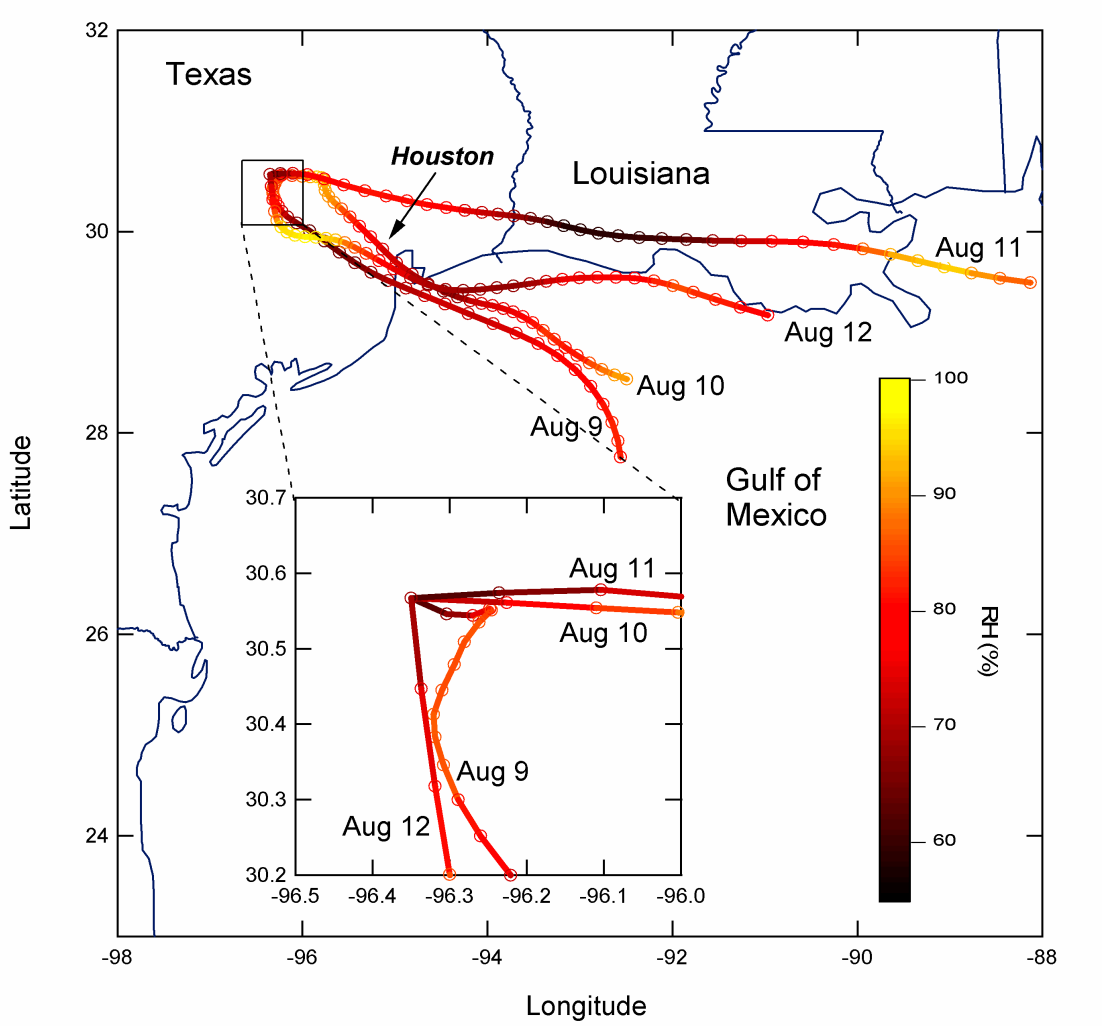

Figure 6. Thirty-six hour back-trajectories calculated using NOAA HYSPLIT with the Eta Data Assimilation System (EDAS) meteorological dataset. These trajectories were calculated for an arrival time of 12:00 CDT and a final height of 50 m. The shading of the trajectories is used to represent the RH history of the sampled air.

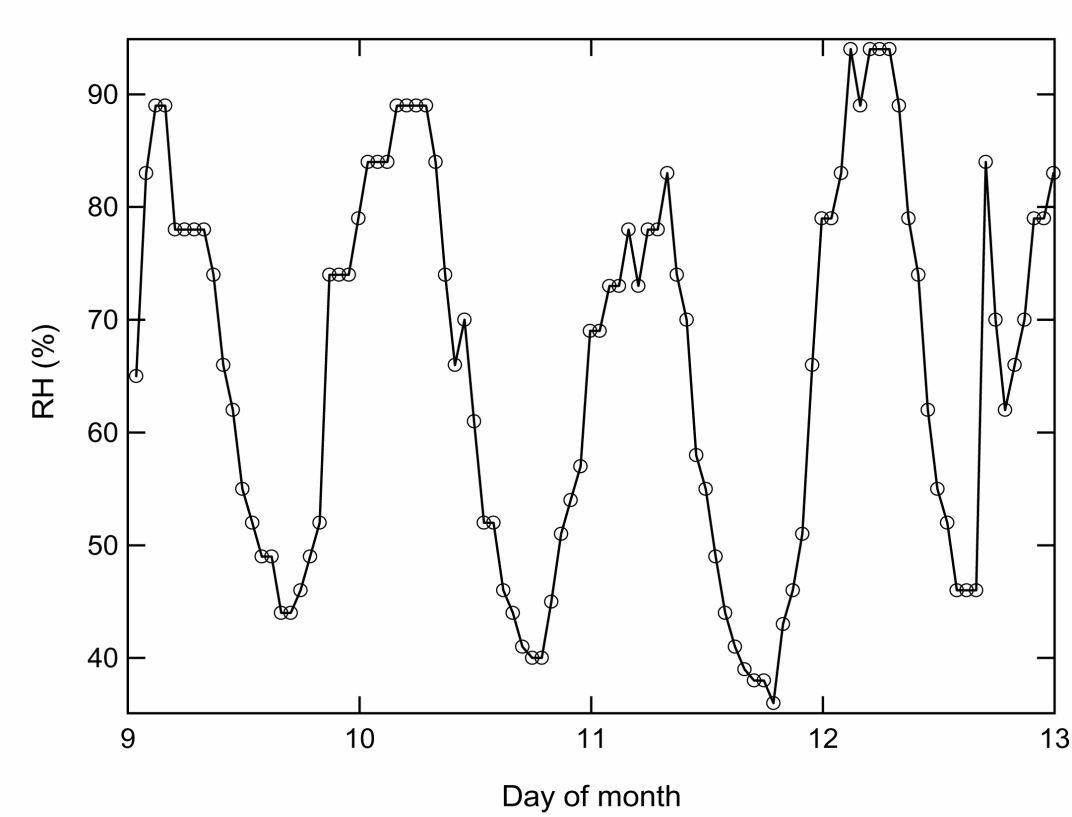

Figure 7. Relative humidity measured at Easterwood Airport (CLL) in College Station during the study period.

4. Results

4.1. Hygroscopic Growth at Fixed RH

Similar to what has been observed at this location prior to and since this sampling period, two distinct modes were present in almost all of the measured hygroscopic growth distributions, with the more hygroscopic of these typically accounting for about 80 to 90% of the total concentration. A typical fixed RH growth factor distribution for 160 nm dry diameter particles is shown in Figure 8. Hygroscopic growth distributions measured at a fixed relative humidity of 85% were used to partition this more hygroscopic mode into soluble and insoluble fractions to assess the presence and size of any insoluble inclusions in the particles. For these calculations, it was assumed that the aqueous solution activity and density were represented by empirical fits described by Tang and Munkelwitz (1994) for ammonium sulfate. A more detailed description of the technique used to ascribe the soluble fraction of the aerosol based on hygroscopic growth is provided in Gasparini et al. (2004). The calculated fractions are somewhat dependent upon the salt assumed to represent the soluble component. For example, 160 nm dry particles that have a growth factor of 1.4 could be composed of 53.3% ammonium bisulfate, 56.4% ammonium nitrate, or 62.7% ammonium sulfate by volume. However, these fractions are used only to provide a rough description of the likely particle composition, and are not critical for the analysis that follows. On each of the four days considered here, the soluble fraction was found to increase with increasing particle size. Averaged over the study period, the more hygroscopic population of 160 nm particles had a volumetric soluble fraction of 0.61, while that of the 320 nm particles

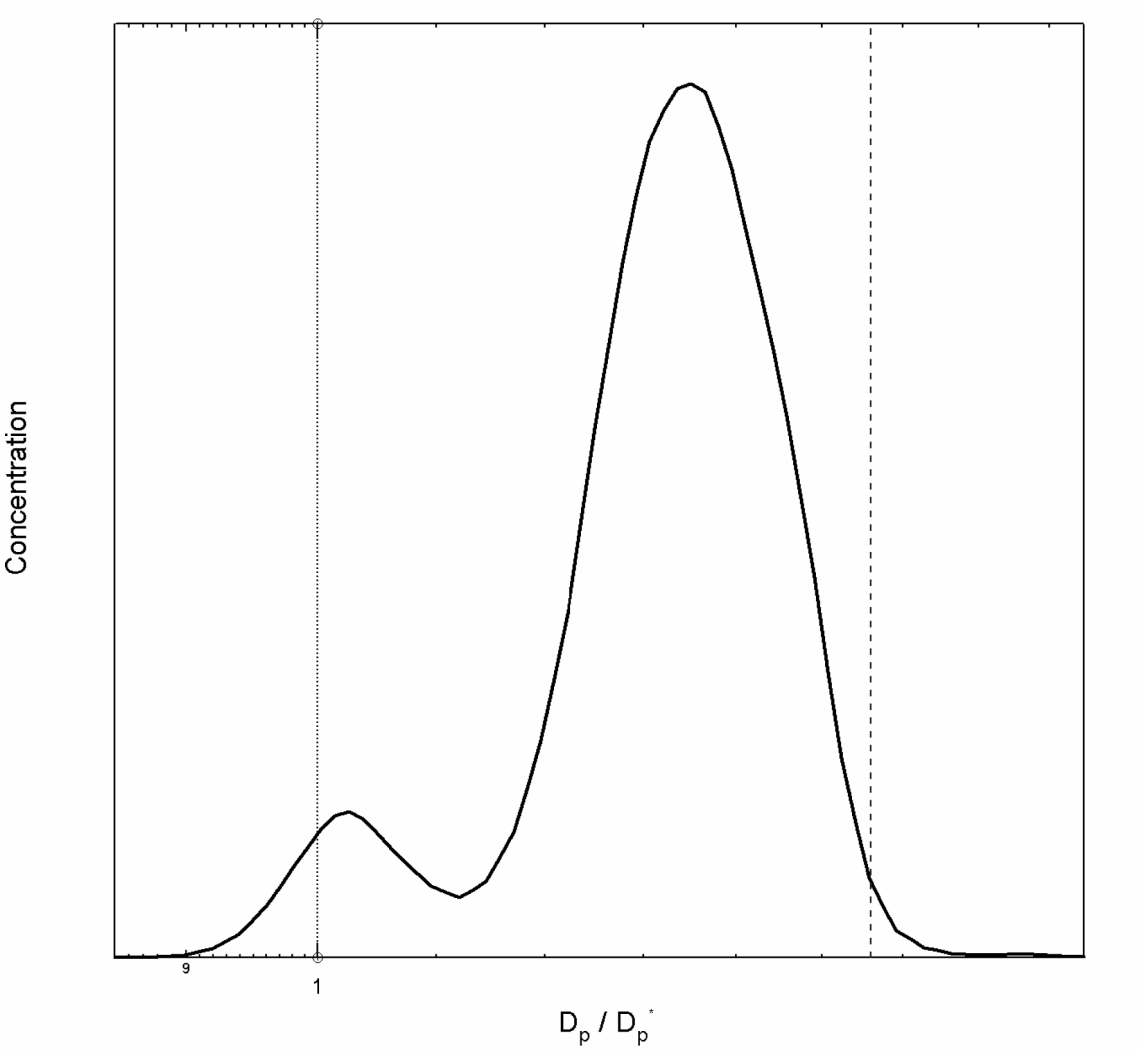

Figure 8. Typical hygroscopic growth distribution for 160 nm particles. The rightmost mode is made up of the more hygroscopic particles for which hysteresis was observed.

was 0.73. This soluble contribution steadily increased over the four-day period with daily average volumetric soluble fractions of the 160 nm particles of 0.50, 0.60, 0.65, and 0.67 on Aug 9, 10, 11, and 12, respectively, and of 0.65, 0.67, 0.80, and 0.82, respectively, for the 320 nm particles. Although the inferred compositions of the 160 and 320 nm particles were slightly different, size distributions measured using a DMA during the sampling period suggested that the majority of the particles of both these sizes were from the same mode. To quantify this, each of the size distributions measured during this period were fitted with a series of lognormals. The average parameters of the lognormal mode to which most of the 160 and 320 nm particles belonged were N = 1770 cm^{-3}, D_{pg} = 188 nm, σ_g = 1.50.

4.2. Observed Hygroscopic Growth Hysteresis

Hygroscopic growth hysteresis was observed in the HS-TDMA data for both 160 and 320 nm particles on each of the four days during this study. Figures 9 and 10 show the results from the first RH scan during each of the four study days for 160 and 320 nm particles, respectively. The points in these figures represent the mean growth factors from the log-normal fits of the distributions. Above about 80% RH, the growth factors measured during the HS1 (lower leg) and HS2 (upper leg) scans were nearly identical. With decreasing RH, these mean growth factors for the more hygroscopic mode diverged as one or more soluble components in the aerosol did not deliquesce. At sufficiently low RH, the mean growth factors along the upper and lower legs converged as the metastable soluble component(s) recrystallized. One noticeable difference between these observed hygroscopic growth hysteresis curves and those obtained for

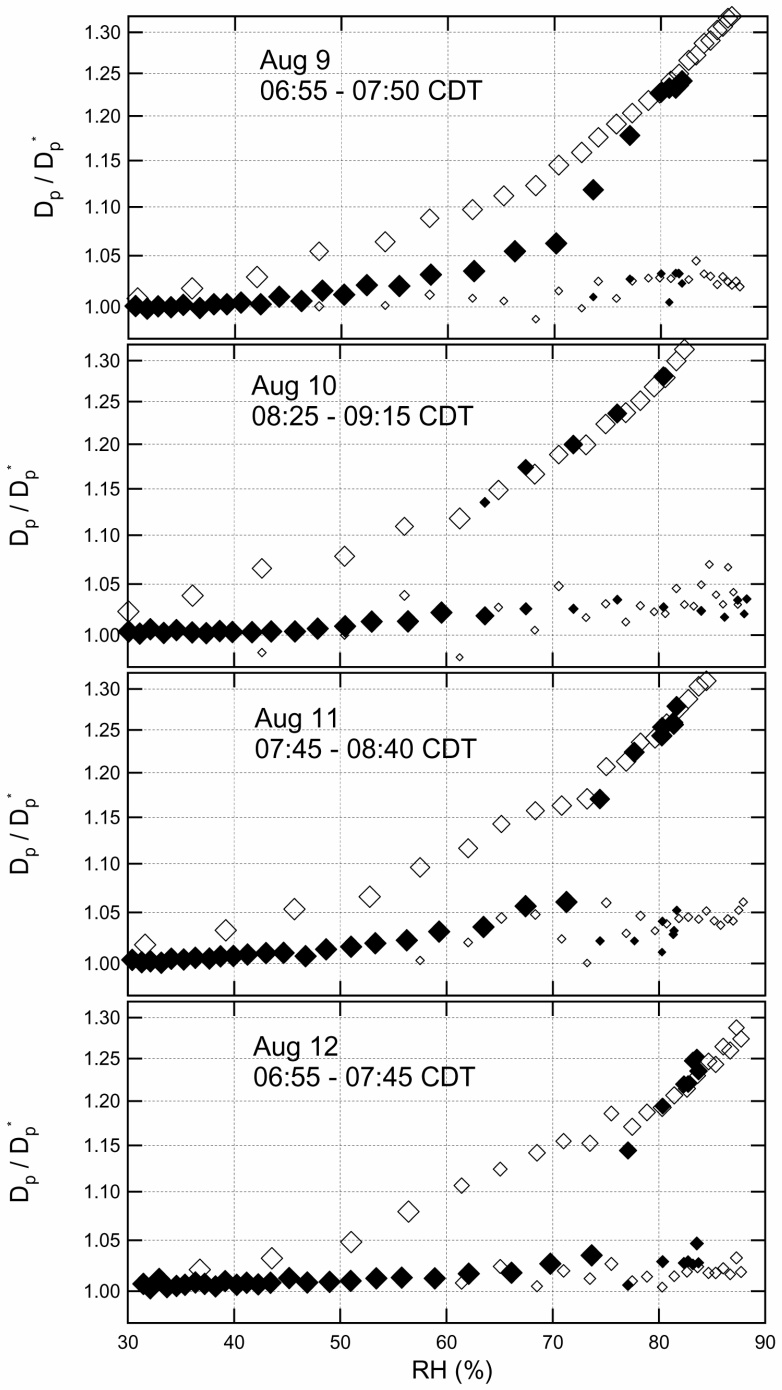

Figure 9. HS-TDMA measurements of 160 nm particles. The hollow markers represent the mean growth factors measured when the aerosol was humidified in Nafion C (upper leg), while the solid markers represent those measured when Nafion C was bypassed (lower leg). The marker size reflects the concentration within each mode when multiple modes were present. Only the first measurement on each of the four sampling days is shown.

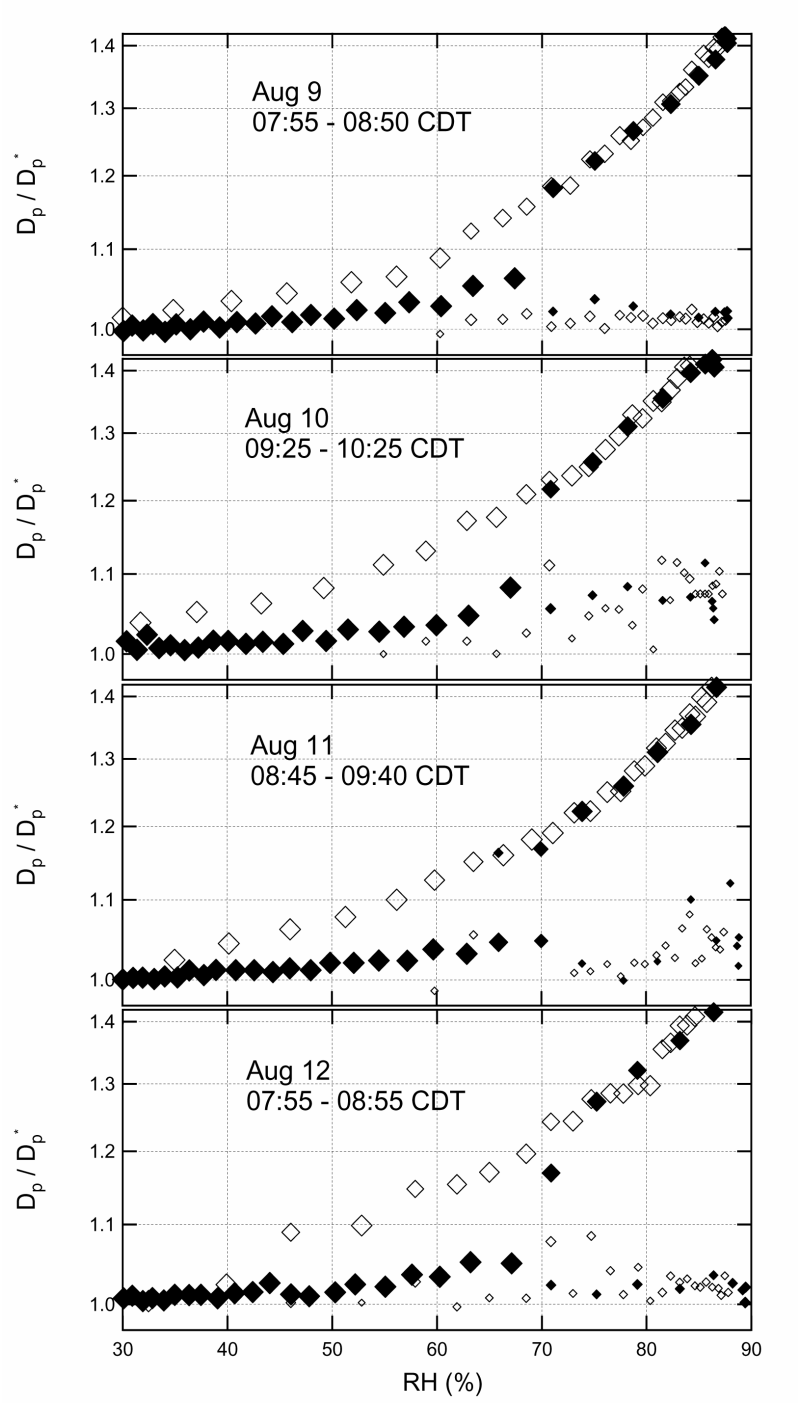

Figure 10. Same as in Figure 8, but for 320 nm particles.

pure salts is the non-zero growth along the lower leg at RH below that of deliquescence. This indicates that soluble organic and / or inorganic compounds with deliquescence humidities below that of the primary salt are internally mixed in the aerosol. For comparison with the AS-TDMA data, it is expected that metastable particles that are dried and then returned to ambient RH should shrink by a factor equal to the ratio of the growth factors along the upper and lower legs of the observed hysteresis loop. Those particles that are not returned to ambient RH prior to measurement by the downstream DMA (AS3 scans) should shrink by an amount equal to the growth factor corresponding to the ambient RH along either the upper or lower leg, depending on initial state.

Although the same two particle sizes were analyzed using both the AS-TDMA and the HS-TDMA, the two instruments sampled slightly different particle populations since the aerosol was dried when classified in the upstream DMA in the HS-TDMA, but was frequently hydrated when classified in the upstream DMA in the AS-TDMA. However, the similarity between the hygroscopic properties of the 160 nm and 320 nm particles suggests that the compositional differences between the slightly different dry particle sizes measured by the two instruments is negligible.

The RH scan measurements do not provide direct information about the ambient state of the aerosol, but they do indicate over what RH range ambient particles could exist in a metastable state. The minimum and maximum RH for which there was a separation between the growth factors measured with the HS-TDMA when Nafion C was bypassed (HS1) and when it was not (HS2) were recorded for each of the RH scans. The ambient RH was then compared with these ~1 hr average RH minima and maxima.

Figure 11 shows the relationship between these for each of the four days considered. Since the ambient RH remained between the primary deliquescence and crystallization points of the dominant aerosol type, metastable aqueous particles could be present in the ambient aerosol throughout the sampling period.

4.3. Ambient Hydration State

During the study period, 82 separate AS-TDMA measurements were made, of which 46 were discarded due to unacceptable deviation between the instrument and ambient RH. Examples of AS-TDMA measurements for 160 and 320 nm particles are shown in Figures 12 and 13, respectively. In each of the graphs within these figures, only the parameterized fit of the distributions is shown since it more clearly shows the frequent presence of secondary, low concentration, modes. The distributions shown were chosen to represent the range of observations, even though that range was quite narrow. As was true for every measurement made during this study, there exists a clear mode centered at D_p / D_p^* (= final / initial) less than 1.0, which results from initially metastable particles that shrink as they are brought to their thermodynamically favored state. Were a significant fraction of the hygroscopic particles on the lower leg of the hysteresis loop, a secondary mode would exist in the AS1 measurements, with a mean Dp / D_p^* greater than one. If these initially crystalline particles were present in the aerosol, their concentration was too low to produce an identifiable mode, which indicates that almost all particles that could be on either leg of the hysteresis loop were on the metastable (or upper) leg. Tables 2 and 3 summarize the study results for 160 and 320 nm particles, respectively. Each of the values describing the ambient state measurements (AS1 and

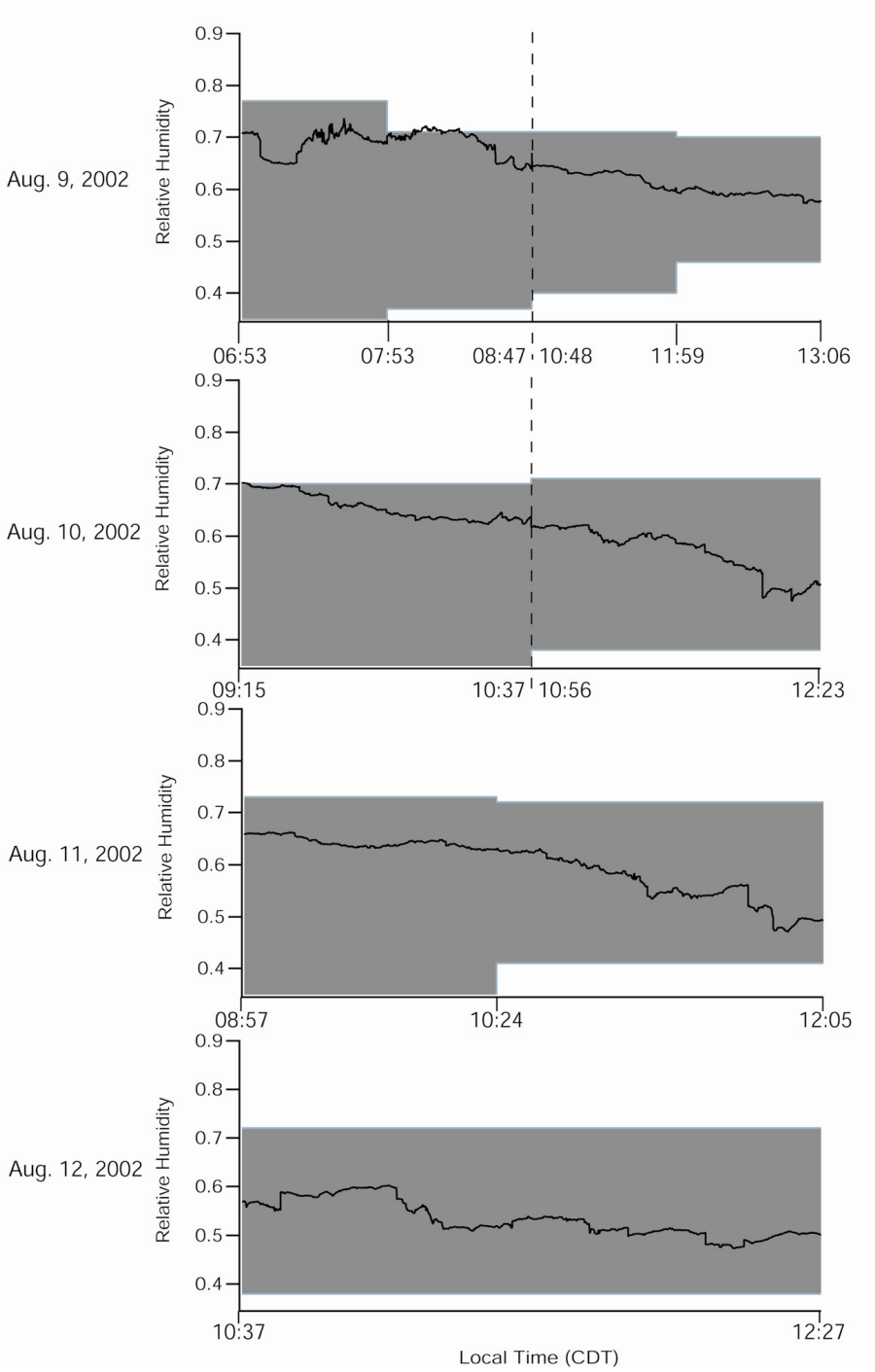

Figure 11. Ambient relative humidity (thick, solid line) during the sampling period on each of the four days. The shaded regions in these graphs indicate the relative humidity range over which hysteresis was observed in the HS-TDMA data. The dashed line in the upper two graphs represents a brief interruption in operation. Metastable aqueous particles may exist when the ambient RH is in the shaded region.

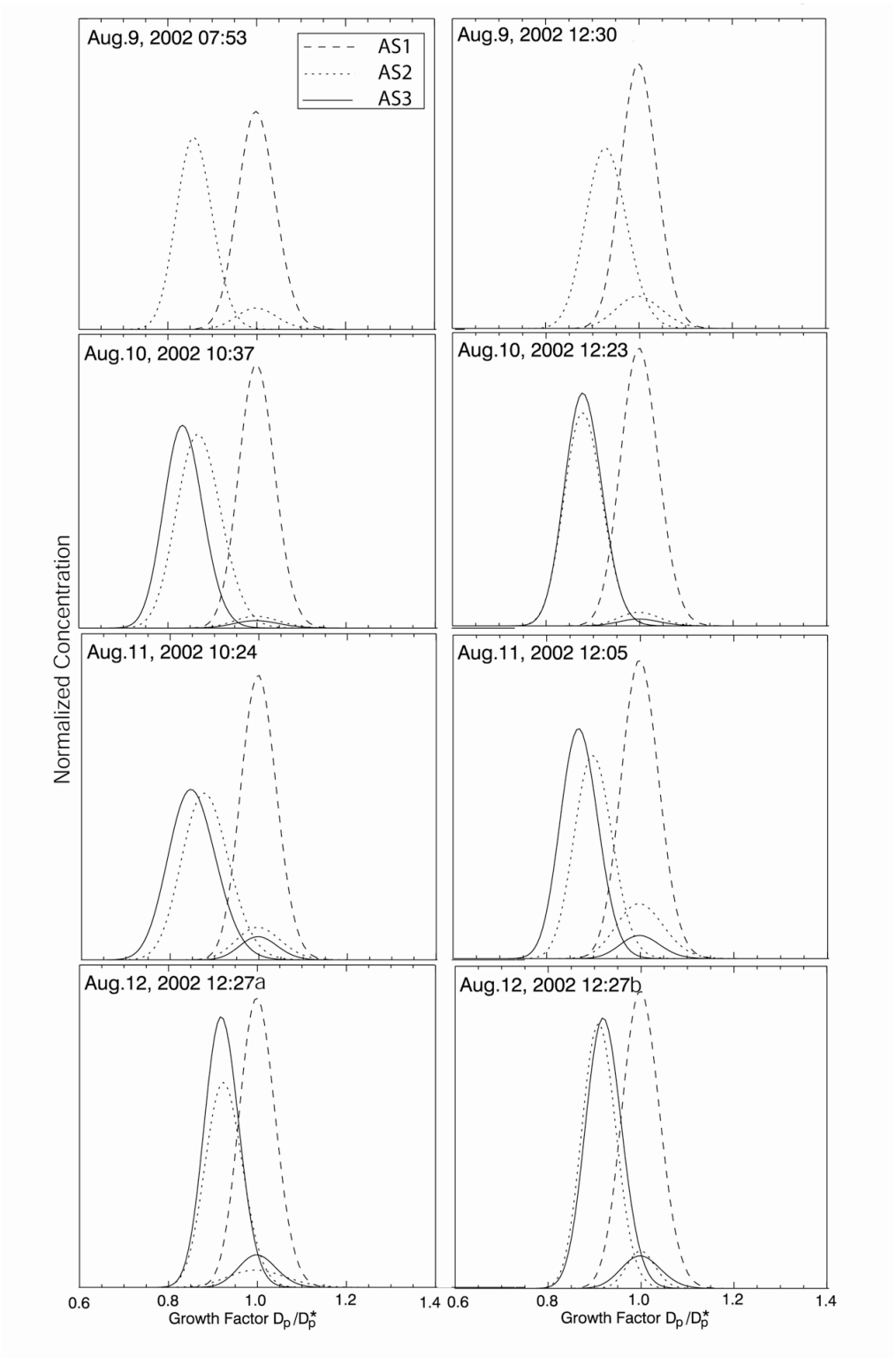

Figure 12. AS-TDMA measurements of 160 nm particles.

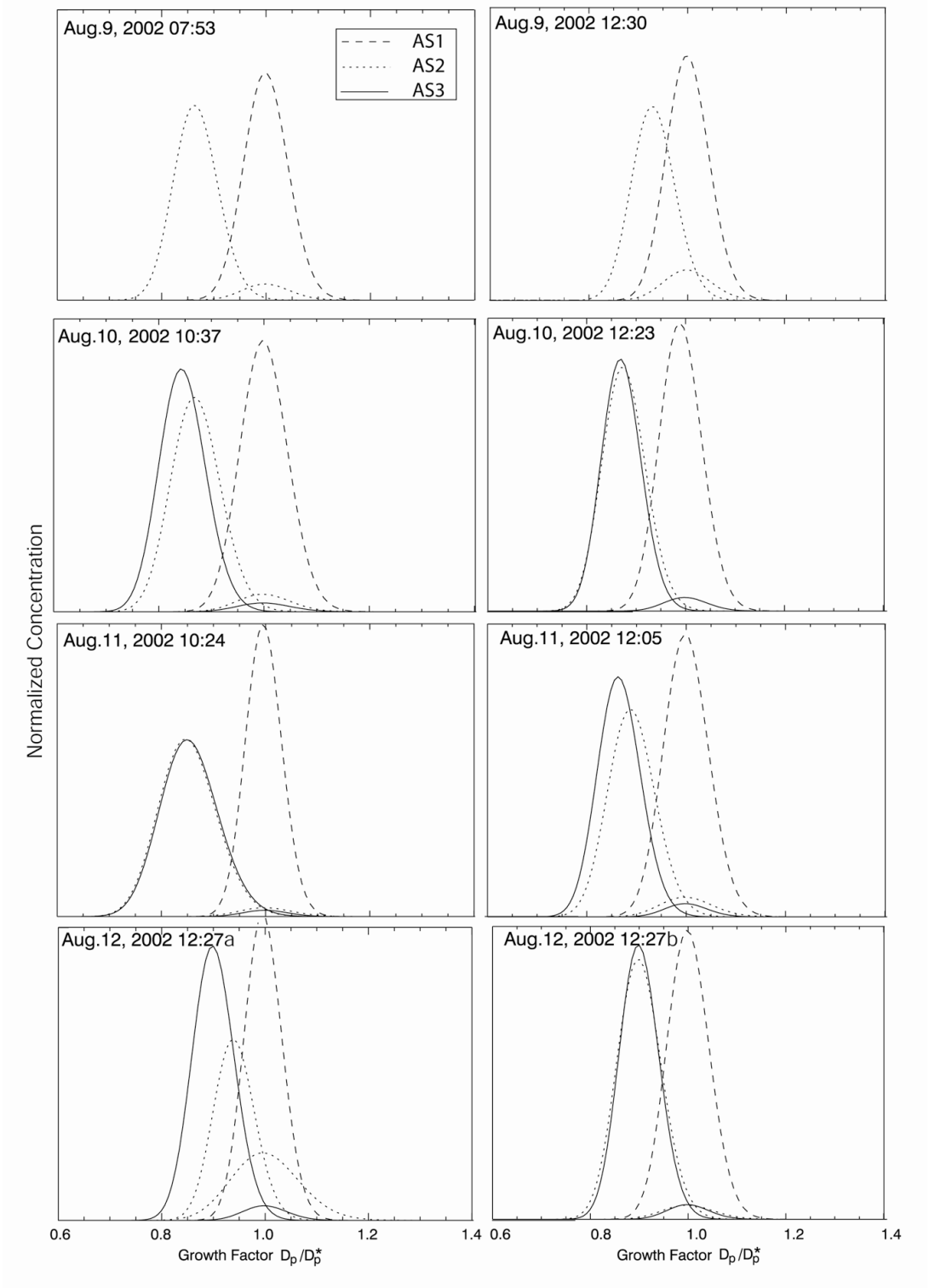

Figure 13. AS-TDMA measurements of 320 nm particles.

Table 2. Summary of measurements of 160nm particles.

Date, Time	Mean Ambient RH	$\frac{(D_p)_{upper\ leg}}{(D_p)_{lower\ leg}}$ AS2	$\frac{(D_p)_{upper\ leg}}{(D_p)_{lower\ leg}}$ HS1, HS2[e]	$\frac{(D_p)_{lower\ leg}}{(D_p)_{dry}}$ HS1	$\frac{(D_p)_{lower\ leg}}{(D_p)_{dry}}$ AS1, AS3	Fraction Metastable[b] (AS2)	Fraction Nonhygroscopic[c] (AS2, AS3)	Fraction Without Hysteresis[d] (AS1, AS2)
9 Aug., 0654–0753	69%	NM	1.07 to 1.15	1.05	NM	NM	NM	NM
9 Aug., 0654–0753	69%	1.16	1.07 to 1.15	1.05	NM	0.904	NM	0.051
9 Aug., 0753–0847	69%	1.16	1.10 to 1.20	1.05	NM	0.870	NM	0.086
9 Aug., 0753–0847	69%	1.19	1.10 to 1.20	1.05	NM	0.730	NM	0.076
9 Aug., 1048–1159	63%	1.10	1.05 to 1.10	1.05	NM	0.769	NM	0.231
9 Aug., 1048–1159	63%	1.10	1.05 to 1.10	1.05	NM	0.769	NM	0.231
9 Aug., 1159–1306	59%	1.09	1.05 to 1.07	1.07	NM	0.810	NM	0.190
9 Aug., 1159–1306	59%	1.08	1.05 to 1.07	1.07	NM	0.846	NM	0.154
10 Aug., 0915–1037	65%	NM	1.10 to 1.17	1.02	NM	NM	NM	NM
10 Aug., 0915–1037	65%	1.15	1.10 to 1.17	1.02	1.04	0.95	0.031	0.050
10 Aug., 1056–1223	57%	1.13	1.05 to 1.10	1.05	1.00	0.933	0.027	0.067
10 Aug., 1056–1223	57%	1.14	1.05 to 1.10	1.05	1.00	0.944	0.028	0.056
11 Aug., 0857–1024	64%	NM	1.07 to 1.15	1.05	NM	NM	NM	NM
11 Aug., 0857–1024	64%	1.14	1.07 to 1.15	1.05	1.02	0.860	0.084	0.140
11 Aug., 1024–1205	56%	1.11	1.07 to 1.12	1.02	1.03	0.769	0.081	0.231
11 Aug., 1024–1205	56%	1.11	1.07 to 1.12	1.02	1.03	0.769	0.081	0.231
12 Aug., 1037–1227	53%	1.09	1.07 to 1.12	1.07	1.01	0.890	0.133	0.110
12 Aug., 1037–1227	53%	1.10	1.07 to 1.12	1.07	1.01	0.904	0.117	0.096

[a]The measurement types (AS1, AS2, AS3, HS1, and HS2) used to determine each of the quantities are also indicated. NM is no measurement.
[b]Defined as the ratio of the concentration within the growth factor mode centered at $D_p/D_p^* < 1$ to the total concentration. A column representing the fraction stable or crystalline is not included since the value would be 0.0 for all measurements.
[c]Defined as the difference between the fraction of particles within the no growth modes measured during the AS2 and AS3 scans.
[d]Defined as the fraction of particles that did not grow during the AS1 scans and did not shrink during the AS2 scans. It is the sum of the nonhygroscopic and hygroscopic, but nondeliquescent fractions. Since initially crystalline particles were not present at sufficiently high concentrations to constitute a mode, this fraction was equivalent to 1.0 – (fraction metastable).
[e]The range of growth factors obtained from the RH scans represents the minimum and maximum growth factors that could be expected from the range of relative humidity values recorded during each observation interval.

Table 3. Summary of measurements of 320 nm particles.

Date, Time	Mean Ambient RH	$\frac{(D_p)_{upper\ leg}}{(D_p)_{lower\ leg}}$ AS2	$\frac{(D_p)_{upper\ leg}}{(D_p)_{lower\ leg}}$ HS1, HS2[e]	$\frac{(D_p)_{lower\ leg}}{(D_p)_{dry}}$ HS1	$\frac{(D_p)_{lower\ leg}}{(D_p)_{dry}}$ AS1, AS3	Fraction Metastable[b] (AS2)	Fraction Nonhygroscopic[c] (AS2, AS3)	Fraction Without Hysteresis[d] (AS1, AS2)
9 Aug., 0654–07:3	69%	1.16	1.13 to 1.18	1.05	NM	0.929	NM	0.032
9 Aug., 0654–07:3	69%	1.17	1.13 to 1.18	1.05	NM	NM	NM	NM
9 Aug., 0753–0847	69%	1.20	1.10 to 1.18	1.02	NM	0.933	NM	~0
9 Aug., 0753–0847	69%	1.20	1.10 to 1.18	1.02	NM	0.870	NM	0.086
9 Aug., 1048–1159	63%	1.10	1.10	1.07	NM	0.791	NM	0.209
9 Aug., 1048–1159	63%	1.10	1.10	1.07	NM	0.769	NM	0.231
9 Aug., 1159–1306	59%	1.10	1.07 to 1.13	1.07	NM	0.856	NM	0.144
9 Aug., 1159–1306	59%	1.08	1.07 to 1.13	1.07	NM	0.810	NM	0.190
10 Aug., 0915–1037	65%	1.15	1.10 to 1.18	1.05	1.03	0.930	0.035	0.070
10 Aug., 0915–1037	65%	1.18	1.10 to 1.18	1.05	1.01	NM	NM	NM
10 Aug., 1056–1223	57%	1.16	1.02 to 1.10	1.02	1.01	0.953	0.047	0.047
10 Aug., 1056–1223	57%	1.13	1.02 to 1.10	1.02	1.01	0.933	0.027	0.067
11 Aug., 0857–1024	64%	1.18	1.13 to 1.16	1.07	1.00	0.963	0.022	0.037
11 Aug., 0857–1024	64%	1.17	1.13 to 1.16	1.07	1.00	NM	NM	NM
11 Aug., 1024–1205	56%	1.08	1.10 to 1.13	1.02	1.08	0.606	0.050	0.394
11 Aug., 1024–1205	56%	1.12	1.10 to 1.13	1.02	1.03	0.769	0.081	0.231
12 Aug., 1037–1227	53%	1.06	1.05 to 1.15	1.07	1.04	0.634	0.051	0.366
12 Aug., 1037–1227	53%	1.11	1.05 to 1.15	1.07	1.00	0.899	0.132	0.109

[a]The measurement types (AS1, AS2, AS3, HS1, and HS2) used to determine each of the quantities are also indicated. NM is no measurement.
[b]Defined as the ratio of the concentration within the growth factor mode centered at $D_p/D_p^* < 1$ to the total concentration. A column representing the fraction stable or crystalline is not included since the value would be 0.0 for all measurements.
[c]Defined as the difference between the fraction of particles within the no growth modes measured during the AS2 and AS3 scans.
[d]Defined as the fraction of particles that did not grow during the AS1 scans and did not shrink during the AS2 scans. It is the sum of the nonhygroscopic and hygroscopic, but nondeliquescent fractions. Since initially crystalline particles were not present at sufficiently high concentrations to constitute a mode, this fraction was equivalent to 1.0 – (fraction metastable).
[e]The range of growth factors obtained from the RH scans represents the minimum and maximum growth factors that could be expected from the range of relative humidity values recorded during each observation interval.

AS2) represents an average of four sequential scans, while the values describing the dry scan measurements (AS3) represent an average of two sequential scans. Also included in the tables is a comparison between the change in particle size measured during the ambient state measurements, and that predicted based on the two possible growth factors at the same RH measured with the HS-TDMA. These complementary measurements were in agreement for most of the sampling intervals. Those differences that were observed were likely caused by variability in the aerosol over the averaging times for each of the instruments. Consistent with the observed non-zero growth of the particles on the lower leg of the hysteresis loop in the HS-TDMA data, the initially metastable particles that were returned to ambient RH were slightly larger than those for which the RH remained low. This size difference is attributed to water uptake by other soluble compounds, probably some or all of which were organic.

5. Conclusions

Despite the spatial and temporal specificity of this study, the data collected suggest that ambient hygroscopic particles frequently remain aqueous even after the ambient RH falls below that at which thermodynamics would dictate that the particles crystallize. This result is not necessarily surprising based on laboratory and theoretical studies that show that many common aerosol types will exhibit hygroscopic growth hysteresis, and that particles may exist on the metastable leg of that hysteresis loop for extended periods of time. However, the complexity of the ambient environment, and of the ambient aerosol, makes the accuracy of applying or extrapolating these laboratory and theoretical results uncertain. Although no attempt to directly measure the aerosol

composition was made in this study, the measured hygroscopic properties are consistent with a mixture of ammonium sulfate and soluble and insoluble organic compounds, which is a representative mix for aerosols in many regions around the world. The expectation that a significant fraction of hygroscopic particles will be aqueous when the ambient RH is below their deliquescence RH has important implications for their radiative impact, and for our ability to accurately model their behavior and evolution. Although the aerosol sampled and the meteorological conditions during sampling are not believed to be atypical, it would still be beneficial to augment these data with similar measurements made at different locations, different times of the day, and different months of the year.

CHAPTER III

DIURNAL CYCLES IN THE HYGROSCOPIC GROWTH CYCLES OF AMBIENT AEROSOL POPULATIONS[*]

1. Introduction

The properties, impacts, and lifetime of an aerosol are strongly dependent upon its hygroscopic behavior. Particle size and water content directly affect everything from the light scattering efficiency of a particle, to its role in heterogeneous reactions (Dentener and Crutzen, 1993) and gas-aerosol partitioning (Ansari and Pandis, 2000). Although hygroscopic behavior can not be unambiguously related to aerosol composition, it can be used to infer the relative abundance of soluble and insoluble species as a function of particle size (Gasparini et al., 2004). If the bulk composition of an aerosol can be constrained with supplementary measurements, the hygroscopic behavior of an aerosol can often be used to determine the soluble compounds present. Identification of aerosol types based only on hygroscopic growth at a fixed RH is challenging since many species exhibit similar growth. Furthermore, the hygroscopic growth of a particle is not only determined by the properties of those soluble species present, but also by the unknown abundance of insoluble compounds. A characteristic that is more uniquely related to aerosol composition is the hysteresis observed in hygroscopic growth as RH is increased or decreased. The hygroscopic behavior of pure ammonium sulfate particles is presented in Figure 14 to provide an example of this

---

[*] Reproduced by permission of American Geophysical Union. Santarpia, Joshua L., Runjun Li, Roberto Gasparini and Don R. Collins, Diurnal Variations in the hygroscopic growth cycles of ambient aerosol populations, *Journal of Geophysical Research*, in press, 2004. Copyright [2004] American Geophysical Union.

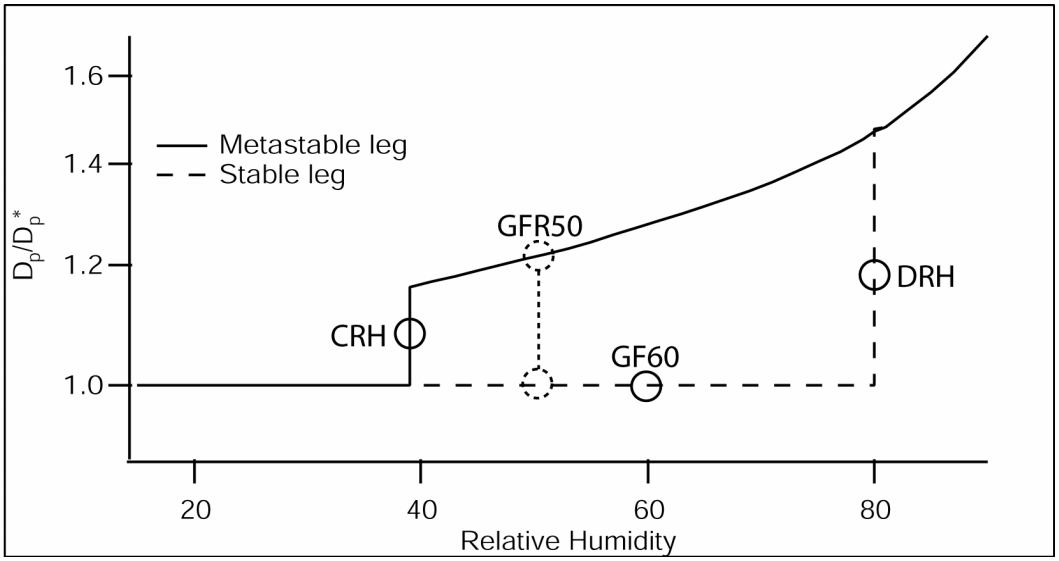

Figure 14. Hysteresis behavior of ammonium sulfate particles. The points along the curve represent the parameters used to describe the hysteresis properties of the ambient aerosol.

hysteresis. A crystalline particle exposed to increasing RH will remain unchanged until reaching its deliquescence relative humidity (DRH). After the particle reaches its DRH, it takes on water to become an aqueous droplet, and continues to grow with increasing RH. As the RH the aqueous aerosol is exposed to decreases, the particle will shrink as water evaporates, but will remain aqueous as a metastable solution droplet even as the RH is reduced below the DRH. After the RH is reduced to the crystallization relative humidity (CRH) of the aerosol, the particle releases all remaining water and returns to a crystalline state. The existence and appearance of this type of loop in a plot of growth factor vs. RH that results from this hysteresis can be used to identify the ratios of certain soluble ions.

Hysteresis in the hygroscopic response of an aerosol has been observed in the laboratory for inorganic salts such as ammonium sulfate [$(NH_4)_2SO_4$], letovicite [$(NH_4)_3H(SO_4)_2$], ammonium bisulfate [NH_4HSO_4], ammonium nitrate [NH_4NO_3], and sodium chloride [NaCl] (Tang and Munkelwitz, 1977; Cohen et al., 1987; Tang and Munkelwitz, 1994; Dougle et al., 1998). Hysteresis has also been observed for some organic compounds that are commonly found in atmospheric aerosol particles (Peng and Chan, 2001). While there has been general consensus on the behavior of some salts such as ammonium sulfate, differences in experimental conditions and characterization techniques have resulted in some discrepancies in reported values for other species. Disagreement regarding the value, and even existence, of CRH for ammonium bisulfate has been attributed to impurities that may have heterogeneously seeded the crystallization (Martin, 2000). The behavior of ammonium nitrate has also proven

difficult to observe due to its high volatility at ambient temperatures. Compounds such as sulfuric acid (H_2SO_4) exhibit no hysteresis since they remain aqueous across the entire spectrum of RH.

In contrast to the specific compounds that are studied in the laboratory, the ratio of ammonium to sulfate within atmospheric aerosol particles varies over a continuum. If this ratio is very low (much less than 1:1) the hygroscopic behavior of the particle will be similar to that of sulfuric acid, exhibiting no hysteresis. As the ammonium to sulfate ratio is increased towards 1:1, the hygroscopic behavior of the particle will more closely resemble that of ammonium bisulfate, which still may not exhibit hysteresis under typical atmospheric conditions. If the ratio is further increased into a regime where the ionic balance resembles letovicite (3:2) or ammonium sulfate (2:1), hysteresis will become pronounced. This indicates that for an aerosol in which ammonium and sulfate are the primary inorganic soluble species, the acidity of the aerosol will be reflected in the degree to which it exhibits hygroscopic growth hysteresis. This link may be useful for understanding the health impact of an aerosol since there is evidence that impact is dependent upon acidity (Gwynn et al., 2000). Aerosol acidity has also been shown to influence secondary organic aerosol (SOA) production (Jang et al., 2002). In the study of these and other effects, inference of particle acidity through measurements of hygroscopic behavior can complement measures of total or fine-mode aerosol acidity that may not capture any dependence on particle size that exists.

Many techniques have been developed to measure the hygroscopic behavior of ambient aerosols. A number of research groups, applying a range of humidity control

approaches, have employed nephelometers to measure the RH dependence of the light scattering properties of an aerosol (Rood et al., 1985; ten Brink et al., 2000; Day et al., 2000). Although these measurements offer no information on the uniformity or size dependence of the hygroscopic properties, the fast time response of nephelometers permits rapid variation of RH to characterize evolving aerosols at the surface, or spatially heterogeneous aerosols from on board aircraft. Gas chromatographs coupled with thermal conductivity detectors (GC-TCD) have been used to directly measure the liquid water present within an aerosol collected on a filter (Chang and Lee, 2002; Lee and Chang, 2002). As with variable-RH nephelometers, use of a GC-TCD provides only a bulk measure of the hygroscopic properties of an aerosol, although it benefits from its relative insensitivity to other properties of the aerosol such as size distribution. The Tandem Differential Mobility Analyzer (TDMA; Liu et al., 1978) has become the most commonly employed instrument for observing the size-resolved hygroscopic behavior of an ambient aerosol (e.g., McMurry and Stolzenburg, 1989; McMurry et al., 1996). Most often, the RH an aerosol is exposed to within a TDMA is fixed in order to minimize the time needed to measure hygroscopic growth at several distinct particle sizes. By measuring the response of an aerosol to a range in RH, it is possible to characterize the upper and lower legs of any hysteresis loop present, which provides much greater insight into the composition of the hygroscopic species than fixed RH measurements alone.

In the following, we describe data collected using a humidity-scanning TDMA (HS-TDMA) to examine the hygroscopic behavior of particles in Houston and College Station, TX. Although no direct measurements of composition were made during this

study, the aerosol in this region at the same time of year was characterized extensively during both the Texas Air Quality Study (TexAQS) in 2000 and the Houston Supersite campaign in 2000 and 2001. Russell et al. (2004) described the daily mean aerosol composition in southeast Texas based on PM2.5 data recorded during the Houston Supersite project. They showed that average daily organic carbon to elemental carbon (OC/EC) ratios were higher than would be expected solely from primary emissions, suggesting that secondary OC is important in the region. Their analysis also showed that the ammonium to sulfate ratio varied from about 1.44 to 1.70. Nitrate comprised only about 5.5% of the average fine mode aerosol mass concentration, while sulfate comprised 32%. The corresponding molar ratio of SO_4^{2-} : NO_3^- of about 3.7:1, coupled with the likely association of nitrate with species other than ammonium, suggests that, on average, ammonium is typically associated with sulfate.

2. Methodology

Sampling was conducted in College Station, TX between August 3 and August 20, 2002, and in Houston, TX between September 17 and September 24, 2002. In Houston, sampling was conducted at ground level in a climate-controlled trailer located on the east side of the city, just north of the ship channel. This region is characterized by a high concentration of industrial and petrochemical refining facilities. Measurements in College Station were made either from within a room on the roof above the 12^{th} story of the Eller Oceanography and Meteorology Building on the campus of Texas A&M University, or on the 10^{th} floor of the same building. The height of these sampling locations minimized the influence from local sources. Since the prevailing winds during

the study period were typically from the south or southeast (Figure 15), the aerosol properties and meteorology in Houston and 100 miles to the northwest in College Station are expected to be similar, with the primary differences attributable to local pollution sources in the Houston area.

A schematic of the TDMA system used in this study is shown in Figure 16. Three identical Permapure PD-070-18T-24SS Nafion tube bundles were used within the TDMA to create the desired RH profiles. Two High Flow differential mobility analyzers (HF-DMAs) designed by Aerosol Dynamics, Inc. (Stolzenburg et al., 1998) were employed in the instrument to enhance the count rates during the necessarily rapid measurements. Complementary measurements of aerosol size distributions spanning a diameter range of 10 to 500 nm were used only to determine aerosol volume concentrations within that size range. The primary measurements used in this study were made with the HS-TDMA. Within this instrument, the aerosol sample is dried in Nafion A to an RH of less than 20% prior to classification by the upstream DMA. Following a single measurement at a fixed RH of 85%, the relative humidity between the two DMAs slowly decreases from about 85% to 30%, and then slowly increases back to 85%. While the RH is varied, the growth factor distribution is continuously measured as the downstream DMA scans through particle size over a period of approximately 40 s. Nafion B is bypassed during the decreasing RH measurements and, as a result, the aerosol is exposed to the maximum RH it experiences within the instrument just as it enters the downstream DMA. If the sampled aerosol exhibits hysteresis, the growth factors measured during this portion of the humidity scan describe the lower leg of the

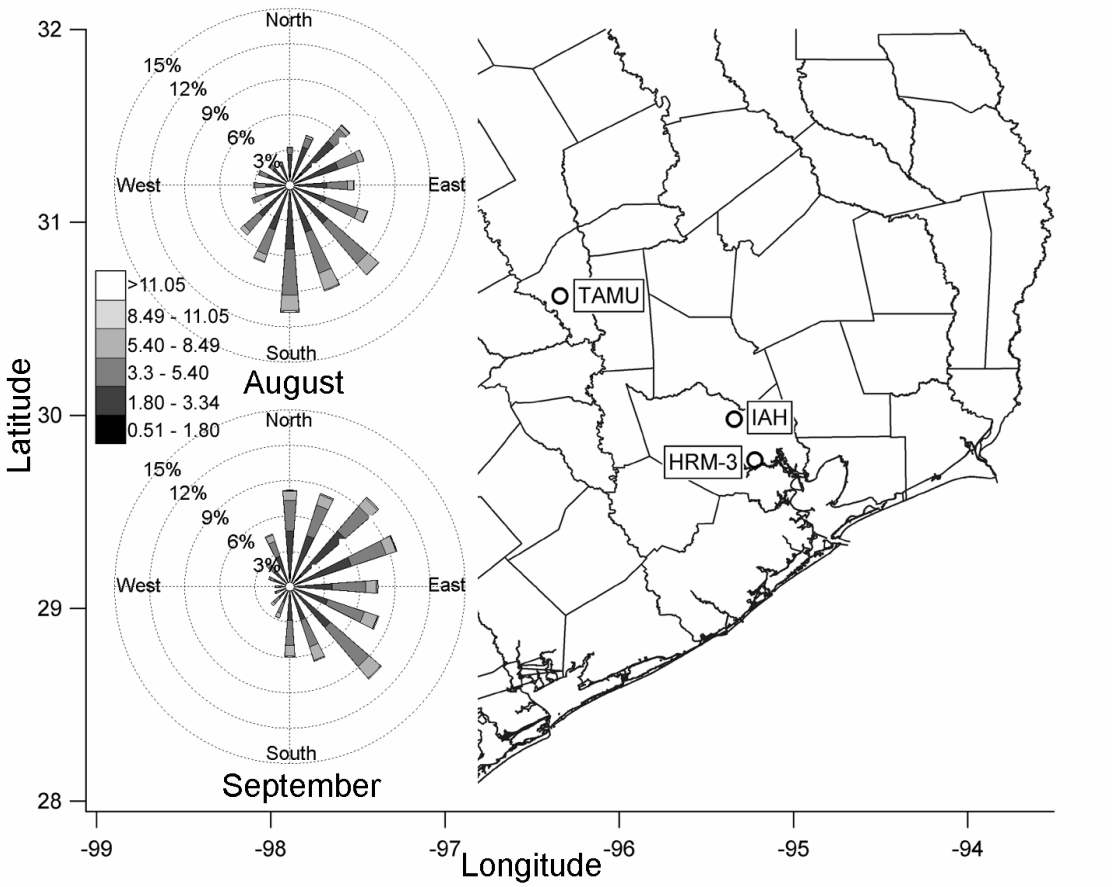

Figure 15. Map showing the two sampling sites (TAMU and HRM-3), and wind roses for the months of August and September. Wind roses were created from measurements made at the Bush Intercontinental Airport in Houston (IAH) using data from 1961 to 1990, and were obtained from the United States Department of Agriculture Natural Resources Conservation Service.

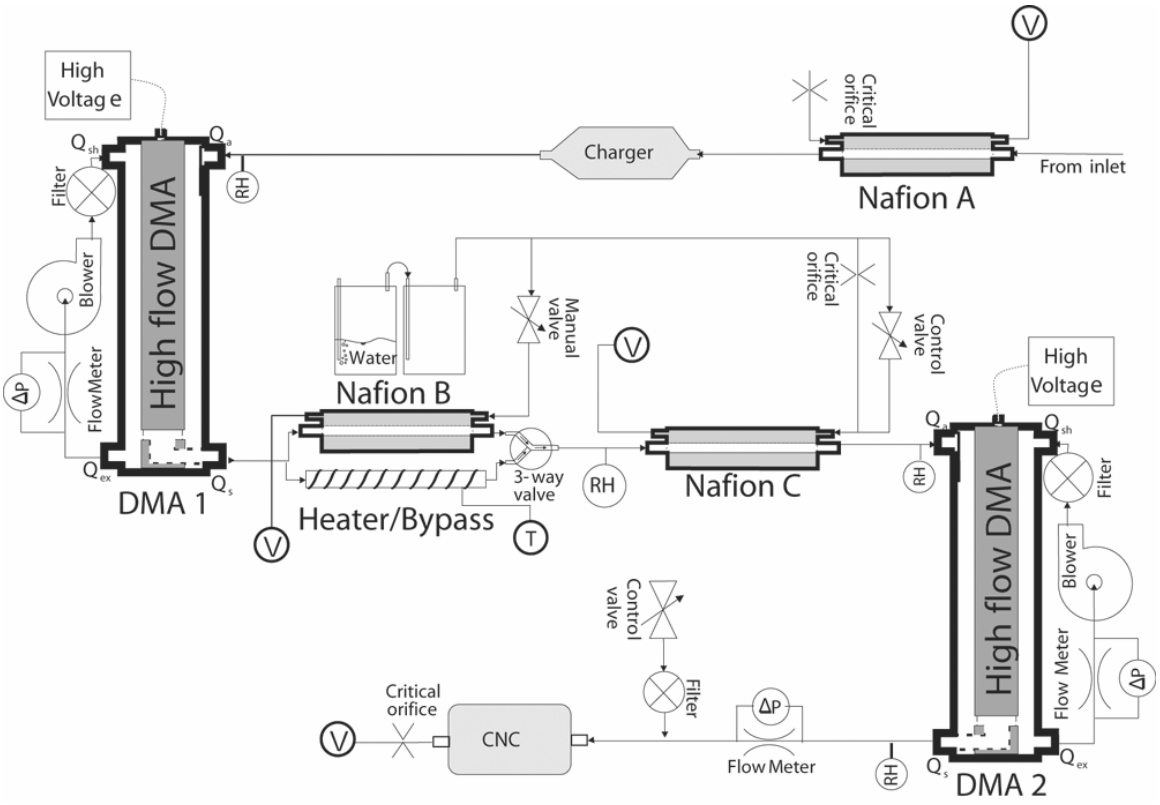

Figure 16. Schematic of the RH scanning and temperature scanning TDMA. Circled V indicates connection to vacuum, circled T indicates a temperature probe, and circled RH indicates the location of an RH probe.

hysteresis loop. During the increasing RH measurements, the aerosol classified by the upstream DMA is exposed to a high (>85%) RH within Nafion B and then returned to a lower RH in Nafion C before entering the downstream DMA. This RH conditioning ensures that all hygroscopic particles are initially hydrated so that the growth factors measured describe the metastable (or upper) leg of any hysteresis loop. The total time to measure both the upper and lower leg of the hysteresis loop varied between 30 and 45 minutes. Despite the fact that the sheath flow RH is not controlled, there is relatively little uncertainty in the RH that the aerosol particles experience in each DMA. Despite the fact that there are differences in the RH of the sheath and aerosol flows, the experimental setup still allows accurate determination of the RH relevant to the measurement. Since the maximum RH, during a lower leg measurement, and the minimum RH, during an upper leg measurement, occur within the DMA, the RH measurement made at the outlet of the DMA is the RH relevant to both the growth factor observed and to any change in hydration state. Initially, these measurements were made for particles with dry diameters ranging from 12 to 400 nm. It was observed that the larger particle sizes displayed the hysteresis behavior most clearly. Measurements were then focused on 160 nm and 320 nm particles. This was further restricted to 160 nm dry diameter particles because the concentration of those particles was much higher, allowing easier interpretation of the changes in hysteresis.

The growth factor distributions measured with the HS-TDMA were parameterized by fitting them with one or more log normal distributions. Although as many as four modes would sometimes be necessary to describe a single HS-TDMA

distribution, a single mode typically dominated the distribution. Occasionally, two modes would be of almost equal magnitude, but this occurred only in the vicinity of phase transitions (deliquescence/crystallization). Once the growth factor distributions were fitted, the parameters describing the dominant hygroscopic mode were used to describe the hysteresis properties of the aerosol. For this study, deliquescence RH (if any), crystallization RH (if any), growth factor of the lower leg at 60% RH (GF60), and the ratio of the growth factors on each leg of the hysteresis loop at 50% RH (GFR50) were chosen to represent the different aspects of hysteresis properties observed in each HS-TDMA measurement. Each of these parameters is identified in Figure 14. The DRH is determined as the RH at which at least half of the particles measured during a lower leg measurement have a growth factor that is equivalent to the growth factor measured at the same RH in the corresponding upper leg measurement. Similarly, the CRH is defined as the RH at which at least half of the particles measured during an upper leg measurement have a growth factor that is equivalent to the growth factor measured at the same RH in the corresponding lower leg measurement. The difficulty in determining an absolute CRH or DRH is complicated by the mixed composition of the ambient aerosol. Ambient aerosol often does not display sharp transitions at deliquescence and crystallization. Therefore, defining a precise RH at which these transitions occur can be extremely difficult. The CRH is particularly difficult determine because the change in growth factor is small compared to that of deliquescence in most cases. The 60% RH growth factor, the deliquescence RH, and the crystallization RH were each normalized with respect to their maximum and minimum daily values according to the following:

$$V_N = \frac{V_o - V_{\min}}{V_{\max} - V_{\min}}$$

In the above, V_N represents the normalized value, V_o represents the observed value and V_{max} and V_{min} represented the observed maximum and minimum values observed for that parameter on each day. This was done to reduce the effect of day-to-day variations in the composition of the soluble fraction of the aerosol. Only days with 5 or more measurements were used in this analysis to ensure that reasonable maximum and minimum values were obtained.

Intermittent aerosol volatility measurements were also made during a few of the study days. For these measurements, the temperature in the heated tube shown in Figure 16 is initially raised to just over 300° C. Over a period of 45 minutes the heater is then allowed to cool to ambient temperature again. After exiting the heated tube, the non-volatile fraction of the initially monodisperse aerosol is humidified to ~85% RH. This post-heating humidification permits identification of the hygroscopic and non-hygroscopic fractions to enable examination of the volatility behavior of the two populations. Growth factor distributions are recorded approximately every minute, resulting in a temperature resolution of about 10° C. By determining the temperature at which most of the hygroscopic particles volatilize, the dominant inorganic species present can be inferred.

The objective of this analysis is to identify variables that are correlated with hygroscopic growth behavior. A range of environmental parameters were considered. Atmospheric observations from automated local weather stations (Easterwood Airport in

College Station and Bush Intercontinental Airport in Houston) were used in conjunction with the aerosol measurements. These meteorological measurements, which are recorded hourly, were linearly interpolated to the times of HS-TDMA scans. The atmospheric variables considered in this analysis are temperature, relative humidity, and wind direction. Any process which changes the aerosol composition may also add mass to the aerosol. This additional mass might be observed in the aerosol volume or mass concentrations. Measured size distributions were used to determine the sub-500 nm aerosol volume concentration in College Station. The size range covered was usually sufficient to capture the peak in the fine mode volume distribution. The volume distributions were then fit with a series of log normal distributions. The volume in each of the modes is then summed to determine a cumulative fine mode volume. In this manner, so long as the peak of a volume distribution is captured, the volume within the entire mode can be determined from the log normal fit. Because aerosol size distributions were not measured in Houston, hourly PM2.5 data recorded by the Texas Commission on Environmental Quality were used in the analysis of the data there.

In order to gain insight into the mechanisms responsible for observed changes in the hygroscopic growth hysteresis, correlations with the range of aerosol and environmental parameters discussed above were examined. In cases where these analyses showed some significant relationship with more than a single variable, correlations combining all appropriate variables were evaluated. In all cases, measured aerosol volume concentration or PM2.5 mass concentration was considered together with RH and temperature. To be confident that the results were not skewed by rapid

meteorological changes or atypical conditions, measurements were omitted if they were made while the wind was changing dramatically (more than 90 degrees of change in a 2 hour period), while the dew point was below 15.5° C, while the temperature was above 35° C, and while it was raining. In addition, when the temperature was below 25° C, almost no correlation could be observed between GFR50 and any atmospheric variable. Therefore, all data points below 25° C were excluded from those analyses to ensure that the existing relationships were not obscured. Using these relationships, inferences can be made regarding the cause of the observed changes in hysteresis properties.

3. Observations and Results

Examination of the parameterized HS-TDMA data indicated that the degree of hysteresis varied cyclically over a twenty-four hour period. An example of this daily transformation is shown in Figure 17. A clearly defined hysteresis loop was commonly observed between late evening and early morning. Beginning in mid-morning, growth factors along the lower leg of the hysteresis loop began to increase. By afternoon, the separation between the lower and upper legs of the hysteresis loop was very small, and occasionally no hysteresis was observed. This trend usually began to reverse in late afternoon or early evening. These changes were observed to some degree on every day that measurements were made and seemed to occur in an incremental and consistent pattern. Due to the rate that changes in aerosol composition were occurring, the 30 to 45 minute measurement time occasionally resulted in different growth factors measured for RH above deliquescence during the upper and lower leg measurements (Figure 17 at 12:21). The expectation that the diurnal changes in the hysteresis properties of the

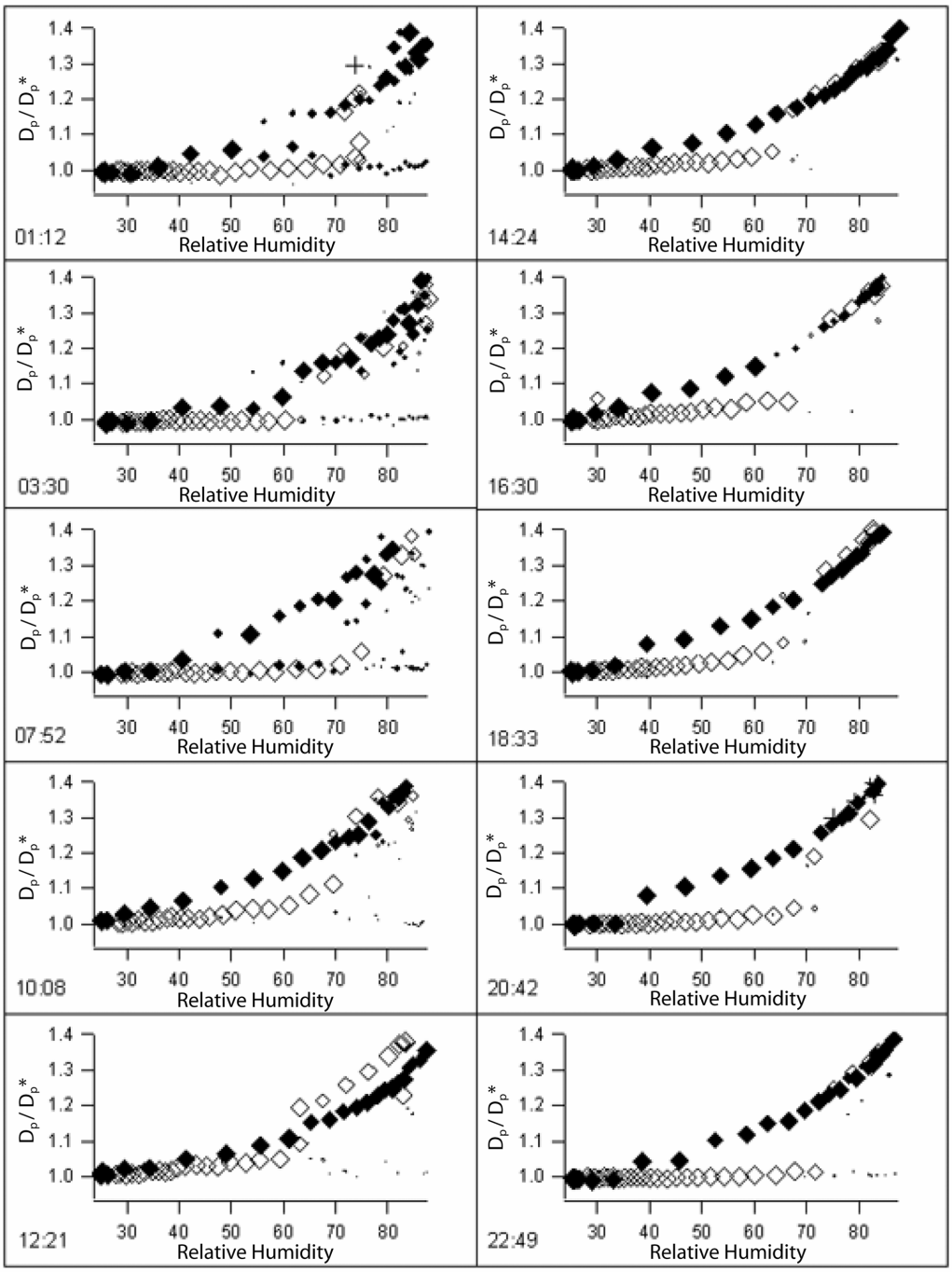

Figure 17. Parameterized RH Scan measurements from August 13, 2002. Solid diamonds represent measurements made when humidity was decreasing (metastable leg) and open diamonds represent measurements made while humidity was increasing (stable leg). Diamond size reflects the fraction of the total concentration in the given mode. Initially the hysteresis is very distinct, but it begins to collapse by the 10:08 measurement. By 20:42 the hysteresis has once again become distinct.

aerosol would be correlated with the diurnal cycle of an atmospheric variable such as temperature or relative humidity motivated the attempt to establish relationships between these variables.

Variability in the composition of the inorganic fraction of the aerosol is likely responsible for part or all of the observed cycles in hygroscopic properties. Based on local aerosol compositional climatology, it is expected that NH_4^+, SO_4^{2-}, and NO_3^- are the primary inorganic ions present in the soluble fraction. Several possible explanations for the observed changes were explored; however, the most plausible of these possibilities is the addition of SO_4^{2-} during the day. If ammonia concentrations are high enough for ammonium nitrate to be present early in the morning, the ammonium to sulfate ratio is expected to be greater than 2:1. As sulfate is added to the aerosol, it would initially displace the nitrate, decreasing the overall ammonium to sulfate ratio. The DRH of a mixture of ammonium nitrate and ammonium sulfate is less than that of pure ammonium sulfate (Rood et al., 1985). Therefore, this initial change would lead to an increase in DRH. However, after the nitrate has been fully displaced, sulfate would continue to condense on, or be formed within, the particles. This increase in sulfate would further decrease the ammonium to sulfate ratio and increase the particle acidity. Both gas phase and aqueous phase sulfate production are likely to be enhanced in the afternoon when OH·, O_3, and H_2O_2 concentrations are highest, and when convective clouds are abundant in this region.

The size-resolved aerosol volatility measurements were used to further constrain the composition of the soluble component of the aerosol. Figure 18 shows one

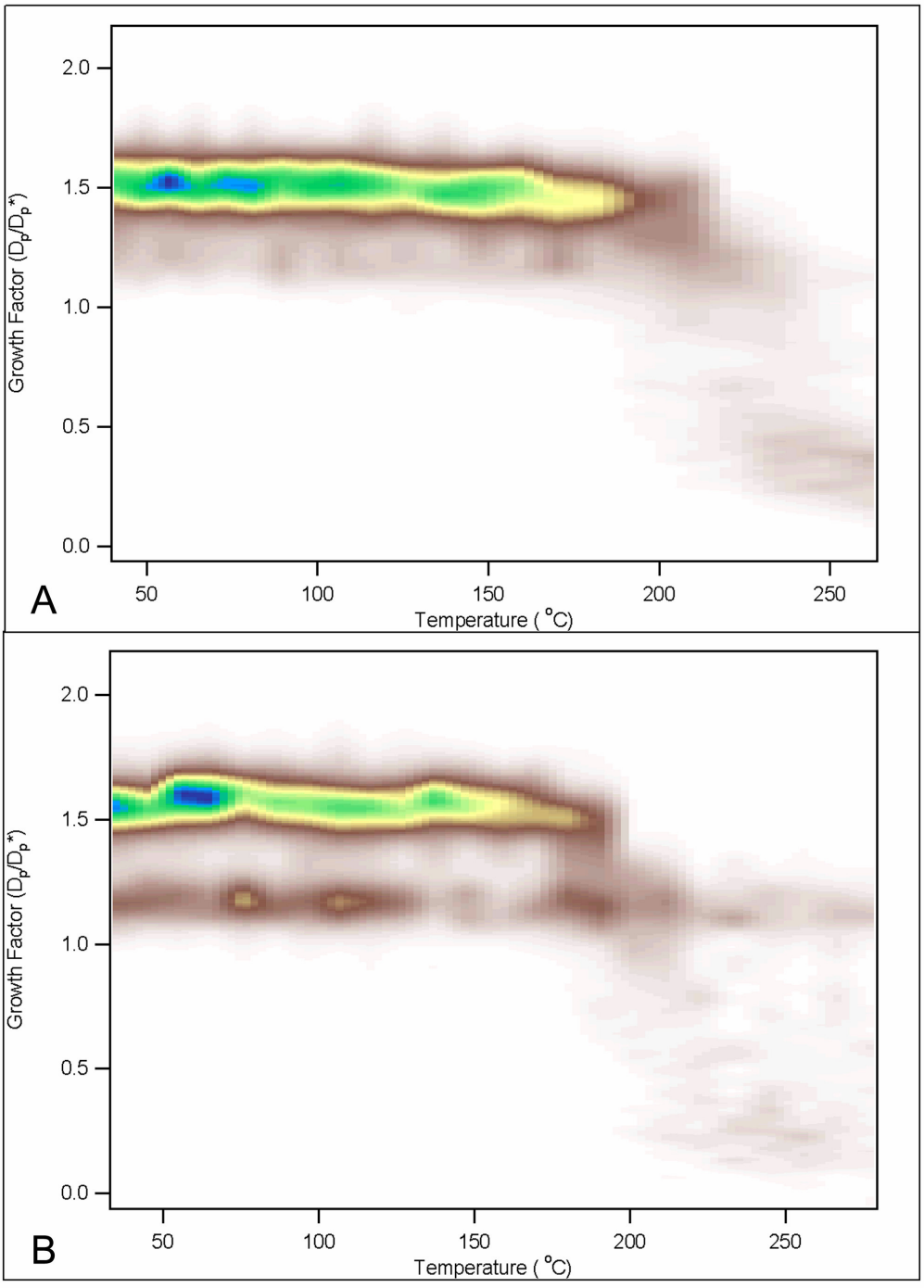

Figure 18. Temperature scan measurements (a) from College Station and (b) from Houston. The sharp drop in concentration in the hygroscopic mode between 180 and 200° C degrees in both plots suggests that ammonium and sulfate are the primary ions in the soluble fraction of the aerosol. Both measurements also indicate the presence of residuals that do not volatilize below 300° C.

temperature scan made on August 28 at the College Station site and one from September 18 at the Houston site. Consistent with other temperature scans made throughout each period, the hygroscopic fraction of the aerosol volatilized at temperatures between 180° and 200° C on both of these days. Published values of the volatility temperature for $(NH_4)_2SO_4$ range from about 200° to 240° C (Pinnick et al., 1987; Jennings and O'Dowd, 1990; Clarke, 1991; O'Dowd et al., 1992; Brooks et al., 2002), while that of NH_4HSO_4 is about 147° C (Brooks et al., 2002). The similarity between the volatility properties of the measured aerosol and those of pure sulfates supports the conclusion that the primary volatile fraction of most of these hygroscopic particles is some combination ammonium and sulfate ions, since other common aerosol species volatilize at significantly different temperatures. These measurements also show that non-refractory residuals that do not volatilize at temperatures as high as 300 ^{o}C are present within most or all of the hygroscopic particles. These residuals are believed to be composed of some combination of ash, mineral dust, and organic and elemental carbon.

As noted in the methodology, several quantities were used to characterize the shape of the hygroscopic growth hysteresis loop. These include the DRH, the CRH, the growth factor at 60% RH along the lower leg (GF60), and the ratio of the growth factor of a particle on the upper leg of the hysteresis to that of one on the lower leg at 50% RH (GFR50). Each of these was selected to represent a different aspect of the change that was observed to occur, as described at the beginning of the section. These quantities were compared with the aforementioned atmospheric variables (temperature, RH, and

wind direction), as well as the measured aerosol volume or PM2.5 mass concentration. Results for College Station and Houston are presented separately below.

The analysis within this paper is focused on the interpretation of compositional variability based on hygroscopic behavior. Even so, there are aspects of the behavior itself that are of importance. Despite the differences between the two sites, the relationships between ambient RH and the CRH and DRH of the aerosol were quite similar. While CRH was difficult to determine with an accuracy that could be used to track changes in the aerosol composition, the measurements were clear enough to determine that the CRH was, in all cases, well below the ambient RH. The measurements also indicate that the ambient RH exceeded the DRH during each 24-hour period. This would suggest that most, if not all, of the aerosol particles that exhibit hysteresis in their hygroscopic growth should remain in an aqueous state throughout the day. This assertion is supported by measurements during this same period of the ambient hydration state of size-resolved particles (Santarpia et al., 2004).

Measurements made in College Station suggest a strong relationship between increasing temperature and the observed compression of the hygroscopic growth hysteresis loop. This relationship is shown in correlations with DRH (Figure 19a), GF60 (Figure 20a), and GFR50 (Figure 21a). This compression also appears closely related to a decrease in ambient RH (Figure 19-21b). The similarity in the strength of correlation with temperature and RH is not surprising since the ambient temperature and RH are very strongly anti-correlated in this dataset (Figure 22a), suggesting that the dew-point was fairly constant over the sampling period. Correlations of DRH, GF60, and GFR50

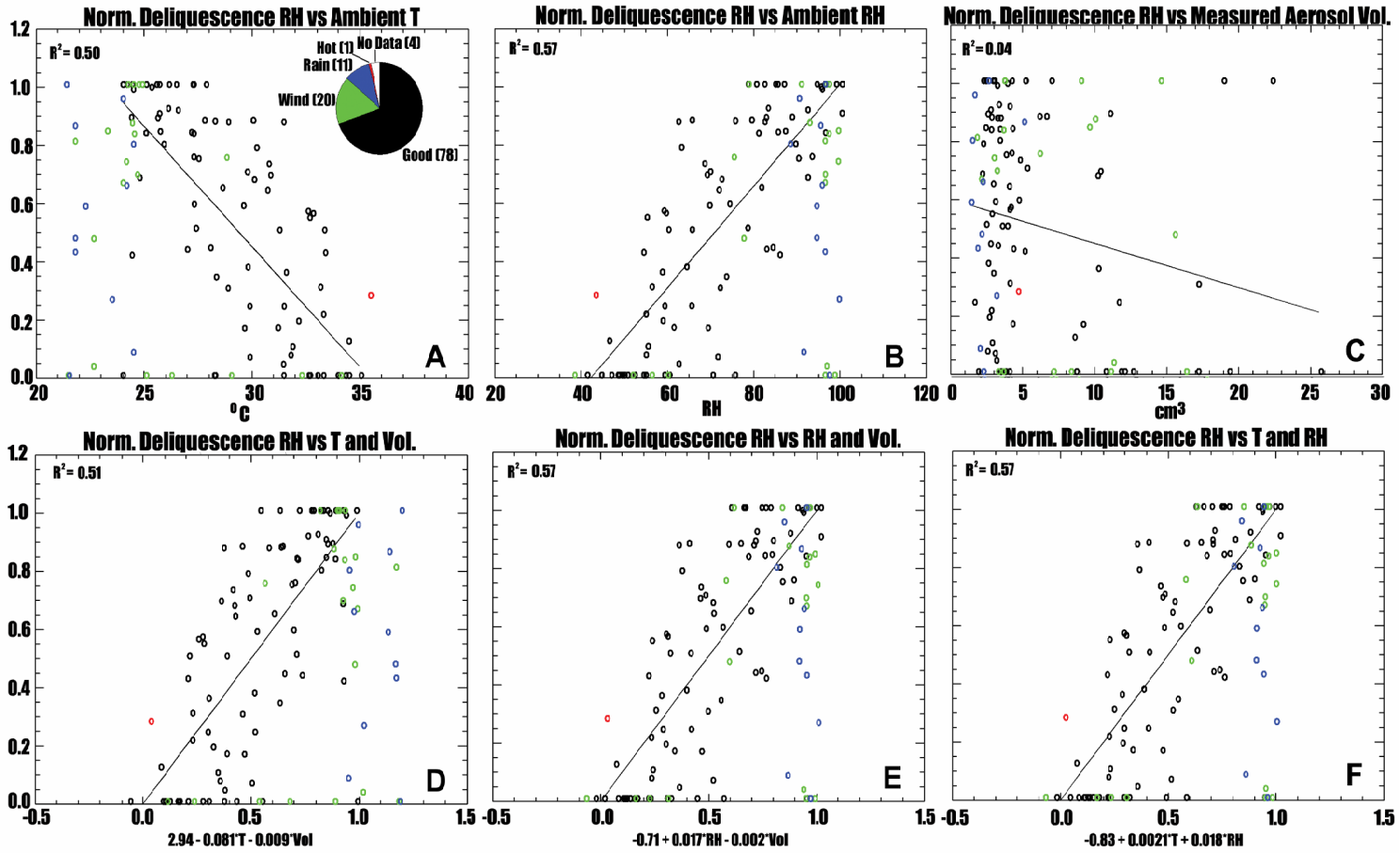

Figure 19. Scatter plots showing relationships with normalized DRH measured in College Station from August 3 to August 20, 2002. Variables for which correlations were evaluated include temperature, RH, aerosol volume concentration, and linear combinations of these. Each point represents an individual hysteresis measurement and all measurements made during this period are shown. Only the black (good) data points are used to determine the R^2 values. The fractions of excluded data (31%) are shown in the pie chart with colors representing the reason for excluding each measurement. In D-F the functions along the x-axis are the best-fit functions for the data as determined by the analysis.

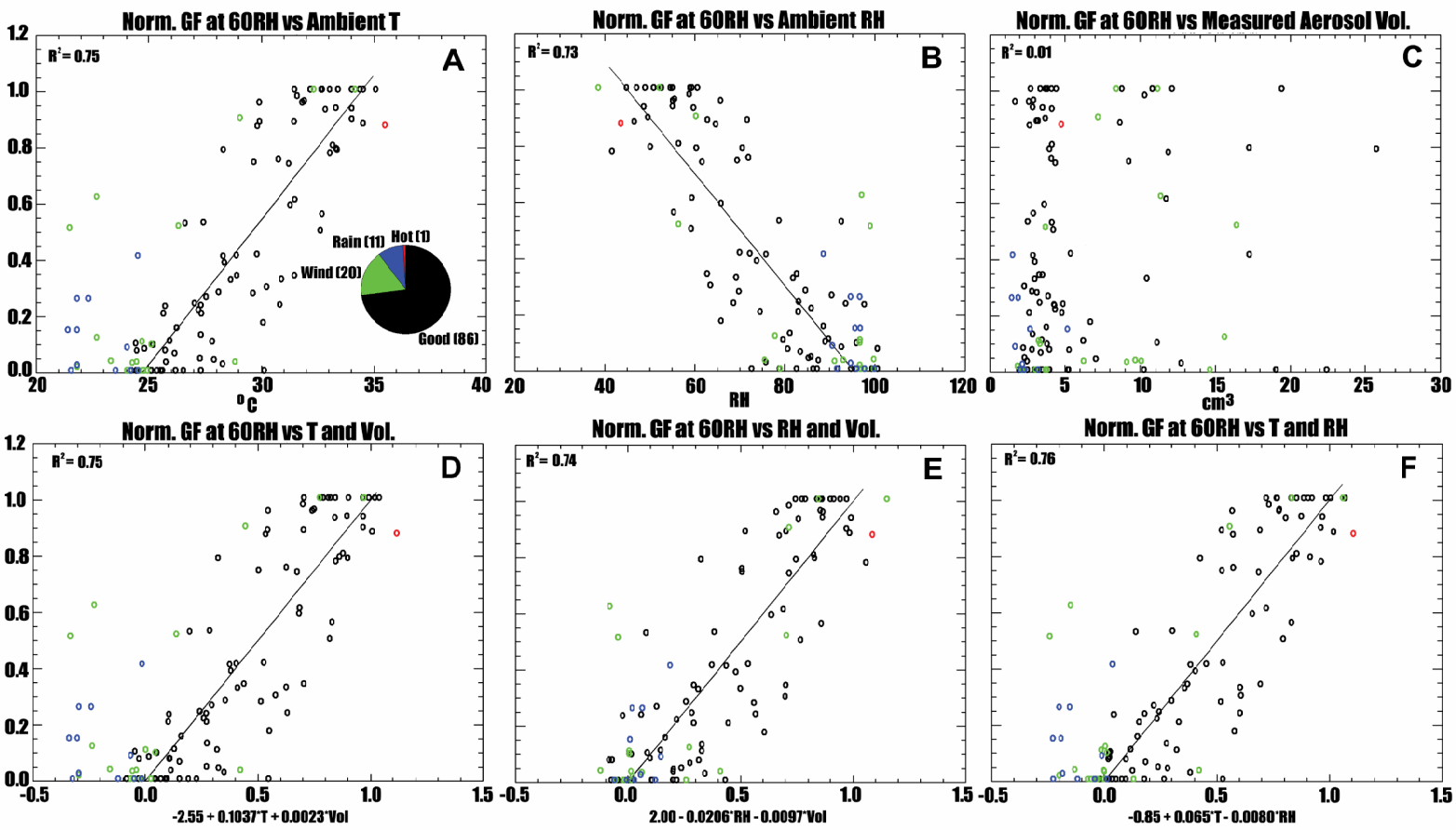

Figure 20. Scatter plots showing relationships with normalized growth factor at 60% RH (NGF60) measured in College Station from August 3 to August 20, 2002. Variables for which correlations were evaluated include temperature, RH, aerosol volume concentration, and linear combinations of these. Each point represents an individual hysteresis measurement and all measurements made during this period are shown. Only the black (good) data points are used to determine the R^2 values. The fractions of excluded data (27%) are shown in the pie chart with colors representing the reason for excluding each measurement. In D-F the functions along the x-axis are the best-fit functions for the data as determined by the analysis.

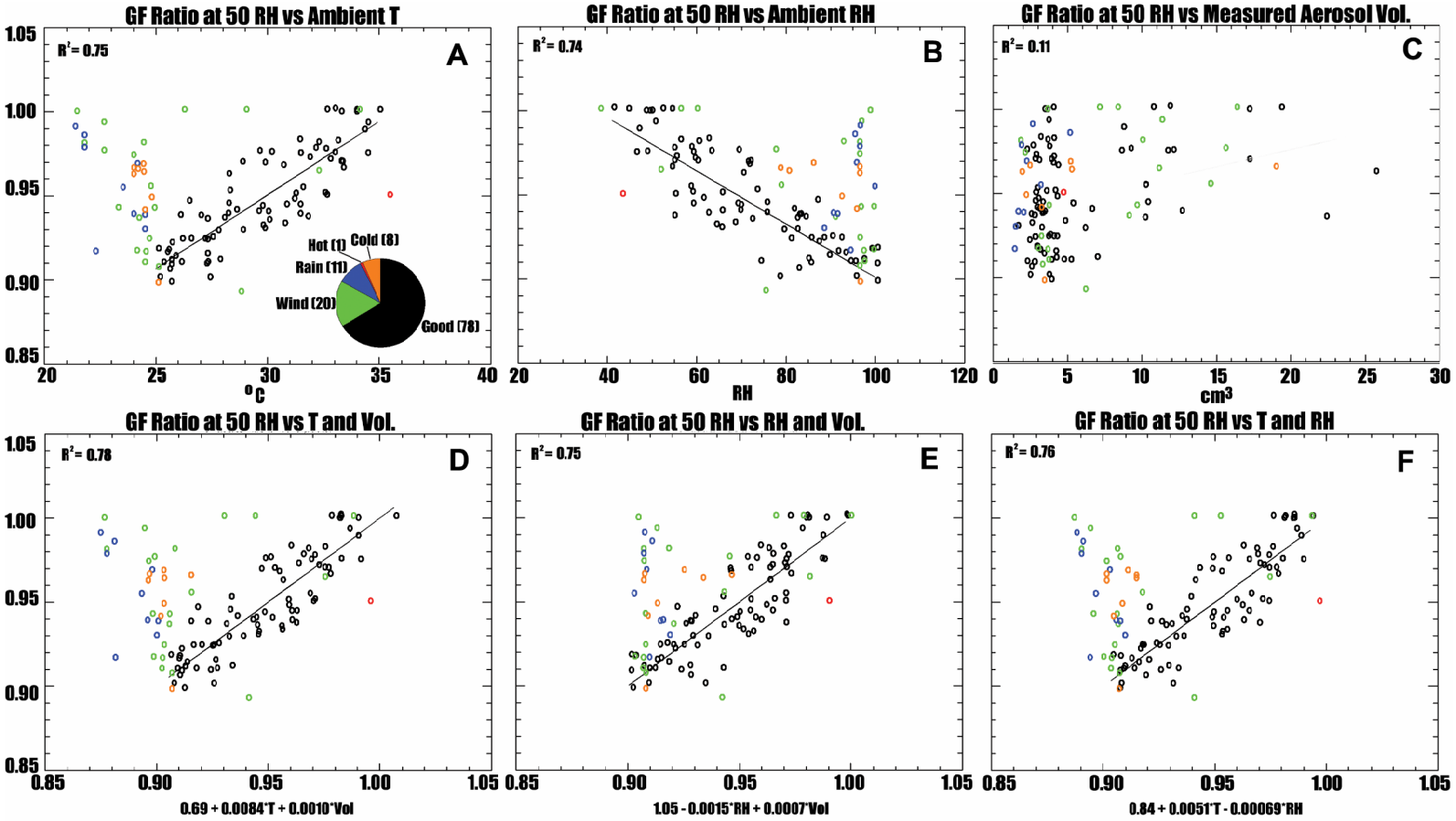

Figure 21. Scatter plots showing relationships with growth factor ratio at 50% RH (GFR50) measured in College Station from August 3 to August 20, 2002. Variables for which correlations were evaluated include temperature, RH, aerosol volume concentration, and linear combinations of these. Each point represents an individual hysteresis measurement and all measurements made during this period are shown. Only the black (good) data points are used to determine the R^2 values. The fractions of excluded data (34%) are shown in the pie chart with colors representing the reason for excluding each measurement. In D-F the functions along the x-axis are the best-fit functions for the data as determined by the analysis.

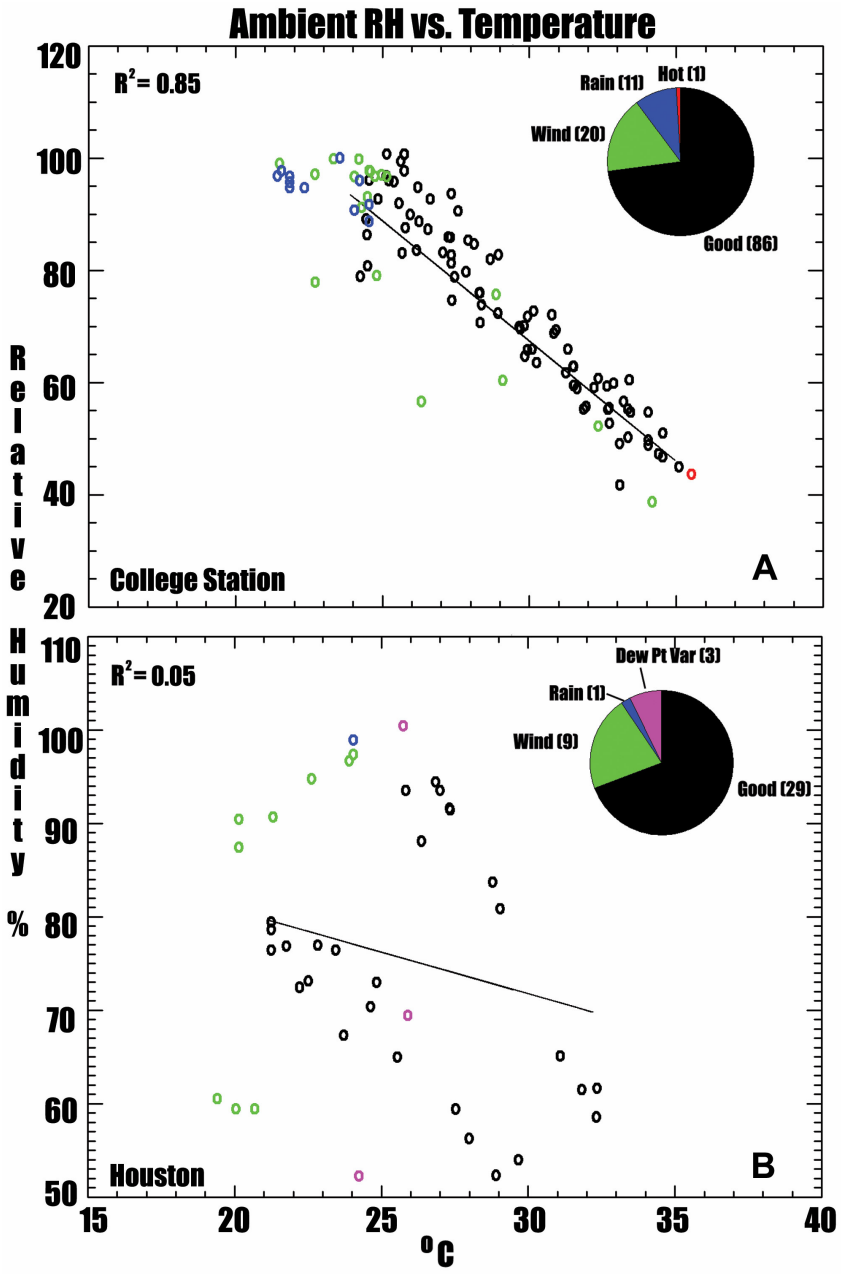

Figure 22. Scatter plots showing the relationship between ambient temperature and ambient RH during the sampling periods in College Station (a) and Houston (b). Each point represents the RH at the midpoint of each hysteresis measurement, and all measurements made during each period are shown. Only the black (good) data points are used to determine the R^2 values. The fractions of excluded data (27% (a); 31% (b)) are shown in the pie chart with colors representing the reason for excluding each measurement.

with wind direction have very low R^2 values, which implies that variability in aerosol source region is not closely related to the observed changes in hysteresis. When both RH and temperature are considered together in the analysis, the R^2 values improve (Figure 19-21f), but only slightly. By itself, aerosol volume does not seem to be strongly correlated with any of the characteristics of the hysteresis loop (Figure 19-21c), but when combined with temperature or RH, it does seem to improve the correlation (Figure 19-21d and e). This indicates that, while other effects may obscure it, the volume concentration of pre-existing aerosol may be important.

Fewer measurements were made in Houston than in College Station, and those that were made were often influenced by local aerosol sources, which complicated interpretation of changes in DRH and GF60. Despite the greater temporal heterogeneity of the aerosol observed in Houston, cyclic changes similar to those observed in College Station were detected. For the measurements made in Houston, the relationship between GFR50, temperature, and RH was similar to that in College Station (Figure 23), indicating that the same type of change in the aerosol was also occurring at this location. Correlations with temperature or RH individually were not as strong as those seen with the College Station data (R^2 values of 0.08 for temperature and 0.47 for RH, as compared to ~0.75 for both in College Station). The dew point in College Station was very stable throughout the measurement period, consistent with typical August weather conditions in this region. The dew point in Houston, however, was more variable, as shown by the complicated relationship between temperature and RH (Figure 22b). As with the data collected in College Station, there was no indication that local source region, as

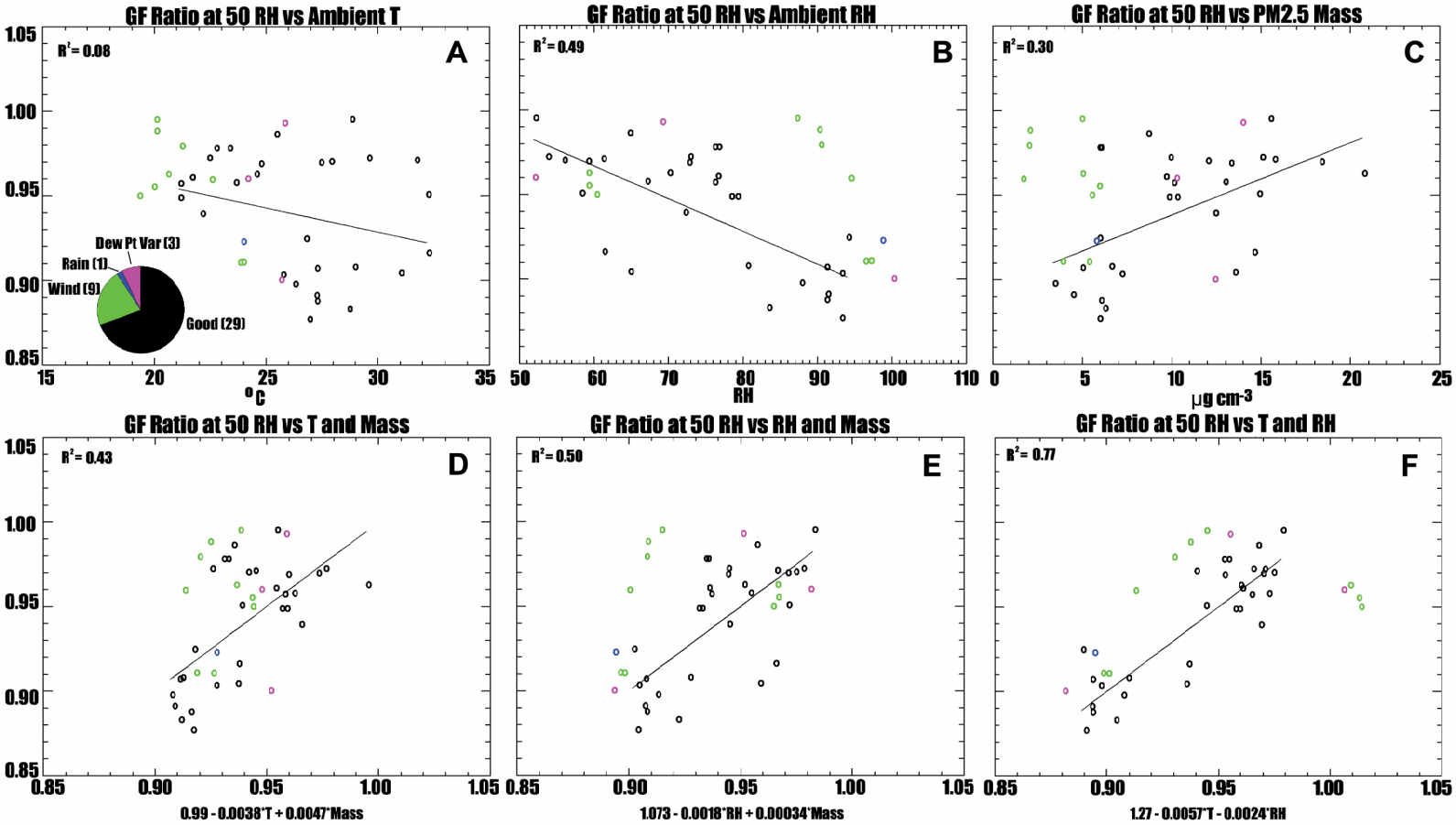

Figure 23. Scatter plots showing relationships with growth factor ratio at 50% RH (GFR50) measured in Houston from September 17 to September 24, 2002. Variables for which correlations were evaluated include temperature, RH, PM2.5 mass concentration, and linear combinations of these. Each point represents an individual hysteresis measurement and all measurements made during this period are shown. Only the black (good) data points are used to determine the R^2 values. The fractions of excluded data (31%) are shown in the pie chart with colors representing the reason for excluding each measurement. In D-F the functions along the x-axis are the best-fit functions for the data as determined by the analysis.

determined by wind direction, was related to the observed changes in hysteresis. Since size distribution measurements like those made in College Station were not available in Houston, measurements of PM2.5 mass concentration were used to examine the influence of pre-existing aerosols on observed changes. The relationship between PM2.5 mass concentration and the changes in hysteresis behavior (Figure 22c) is considerably stronger than the relationships between volume concentration and the changes observed in College Station.

4. Discussion

The overall results of this analysis suggest that the hygroscopic fraction of the aerosol in both College Station and Houston experiences some cyclic change in its composition that is correlated with ambient temperature, RH, and aerosol volume/mass concentration. Based on the regionally-representative aerosol composition presented by Russell et al. (2004), and on measurements of both the DRH and aerosol volatility, it is believed that this change is related to changes in the soluble ion ratio in the particles. The mechanism(s) responsible for that change were investigated.

The ISORROPIA aerosol thermodynamics model (Nenes et al., 1998a, b) was used to examine the possibility that changes in temperature could be directly responsible for the observed changes in hygroscopic growth hysteresis. To reflect the regionally-representative aerosol composition described by Russell et al. (2004), the model was initiated with a sulfate to nitrate molar ratio of 3.7:1 and enough ammonium to balance the charge. Temperature was varied between 20° C and 34° C, while water vapor was held constant, resulting in a corresponding decrease in RH from 98% to 42%. Over this

temperature and RH range, approximately 27% of the aerosol phase nitrate would be lost to the gas phase along with 3% of the ammonia. As discussed above, the loss of nitrate with increasing temperature would lead to an increase in the DRH of the aerosol. Accompanying this change must be one or more additional transformations that result in more significant changes since the observed evolution in DRH with increasing temperature is opposite of that which would be expected due to nitrate loss.

Since nitrate represents such a small fraction of the aerosol and its loss due to increasing temperature does not explain the dependence of hygroscopic behavior on temperature, the almost-daily cycle of collapse and then separation of the upper and lower legs of the hysteresis loop is very likely due to an increase in sulfate mass. Gas phase production of sulfate is expected to peak in the afternoon when OH· concentration is highest. Convective clouds are abundant in southeast Texas during the late morning and early afternoon, which, coupled with high O_3 and H_2O_2 concentrations, will also contribute to a mid-day maxima in sulfate production through aqueous phase reactions. Therefore, if excess ammonia is not available, the ammonium to sulfate ratio will decrease in the late morning and early afternoon, coincident with increasing temperature and decreasing RH. There may also be feedbacks that further alter aerosol hygroscopic behavior in response to increased sulfate concentration. For example, addition of SOA to the increasingly acidic hygroscopic particles may be enhanced through acid-catalyzed reactions (Jang et al., 2002; Czoschke et al., 2003). Many recent studies (Hansson et al., 1990; Saxena et al., 1995; Hansson et al., 1998; Xiong et al., 1998) have shown that

organics may significantly change the DRH and CRH of a hygroscopic aerosol and may also cause it to absorb water prior to deliquescence.

Based on the extent to which hygroscopic behavior varied throughout a day, use of seasonal or even daily averages of the ammonium to sulfate ratio could lead to misconceptions about the behavior and influence of the aerosol. For instance, Russell et al. (2004) state that the ratio of ammonium to sulfate is approximately 1.5:1 during the late summer. However, our examination of the hygroscopic properties of these particles suggests that over the course of the day the ammonium to sulfate ratio might vary between 2:1 and less than 1:1. Evidence for this cyclic variation in the ammonium to sulfate ratio was also found in data collected during TexAQS 2000. Measurements made with the particle into liquid sampler (PILS; Weber et al., 2001) between August 13, 2000 and September 13, 2000 were used to determine the ammonium to sulfate ratio within the fine mode aerosol. These data suggest that the peak NH_4:SO_4 of about 1.92 occurs between 04:00 and 08:00 and that this ratio declines sharply after 10:00 to approximately 1.76 (Rodney Weber personal communication, 2004). Even though the PILS data does not indicate as dramatic a change as was observed in this study, the qualitative behavior is the same.

A conceptual model that can explain the observed behavior is shown in Figure 24. In the early morning, when the temperature is at a minimum and RH at a maximum, the ammonium to sulfate ratio in the aerosol will typically be 2:1 or higher. Since sulfate will not be efficiently produced through either gas or aqueous phase reactions at this time, the aerosol can be fully neutralized by the existing ammonium. Following sunrise,

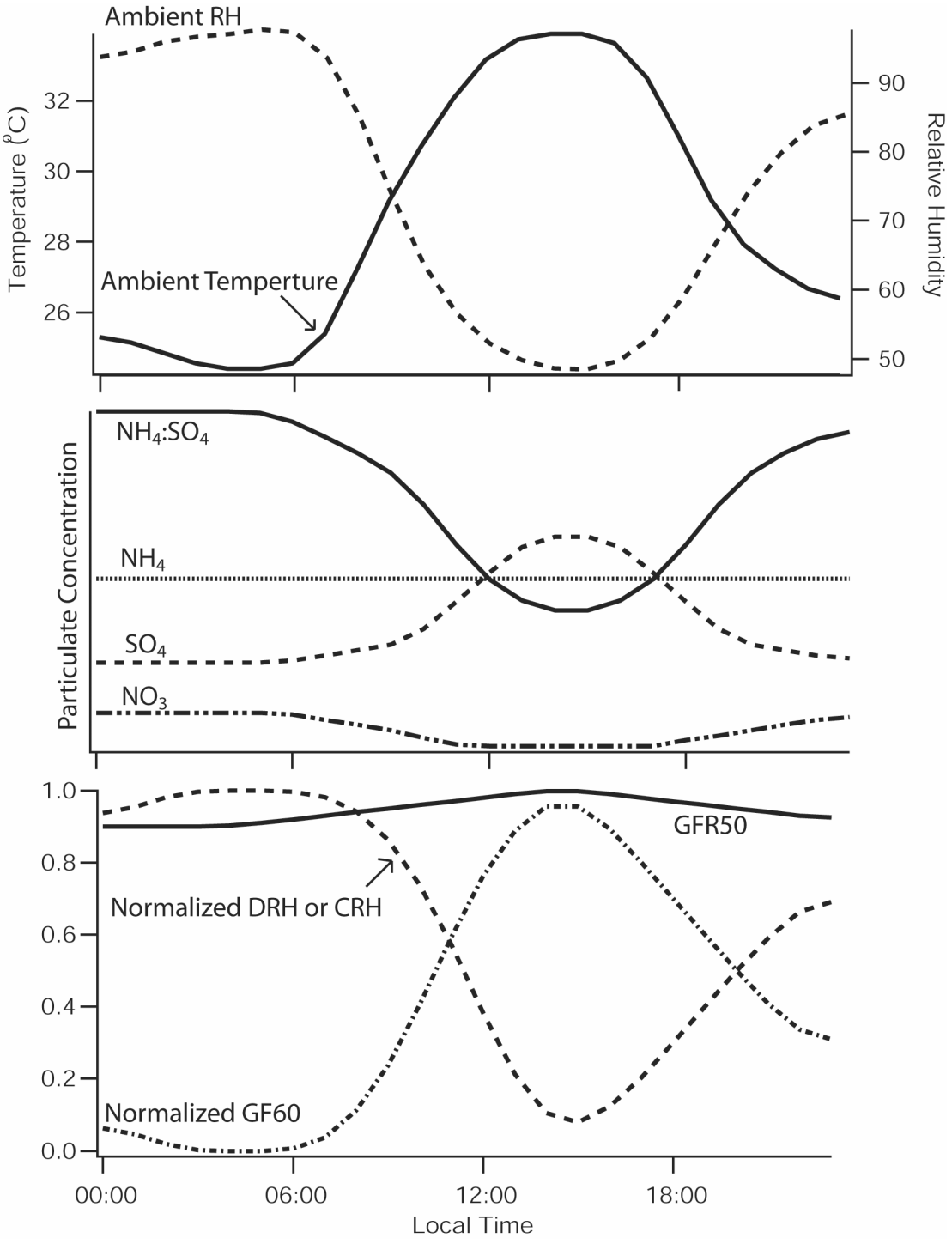

Figure 24. Conceptual model that explains the cycles observed in aerosol hygroscopic behavior.

gas phase and aqueous phase sulfate production increases. When the nitrate that was initially associated with ammonium has been completely displaced by sulfate, the ammonium to sulfate ratio will begin to decrease. As sulfate production peaks in the mid-afternoon, the ammonium to sulfate ratio will be at a minimum and the aerosol acidity will be at its peak daily value. Already high SOA production resulting from high oxidant concentrations may be further enhanced during this period through acid-catalyzed reactions on the sulfate aerosol. The decreasing ammonium to sulfate ratio also impacts the phase of the aerosol. The transition from high to low ammonium to sulfate ratio results in a CRH cycle that is in phase with the ambient RH cycle. This prevents the ambient RH from falling below the CRH, which causes the hygroscopic aerosol to remain aqueous throughout the day. This cycle in particle acidity may also be of significance with respect to the impact of the aerosol on human health. A recent study by Gwynn et al. (2000) demonstrated that respiratory hospitalization and mortality rates had very high correlations with both H^+ and SO_4^{2-} concentrations in the particulate phase. Unfortunately, the peak in aerosol acidity inferred from these data occurs at a time when outside activity is expected to be high.

In summary, the results of this study suggest that the aerosol in southeast Texas is subject to variations in the relative concentration of ammonium and sulfate throughout the day. This diurnal variation in the ammonium to sulfate ratio is likely caused by an enhancement in sulfate production during the late morning and afternoon. Although data were only collected in a limited geographical area, the aerosol in this region is similar to

that in many other parts of the world, suggesting that this type of cycle may influence aerosol properties elsewhere.

CHAPTER IV

ESTIMATES OF AQUEOUS-PHASE SULFATE PRODUCTION USING TANDEM DIFFERENTIAL MOBILITY ANALYSIS

1. Introduction

Aerosol-cloud interactions are not only important to the fundamental properties of clouds, but are also important in shaping the distribution and chemical composition of the aerosol. Clouds may modify aerosol populations simply by preferentially scavenging and precipitating cloud condensation nuclei (CCN), or by adding mass to the activated aerosol through aqueous phase reactions. This additional material can change the size, composition, and hygroscopic properties of the aerosol. Arguably, the most important reactions occurring in this manner involve the transformation of dissolved compounds containing S(IV) such as sulfur dioxide, SO_2, into compounds containing S(VI) such as the sulfate ion (SO_4^{2-}). Although sulfate may be produced through several oxidation pathways, reactions involving ozone (O_3) and hydrogen peroxide (H_2O_2) are typically deemed the most important (Seinfeld and Pandis, 1998).

Sulfate production through cloud-processing is a significant source of sulfate mass. McHenry and Dennis (1994) found that more than 60% of the sulfate present in the ambient aerosol in the central and eastern United States is likely produced by non-precipitating clouds. Hegg and Hobbs (1986) and Langer and Rodhe (1991) have also predicted that aqueous phase production of sulfate is the most important pathway for the production of sulfate on a global scale. Despite its importance, the detection of aqueous

phase conversion of S(IV) to S(VI) is problematic due to variability in cloud liquid water content and to the temporal and spatial variability in the concentrations of the reacting species (Kelly et al., 1989). The dependence of aqueous phase reaction rates on the concentration of multiple oxidants, and on the concentration and composition of available CCN, makes extrapolation of laboratory measurements to real clouds complex.

A number of studies have attempted to detect and quantify in-cloud production of sulfate. Hegg and Hobbs (1982) analyzed filter samples of particulate matter collected aboard a B-23 aircraft during flight segments both up and down wind of wave clouds in western Washington. The filter samples were analyzed for sulfate by ion-exchange chromatography. In most cases, they found a significant increase in sulfate mass (0.93 $\mu g\ m^{-3}$ on average) between the upwind and downwind measurements. From the rates of sulfate production derived from those measurements, they determined aqueous phase oxidation of SO_2 by O_3 to be the dominant mechanism for sulfate production. However, they speculated that the significant uncertainty in the calculated production rates might be due to oxidation by H_2O_2. Hegg and Hobbs (1988) described similar measurements on the Mid-Atlantic and Pacific Northwest coasts of the United States. Measurements in the Pacific Northwest indicated an increase in sulfate mass of 0.97 $\mu g\ m^{-3}$. Through analysis of aerosols collected in the Los Angeles basin using a low-pressure impactor, Hering and Friedlander (1982) concluded that the dominant size mode (0.46-0.65 μm mass-median diameter) was probably produced by droplet phase oxidation mechanisms. They also concluded that these aerosol particles could account for the contribution of sulfates to visibility degradation. A number of recent studies have utilized single-stage

and cascade impactors to measure aerosol distributions and particulate sulfate concentrations in a variety of environments (i.e. Laj et al., 1997 and Sievering et al., 1999). Measured aerosol volatility and aerosol size distributions were used by O'Dowd et al. (2000) to examine growth in accumulation mode particles. They found a significant enhancement in aerosol mode diameter for aerosols sampled under cloudy conditions relative to those sampled under cloud-free conditions. Their volatility analysis suggested that this additional mass had properties typical of sulfuric acid containing aerosol. Their calculations suggest that only aqueous phase production of sulfate could explain the increase in mass they observed. Kramer et al. (2000) employed a variety of instruments including the soluble fraction of aerosols-analyzer (SoFA) to measure the soluble and insoluble fractions of the aerosol with mean diameters from 0.38μm to 2.58 μm. Their findings suggest that the smaller activated particles ($D_p < 0.2$ μm) were subject to the greatest change due to cloud-processing, and had the largest impact on aerosol light-scattering properties. Based on measurements of particle mass concentration, number concentration, and hygroscopic properties in the Pennines of northern England, Yuskiewicz et al. (1999) reported an average increase of 14 to 20% in aerosol mass after passage through the orographic clouds in that region. They estimated that this increase would lead to an 18 to 24% increase in total light scattering by the aerosol.

A differential mobility analyzer (DMA) was first used to examine the effects of cloud-processing by Hoppel et al. (1986). They observed a significant difference in the size distributions of aerosols sampled in air masses that had traversed a region of significant cloud cover relative to those sampled in air masses that had passed through

non-cloudy regions. Aerosols that had not been through cloud had distributions displaying a single peak, while those that had been exposed to cloud displayed a double peak. They attributed this shift in the larger diameter particles to the addition of sulfate mass to particles that had nucleated cloud droplets.

During August and September of 2002 the Cloud-Aerosol Research in the Marine Atmosphere (CARMA) program employed a research aircraft to study the effects of clouds on aerosol properties. During this field program the effect of cloud-processing on aerosol light-scattering efficiency and on sulfate mass concentration were inferred from above-cloud, in-cloud, and below-cloud measurements. Hegg et al. (2004) used data collected during that study to examine the effects of cloud-processing on the mass scattering efficiency of the sampled aerosol. By combing airborne nephelometer measurements with calculated aerosol volume, they found an average increase of 10% in mass scattering efficiency for the processed aerosol. From these measurements they inferred that from 0.06 to 0.85 g m^{-3} of sulfate was produced in cloud. Crahan et al. (2004) directly measured non-sea salt sulfate in the aerosol below cloud and in the cloud water during the CARMA project. These measurements indicated that, on average, 1.16 μg m^{-3} of sulfate was produced in cloud.

2. Methodology

The work presented here employs data collected with a tandem differential mobility analyzer (TDMA;Liu et al., 1978) system. This system was operated on board the Center for Interdisciplinary Remotely-Piloted Aircraft Studies (CIRPAS) Twin Otter (e.g. Gao et al., 2003; Hegg et al., 2004), measured growth factor distributions both

above and below cloud off the coast of California as part of the CARMA-II program in July and August of 2004. By examining the size-resolved hygroscopic properties of aerosol measured before entering (below) and after exiting (above) cloud, the soluble fraction of the aerosol can be inferred for both measurements and the change in sulfate mass due to cloud-processing may be calculated.

During the CARMA-II study, a series of missions were flown from the aircraft base at Marina, California from June 30, 2004 to July 21, 2004. A flight track from July 21, 2004 is depicted in Figure 25b. This location was the site of the previous CARMA campaign (Hegg et al., 2004), and provides excellent conditions to study cloud-processing in the atmosphere. As noted by Hegg et al. (2004), the stratocumulus cloud deck is well understood dynamically, is stable for long periods, and can typically provide adequate in-cloud resonance time for aerosols to undergo significant cloud-processing. During the project, 14 missions were flown; of those missions, 6 missions were excluded from this analysis due to instrument failures, the lack of cloud cover, or the lack of flight legs above cloud. Size-resolved hygroscopic growth measurements are used to examine in-cloud production of sulfate during the remaining 8 missions.

A schematic of the TDMA system used in this study is shown in Figure 26. Two identical Permapure PD-070-18T-24SS Nafion tube bundles were used within the TDMA. Nafion A is used to dry the particles prior to classification by the first DMA, while Nafion B is used to humidify the monodisperse aerosol sample flow to 85% RH between the two DMAs. Two high flow differential mobility analyzers (HF-DMAs)

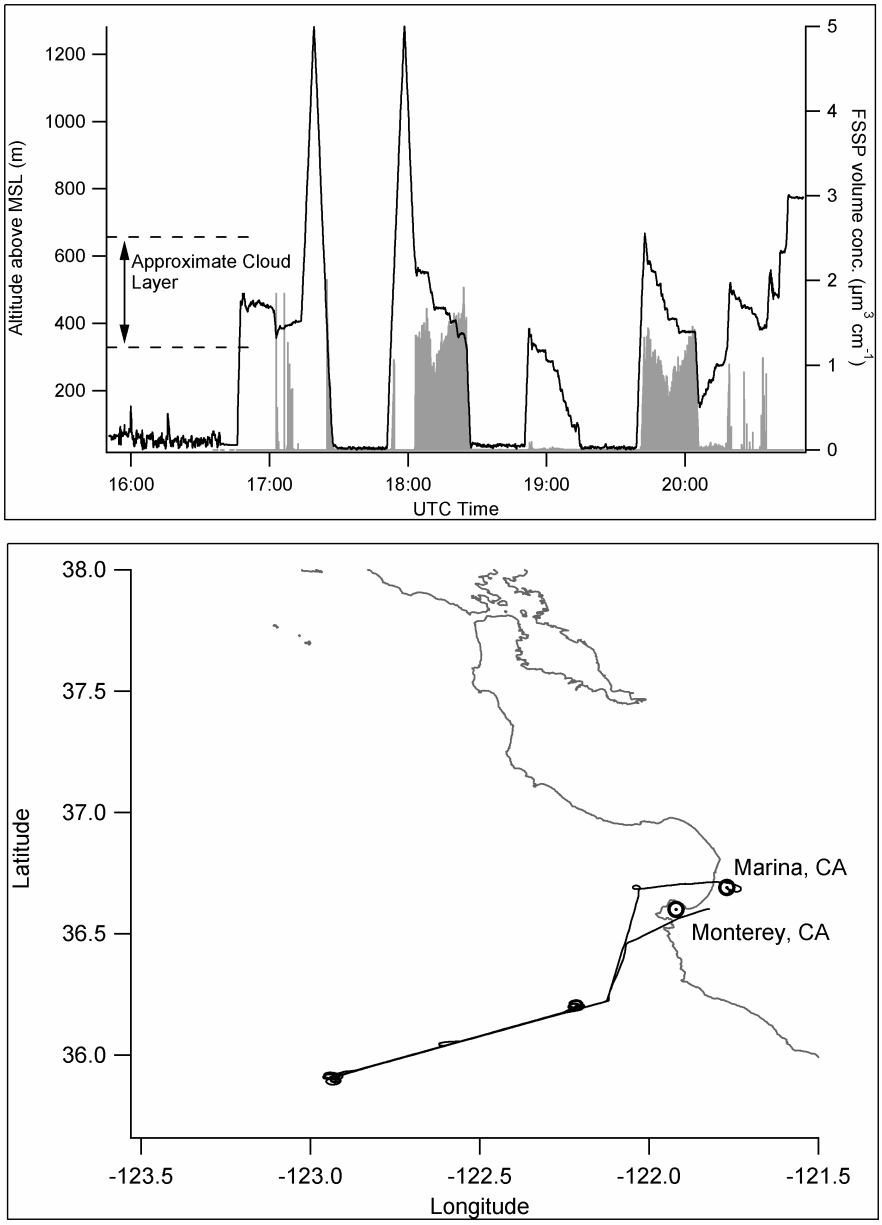

Figure 25. Typical aircraft flight patterns as measured on July 21, 2004. The solid line in (a) show aircraft altitude throughout the flight and the shaded region indicates the measured FSSP volume concentrations. Approximate cloud layer is indicated by the dashed lines. The flight track is shown in (b).

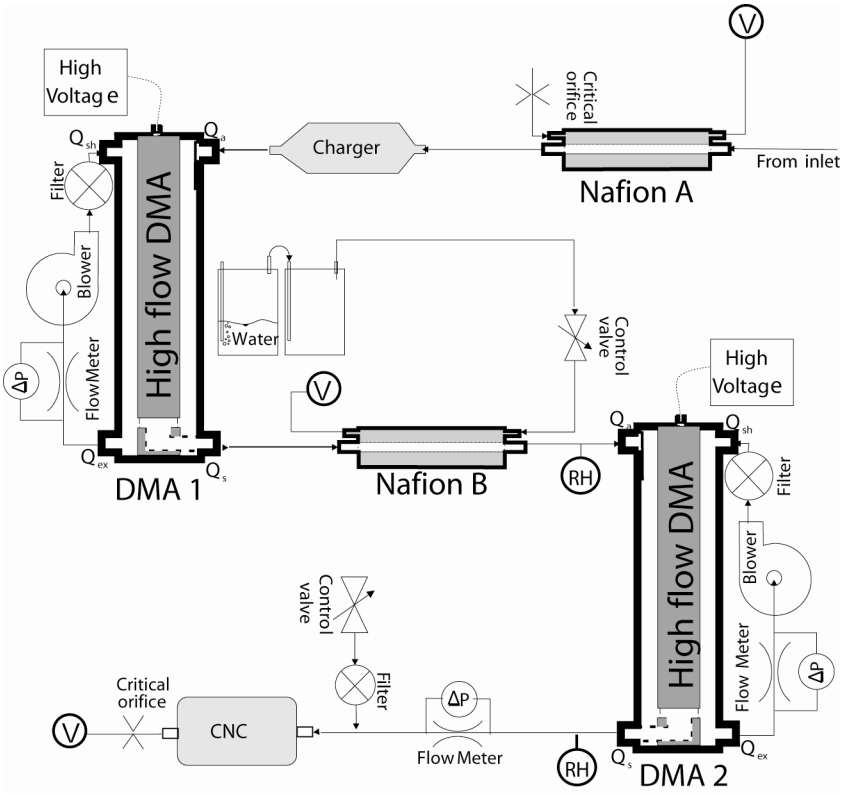

Figure 26. Schematic of the aircraft TDMA. Circled V indicates connection to vacuum and circled RH indicates the location of an RH probe.

designed by Aerosol Dynamics, Inc. (Stolzenburg et al., 1998) were employed in the instrument to enhance the count rates during the necessarily rapid measurements. Hygroscopic growth factor distributions of 0.05, 0.10, 0.15 and 0.20 μm particles at 85% RH were measured using this configuration. The entire system is contained in an aluminum-framed acrylic enclosure. A constant enclosure temperature is maintained throughout a flight by controlling the speed of two vent fans placed directly behind the DMAs. The configuration allows mitigation of the variations in cabin temperature that are often experienced during flight. These temperature variations complicate RH control and, consequently, the interpretation of the measurements.

In order to isolate the effect of aqueous phase sulfate production, the measurements were binned according to their altitude relative to the cloud layer. Measurements of aerosol and cloud droplet size distributions made with a wing-mounted Particle Measurement Systems/Droplet Measurement Technologies (PMS/DMT, Inc.) Forward Scattering Spectrometer Probe 100 (FSSP) were used to determine if the aircraft was in cloud. These measurements were used in conjunction with pressure measurements to determine the pressure-altitude location of the cloud layer. Figure 25a depicts the measured FSSP volume and the pressure altitude of the aircraft, and indicates the approximate location of cloud on July 21, 2004. Using these data, measurements were binned into three categories: below-cloud, in-cloud and above-cloud. During in-cloud measurements, cloud droplets may impact and shatter on the aerosol inlet. The resulting shattered droplets may be sampled by the instruments and result in measurements of aerosol that are not representative of the particles that nucleated the

droplets. During this study, droplet shatter was manifested in the presence of very hygroscopic particles as small as 0.05 μm that were created from evaporated fragments of shattered droplets that formed on sea salt particles. Therefore, measurements made in cloud were not considered in this analysis. In addition, measurements made while the plane was transitioning between categories or when the plane performed spiral ascents were not used. Each of the measured growth factor distributions were inverted and fit with a series of log-normal distributions.

The soluble and insoluble fractions of the aerosol were computed from each size-resolved hygroscopic mode, assuming the soluble fraction was pure ammonium bisulfate (NH_4HSO_4), to examine the difference in soluble volume between above cloud and below cloud measurements. Samples collected using a modified Mohen slotted cloud water collector (Hegg and Hobbs, 1986) were analyzed with ion chromatography, inductively coupled plasma-atomic emission spectrometry and mass spectrometry to determine mass concentrations of sulfate, nitrate, phosphate, chloride, sodium and other metals, and many organic compounds. The average sulfate to nitrate mass concentration ratio measured in cloud water was 3.73:1, but was observed as high as 7.89:1. The limited concentration of nitrate, coupled with the similarity in hygroscopicity of sulfates and nitrates supports the simplifying assumption that only NH_4HSO_4 contributes to the observed hygroscopic growth. The assumption that NH_4HSO_4 is the dominant sulfate species cannot be verified by measurements made during this or the previous CARMA campaign. However, it seems reasonable to assume that aerosol in a coastal setting would be only partially neutralized, since ammonia has primarily continental sources. It

is necessary to consider the possibility that the aerosol in the detraining air above cloud may have a smaller ammonium to sulfate ratio than that below cloud, since aqueous phase oxidation of SO_2 results in the formation of H_2SO_4. Some additional neutralization may occur from the condensation of gas phase ammonia, but without measurements of ammonium the exact amount of neutralization cannot be determined. For simplification, the same soluble material is used both above and below cloud. It must be noted that if H_2SO_4 is the dominant soluble aerosol species then the soluble fraction of the aerosol calculated from the hygroscopic measurements will be less than that represented here.

To alleviate the effect of RH variations, measured growth factors were adjusted to those expected at 85% RH. For each size measured, the mass of NH_4HSO_4 and of insoluble material (density of 1400 kg m^{-3}; Gasparini et al., 2004) that would result in the measured growth factor is calculated for the particles in all hygroscopic modes measured above and below cloud. As shown in Figure 27a, the calculated insoluble mass of each above-cloud particle is then compared with the insoluble masses of particles measured below cloud. Calculations of the change in soluble mass are restricted to those particles whose insoluble masses are within 15% of one another. Since the cloud-processing mechanisms being investigated will not change the insoluble mass of the particle, this ensures that the particles sampled above cloud have similar compositions to those sampled below cloud. The difference in soluble mass is then compared with the results of a simple one-step cloud-processing model that follows the gas phase partitioning set forth in Seinfeld and Pandis (1998) as well as aqueous phase reaction rates for dissolved S(IV) species with O_3 and H_2O_2 presented in the same text. To

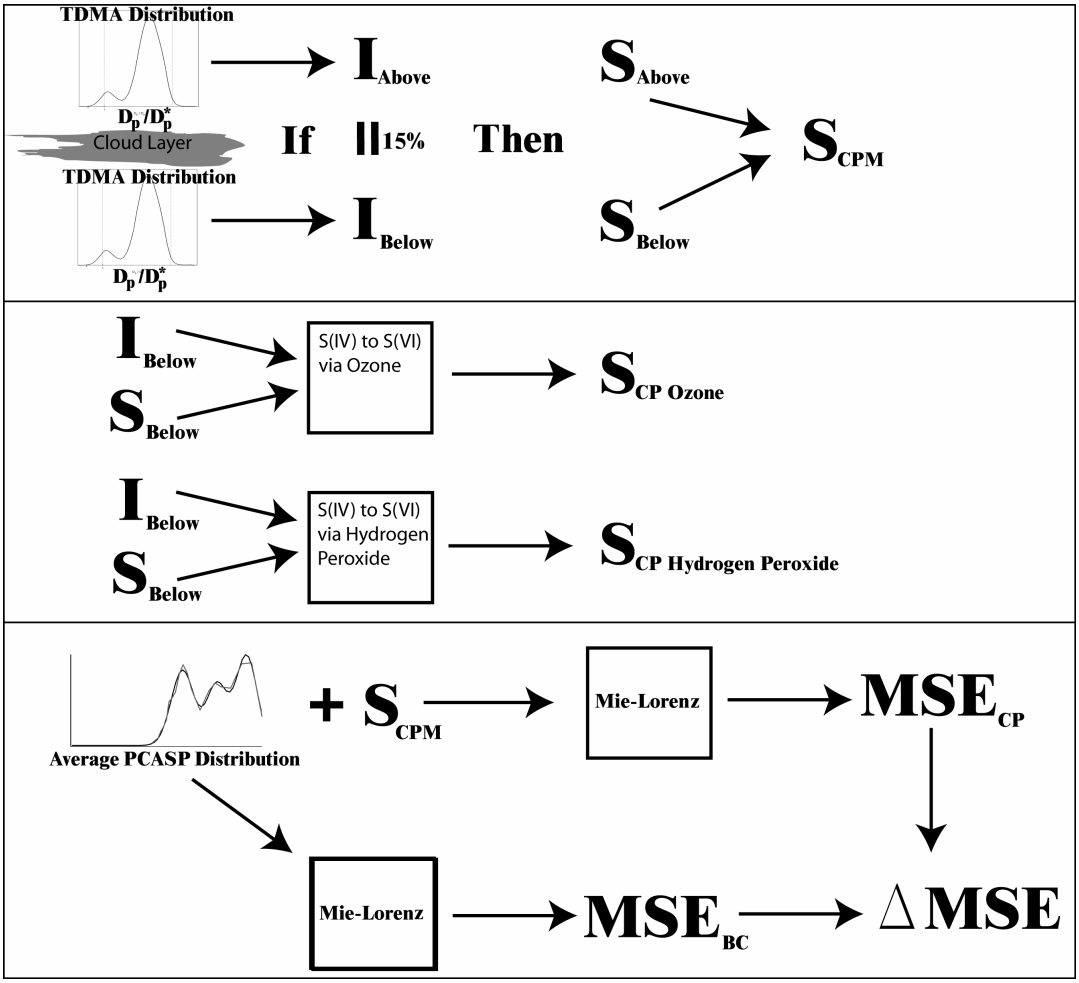

Figure 27. Flow chart of the methodology employed to determine the amount of sulfate produced during cloud processing (CP) reactions and its affect on aerosol mass scattering efficiency (MSE). Capital I indicates insoluble mass and capital S indicates soluble mass.

examine the effect of these reactions on each of the particles, the following quantities are considered: the calculated soluble/insoluble mass below cloud; average cloud liquid water content (LWC); cloud droplet number concentration; gas phase SO_2, O_3, and H_2O_2 concentrations from previous studies (Bates et al., 1992; Heikes et al., 1996; O'Sullivan et al., 1999; Hegg et al., 2004); and the volume mean diameter of the cloud droplets determined from an average FSSP volume distribution shown in Figure 28. The maximum allowable pH was 5.6 to account for dissolved CO_2 (e.g. Seinfeld and Pandis, 1998). The model performs the calculations in a single time-step, assuming the droplet pH is controlled by the dissolution of the soluble fraction of the aerosol into the droplet. This simple model does not consider the effect of the sulfate added during cloud processing on the droplet pH and therefore the reactions rates, since those calculations would have to be done at much shorter time steps to be relevant. This model serves as an aid to interpreting the measurements and is not intended to be cloud-resolving. As shown in Figure 27b, sulfate production due to reactions involving O_3 and H_2O_2 are calculated separately and used as bounds for the total sulfate added during cloud-processing.

Once the sulfate added during cloud-processing was calculated from each of the measurements, the average mass added was used to adjust the average aerosol distribution measured by the Passive Cavity Aerosol Spectrometer Probe 100X (PCASP, PMS/DMT Inc.). This distribution was computed from the average of 1000 below-cloud measurements on each of 5 days during the measurement period. This average distribution was then parameterized with three log-normal distributions and then divided into bins from 0.01 μm to 3.05 μm. By adding the average amount of sulfate mass

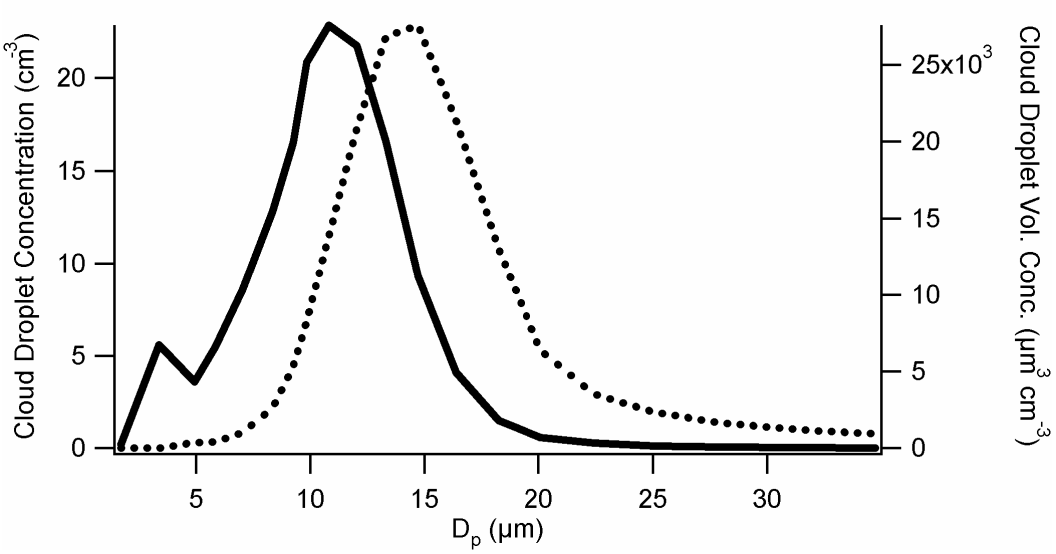

Figure 28. Cloud droplet number and volume distributions derived from bin-averaged FSSP measurements on July 2 and July 21, 2004.

determined from the above and below cloud measurements to each particle in each bin, the aerosol volume distribution was modified to reflect the effects of cloud processing. It is likely that particles less than 0.05 μm are not activated as cloud droplets and will not have sulfate added in this manner; however, since the PCASP cannot resolve particles smaller than 0.10 μm, the population of aerosols below this size is not represented in the parameterized distribution and therefore does not influence the final result. Total scattering at a wavelength of 0.55 μm was calculated for the parameterized PCASP data and for each of the distributions that were modified to reflect cloud-processing using a Mie-Lorenz light scattering model (Bohren and Huffman, 1983). The refractive index of NH_4HSO_4 (1.473 - 0.000i) was used for all particles in the calculations. As shown in Figure 27c, the mass scattering efficiency was calculated from the ratio of the total scattering to the integrated mass of the relevant aerosol distribution calculated using the density of NH_4HSO_4 (1.78 g cm^{-3}). This density is consistent with that used for similar calculations in previous studies (1.8 g cm^{-3}; Yuskiewicz et al., 1999 and Hegg et al., 2004).

3. Results

During the 8 flights from which data were used for this study there were very few measurements made above cloud. Table 4 summarizes the measurements from all 8 flights. The small number of measurements made above cloud limits the observation of particles that have been cloud-processed. Despite this limitation, measurements on three of the eight days exhibited increases in soluble mass that could be attributed to cloud-processing. Figure 29 shows 0.15 μm and 0.20 μm hygroscopic growth factor

Table 4. Measurements and calculations for all days used in the analysis. NA=Not Applicable, NO=Not Observed, NC=Not Calculated.

Date	Number of modes measured above cloud	Number of data pairs with matching insoluble volumes	Average fractional difference in soluble mass in matching data pairs	Average difference in soluble mass of modes excluding those with the same soluble mass	Average difference in soluble mass of all matching modes	Fractional change in mass scattering efficiency when modes with same soluble mass excluded	Fractional change in mass scattering efficiency including all matching modes
07/02/2004	10	8	6.60	4.32E-18	3.22E-18	0.13	0.09
07/06/2004	6	0	NA	NA	NA	NA	NA
07/07/2004	12	12	-0.10	NO	-3.39E-20	NC	NC
07/08/2004	4	8	-0.06	NO	-7.71E-20	NC	NC
07/09/2004	10	24	-0.12	NO	-1.37E-19	NC	NC
07/12/2004	6	5	0.37	4.42E-18	8.33E-19	0.13	0.02
07/20/2004	2	5	0.00	NO	-6.72E-20	NC	NC
07/21/2004	15	26	4.53	5.60E-18	2.65E-18	0.17	0.08

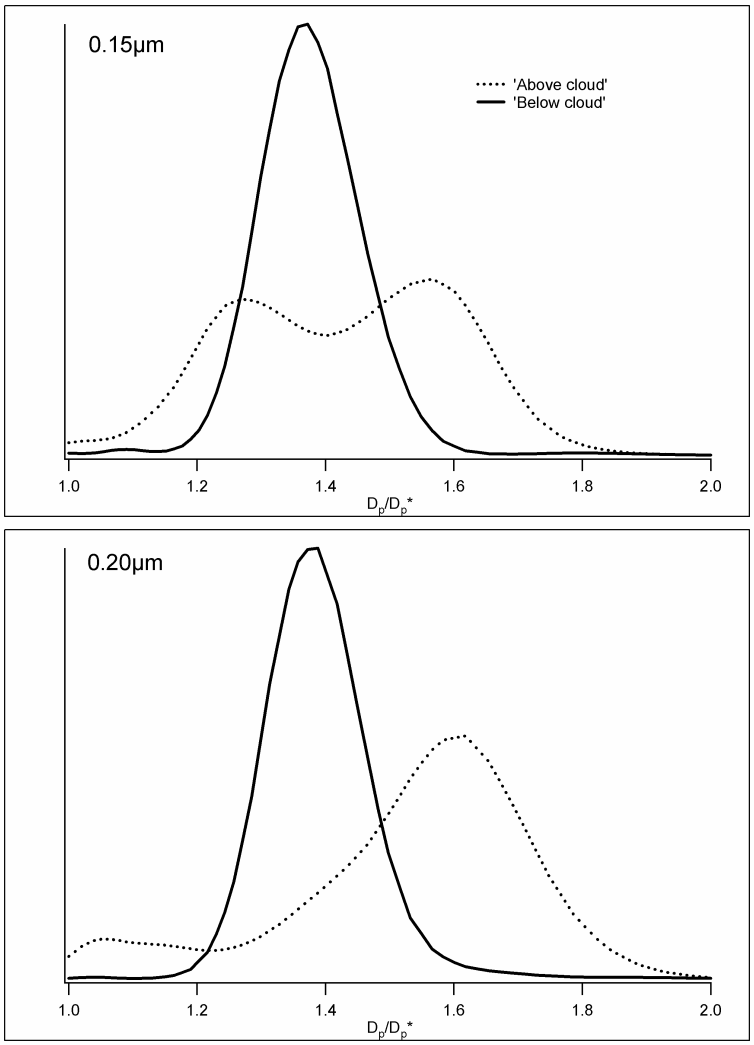

Figure 29. Growth factor distributions from July 21, 2004 measured above cloud (dotted line) and below cloud (solid line).

distributions, from July 21, 2004 displaying a shift in growth factor between above and below cloud measurements. On the remaining five days, particles measured above cloud did not have soluble masses that were significantly different (less than 15% on average) than particles with the same insoluble mass measured below cloud (Table 1). The impact of cloud-processing may not have been detected on these days due to the lack of extensive measurements above cloud. A complete sequence of hygroscopic measurements at the four sizes examined with this system takes approximately 12 minutes. Therefore in a two to three hour flight only 10 to 15 measurements at each size are possible. The time spent above-cloud was limited by the needs of other experiments; thus, the likelihood of capturing aerosol that has been changed by aqueous phase reactions in the detraining cloud air against the background aerosol is significantly reduced.

For the days on which cloud-processing had a discernable impact on the aerosol, the change in soluble mass is consistent with that determined during previous studies. If only those particles observed to have a change in soluble mass greater than 15% are considered, the average mass added ranged from 4.32×10^{-9} μg/particle on July 02 to 5.60×10^{-9} μg/particle on July 21. A single measurement on July 12 indicated an increase in soluble mass of 4.42×10^{-9} μg/particle. The average FSSP cloud droplet number concentration (CDNC) on these days was 250cm^{-3}. By adding the average per-particle sulfate production to each cloud droplet measured by the FSSP, the total sulfate added due to cloud-processing is calculated to be between 1.08μg m^{-3} and 1.4 μg m^{-3}. However, if all data pairs are considered, the average sulfate production is somewhat lower. The

calculated addition would then be 3.22×10^{-9} μg/particle on July 2, 8.33×10^{-9} μg/particle on July 12 and 2.65×10^{-9} μg/particle on July 21. This leads to total sulfate addition of between 0.66 μg m^{-3} and 0.81 μg m^{-3} for the same CDNC. This production is within the range of average produced sulfate mass reported by Hegg, et al. (2004) of between 0.06 μg m^{-3} and 0.85 μg m^{-3}. However, Crahan et al. (2004) reported an average value of 1.16 μg m^{-3} of sulfate added in cloud, which is in better agreement with the average of only those data pairs that exhibited significant changes in soluble mass. Hegg and Hobbs (1982) and Hegg and Hobbs (1988) report average increases in sulfate mass of 0.93 μg m^{-3} in wave clouds over Western Washington and 0.97 μg m^{-3} in stratus clouds over the Pacific Northwest coast, respectively. These measurements are between the two ranges indicated here. Upon consideration of previous results, it seems that either considering all data pairs above cloud or by eliminating those that exhibit little or no change in soluble mass produces results that are consistent with the typical range of sulfate mass added to aerosol through aqueous phase mechanisms in this region.

The model was initiated with the calculated soluble and insoluble masses from the particles sampled below-cloud in each data pair. Model calculations were performed assuming that the aerosol spent 1300s in cloud, which is consistent with in-cloud resonance times typical of the cloud depths observed during the flights (a few hundred meters) and updraft velocities typical of the region (0.1 to 2 m s^{-1}). Gas phase SO_2 concentrations were held at 300 pptv, similar to what has been measured in previous studies in the same region (Bates et al., 1992; Heikes et al., 1996; O'Sullivan et al., 1999). Gas phase O_3 and H_2O_2 were held at 30 ppbv and 1 ppbv, respectively. Cloud

droplet number and volume mean diameter, as determined from the FSSP measurements, were held at 250 cm^{-3} and 13.3μm, respectively. Due to in-cloud variability and poor agreement between instruments, there is some uncertainty in the cloud LWC, which was measured by both a Gerber hot-wire probe and a DMT Cloud Aerosol and Precipitation Spectrometer (CAPS) probe; therefore, a range of values was used in these calculations. As indicated in Figure 30, the measured sulfate addition is in the same range as the theoretical calculations (shaded region). The calculations indicate that the sulfate production observed is more accurately bounded by higher LWC values. These calculations also show that aqueous phase sulfate production by O_3 is very sensitive to the initial soluble volume of the particle so the results vary considerably with initial soluble volume, while the H_2O_2 reactions are largely insensitive to initial soluble volume. The model results suggest that both O_3 and H_2O_2 are important to the observed production of sulfate.

In order to compare more directly with nephelometer measurements of aerosol scattering properties, an average aerosol size distribution was created from 1000 below-cloud PCASP size distributions on each of 5 days during the measurements period and parameterized with three log-normal distributions to capture each mode of the volume distribution between 0.10 μm and 3.05 μm. Both the averaged aerosol volume distribution calculated from PCASP measurements and the parameterized aerosol volume distributions are shown in Figure 31. The corresponding aerosol size distribution was comprised of modes with number concentrations of 306.96 cm^{-3}, 9.25 cm^{-3}, and 0.97 cm^{-3} with mean diameters of 0.20 μm, 0.59 μm, and 1.43 μm, and standard deviations of

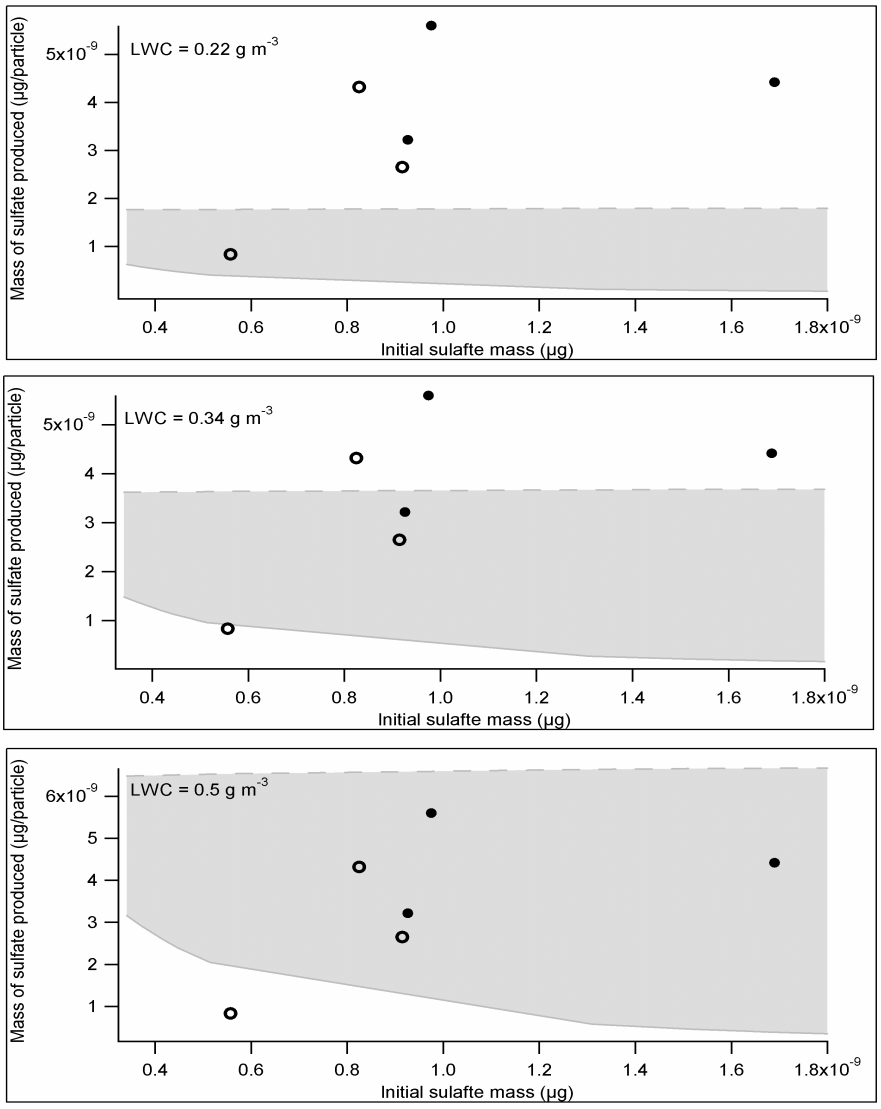

Figure 30. Measurements of soluble mass (assumed NH4HSO4) added during cloud processing (dots) on the 2nd, 12th and 21st of July 2004. The grey region denotes the range of mass that would be expected through reactions involving O3 (dashed line) and H2O2 (solid line) for each particle. Each panel represents calculations for different cloud LWC values. Open circles denote the average of the change in soluble mass for all matching modes and solid dots indicate the average of data points whose soluble volumes differed by more than 15%. The dashed line indicates production by H2O2 pathways and the solid indicates production by O3 pathways.

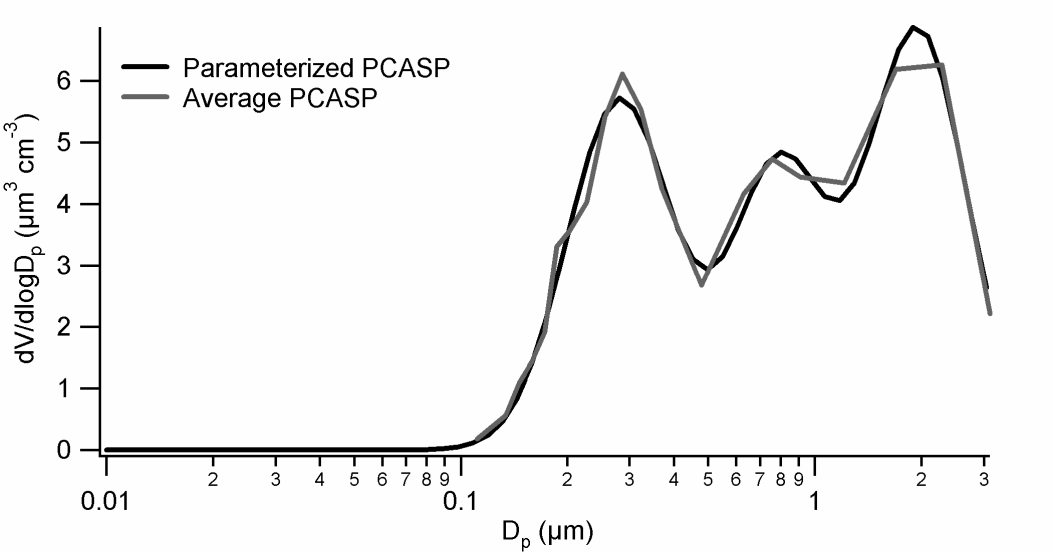

Figure 31. Averaged and parameterized PCASP volume distributions.

1.41 μm, 1.36 μm, and 1.38 μm, respectively. Both the averaged and parameterized distributions are shown in Figures 32a and 32b. These parameters are used to create a distribution to represent the aerosol below cloud. This below cloud distribution is then modified to reflect the addition of soluble mass during cloud-processing. Both the original and the modified distributions are shown in Figure 32a and 32b. From these distributions, aerosol mass scattering efficiencies were calculated. If only those data pairs that had a change in soluble mass greater than 15% were considered, the average change in mass scattering efficiency was 14%. If all data pairs were considered the average change was 6%. Both of these fall well within the range of the measurements of Hegg et al, 2004, whose average change in mass scattering efficiency was approximately 10%. Total scattering curves for these distributions are shown in Figure 32c and 32d.

4. Summary and Conclusions

Size-resolved measurements of aerosol hygroscopic growth were made as a part of the CARMA II field campaign from June 30 to July 21, 2004. Comparing the hygroscopic properties of aerosol in air entering the cloud from below with aerosol in the detraining air above cloud provides a new means to quantify the production rate of aerosol-phase sulfate by aqueous phase reactions in cloud. Despite the rarity of usable above cloud measurements during the experiment, observations of cloud-processed aerosol were observed during three of the eight flights that were examined. Measurements suggest that the sulfate produced in cloud was between 1.08 μg m^{-3} to 1.4 μg m^{-3}, which would lead to an enhancement of 6 to 14% in aerosol mass scattering efficiency at a wavelength 0.55 μm. These measurements are in excellent agreement

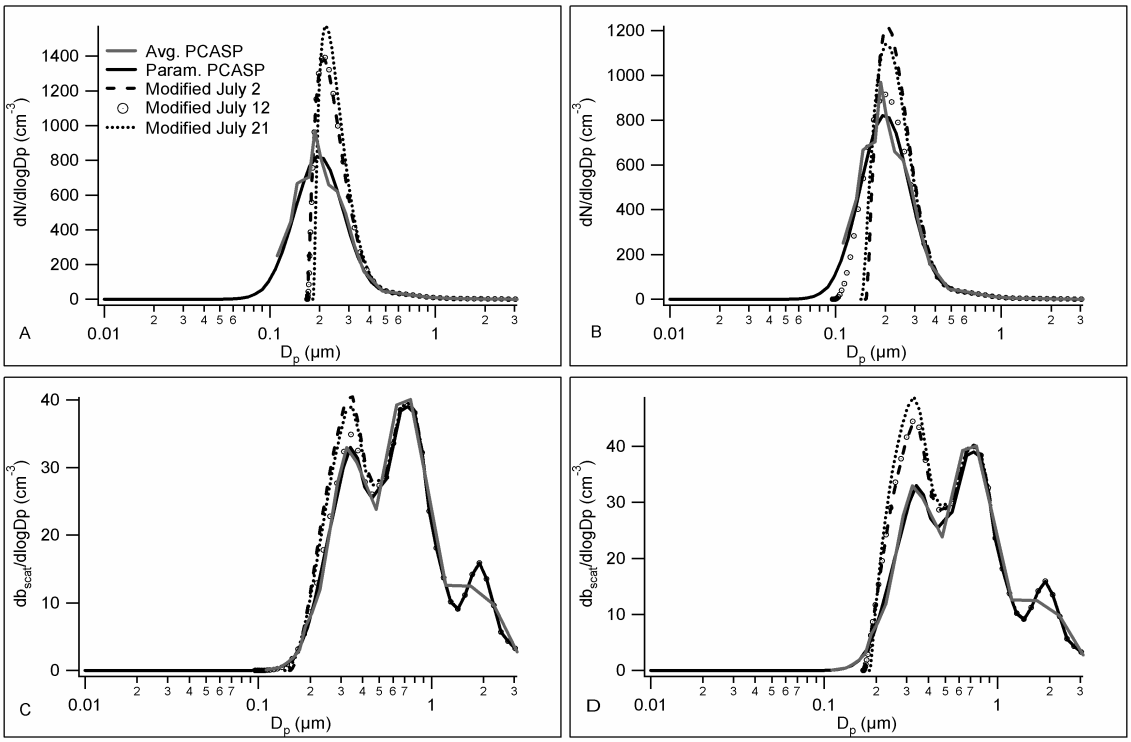

Figure 32. Aerosol concentration and total scattering at 0.55 um derived from PCASP data. The averaged and parameterized PCASP size distributions measured below cloud are denoted by the solid grey and black lines, respectively. The distributions modified by the average amount of soluble volume added to the aerosol on each day that cloud processing was observed is indicated by the dashed and dotted lines. A and C represent calculations considering only those data points whose difference in soluble volume was greater than 15%, while B and D consider all data points with matching insoluble volumes.

with the results of Hegg et al. (2004) and Crahan et al. (2004) and model calculation of the relevant reactions on the observed particles agree relatively well with the calculated values.

For future studies, significant improvements to the experimental design could be implemented. The most critical change should be to increase the time spent in the detraining air above cloud. This would significantly improve the likelihood that observations of cloud-processed aerosol would be made. It would also be advisable to change the particle sizes measured. Due to the compression of the aerosol distribution by cloud-processing, measuring 0.05 μm particles has limited benefits. In this study, no particles of this size were observed to have been cloud-processed. Focusing the measurements on larger particle sizes both increases the chance of observing cloud processed aerosols and focuses the observations on those aerosols that have the greatest impact on the scattering properties.

CHAPTER V

SUMMARY

Experiments were performed in: College Station, Texas; Houston, Texas; and in the coastal Pacific near Monterey, California to study the physical and chemical properties of aerosol in those regions and the nature of the changes those aerosol experience. The initial experiment was concerned with the hydration state of ambient aerosol under ambient conditions. Further experiments were performed to examine diurnal cycles in the hygroscopic growth cycles of aerosols in southeast Texas. Finally experiments were performed near Monterey, California to measure the sulfate added to the ambient aerosol through aqueous phase oxidation of S(IV) in cloud.

Measurements in College Station, Texas determined the ambient hydration state of aerosols in that region. Using a novel TDMA experiment, it was determined that during the month August 70 to 95% of all the particles observed resided in the metastable state. Further, no stable deliquescent particles were observed. This is in agreement with Rood et al. (1985) whose measurements also indicated a predominance of metastable aerosol. These measurements also indicate that the soluble component of the aerosol was probably some combination of ammonium and sulfate, and that the soluble fraction made up 60 to 70% of the aerosol by volume.

Further measurements in College Station and Houston, Texas examined diurnal cycles in the properties of the aerosol. Observations indicated that the hygroscopic growth hysteresis in the aerosol in these two locations changed in a repeatable and predictable way over the course of most days during the study period. The aerosols were

observed to display a clearly defined hysteresis in the early morning hours. Around 10:00 local time the observed hysteresis curves began to collapse, sometimes resulting in no observed hysteresis in the early afternoon. After 16:00 local time the hysteresis began to become more prominent. Correlations with atmospheric variables and parameters describing the change in hysteresis indicated that high RH and and low temperatures, as would be expected in the early morning, corresponded to times when the hysteresis was clearly defined, while low RH and high temperatures corresponded to times when the hysteresis behavior was less prominent. The deliquescence and crystallization point were observed to decrease during the afternoon so that the ambient RH never fell below the crystallization RH, and since during the study period, the deliquescence RH was always exceeded at some point during the day all particles were expected to remain in the metastable state. The shifts in the hysteresis behavior of the aerosols indicate a change in chemical composition, which is believed to be due to the addition of sulfate through both gas and aqueous phase mechanisms that are preferentially more active during mid-day. Growth along the stable leg of the hysteresis was often observed during the early afternoon coincident with the collapse of the hysteresis curves.

A final experiment to examine the production of sulfate in cloud was performed off the coast of Monterey, California. By computing soluble and insoluble aerosol volumes both below cloud and in the detraining air above cloud, the change in soluble mass on an aerosol particle as it passed through a cloud could be calculated. The amount of soluble material produced on the particles was observed to be between 0.66 $\mu g\ m^{-3}$ and 1.4 $\mu g\ m^{-3}$, which is excellent agreement with previous studies. The calculated

increase in mass scattering efficiency from these measurements was between 6 and 14%, also in excellent agreement with previous work.

The ambient hydration state of an aerosol is critical to understanding the aerosol's impact on radiative forcing, visibility, the partitioning of trace gasses to the aerosol phase and secondary aerosol formation. The observed cycle of sulfate production indicates that the aerosol will become more acidic in the afternoon, which not only makes it a better site for SOA production but may increase the health effects associated with the aerosol. The indication of SOA production is further strengthened by the observation of growth along the stable leg in the afternoon. This type of growth is often associated with the presence of soluble organic compounds (Brooks et al., 2003) that may have been produced on the acidified aerosol. One of the primary mechanisms responsible for the production of sulfate on the aerosol particles in Houston was investigated in Monterey. Cloud-processing reactions were observed to produce quite large amounts of sulfate of the particles in coastal California, and indicate that the mechanisms presumed to be responsible for the compositional changes in Houston are quite plausible. Due to the ubiquitous nature of ammonium and sulfate containing aerosols worldwide, the results of these studies may have application outside the individual study areas.

REFERENCES

Ansari, A. S. and S. N. Pandis, The effect of metastable equilibrium states on the partitioning of nitrate between the gas and aerosol phases, *Atmospheric Environment*, 34, 157-168, 2000.

Bates, T. S., J. A. Calhoun, and P. K. Quinn, Variations in the methanesulfonate to sulfate molar ratio in submicrometer marine aerosol particles over the Southern Pacific Ocean, *Journal of Geophysical Research*, 97, 9859-9865, 1992.

Berg, O. H., E. Swietlicki, and R. Krejci, Hygroscopic growth of aerosol particles in the marine boundary layer over the Pacific and southern oceans during the first aerosol characterization experiment (ACE 1), *Journal of Geophysical Research Atmospheres*, 103, 16535-16545, 1998.

Bohren, C. F. and D. R. Huffman, *Absorption and Scattering of Light by Small Particles*, Wiley, New York, 1983.

Brooks, B. J., M. H. Smith, M. K. Hill, and C. D. O'Dowd, Size-differentiated volatility analysis of internally mixed laboratory-generated aerosol, *Journal of Aerosol Science*, 33, 555-579, 2002.

Brooks, S. D., R. M. Garland, M. E. Wise, A. J. Prenni, M. Cushing, E. Hewitt, and M. A. Tolbert, Phase changes in internally mixed maleic acid/ammonium sulfate aerosols, *Journal of Geophysical Research-Atmospheres*, 108, 4487, 2003.

Chang S. Y. and C. T. Lee, Applying GC-TCD to investigate the hygroscopic characteristics of mixed aerosols, *Atmospheric Environment*, 36, 1521-1530, 2002.

Clarke, A. D., A thermo optic technique for in situ analysis of size-resolved aerosol physiochemistry, *Atmospheric Environment*, 25A, 635-644, 1991.

Cocker, D. R., N. E. Whitlock, R. C. Flagan, and J. H. Seinfeld, Hygroscopic properties of Pasadena, California aerosol, *Aerosol Science and Technology*, 35, 637-647, 2001.

Cohen, M. D., R. C. Flagan, and J. H. Seinfeld, Studies of concentrated electrolyte solutions using the electrodynamic balance. 1. water activities for single-electrolyte solutions, *Journal of Physical Chemistry, 91,* 4563-4514, 1987.

Crahan K. K., D. Hegg, D. S. Covert, and H. Jonsson, An exploration of aqueous oxalic acid production in the coastal marine atmosphere, *Atmospheric Environment*, 38, 3757-3764, 2004.

Czoschke, N. M., M. Jang, and R. M. Kamens, Effect of acidic seed on biogenic secondary organic aerosol growth, *Atmospheric Environment*, 37 (30), 4287-4299, 2003.

Day, D. E., W. C. Malm, and S. M. Kreidenweis, Aerosol light scattering measurements as a function of relative humidity, *Journal of the Air & Waste Management Association*, 50, 710-716, 2000.

Dentener, F. J. and P. J. Crutzen, Reaction of N_2O_5 on tropospheric aerosols - impact on the global distributions of NOx, O_3, and OH, *Journal of Geophysical Research-Atmospheres*, 98, 7149-7163, 1993.

Dick, W. D., P. Saxena, and P. H. McMurry, Estimation of water uptake by organic compounds in submicron aerosols measured during the southeastern aerosol and visibility study, *Journal of Geophysical Research-Atmospheres*, 105, 1471-1479, 2000.

Dougle, P. G., J. P. Veefkinda, and H. M. ten Brink, Crystallisation of mixtures of ammonium nitrate, ammonium sulfate and soot, *Journal of Aerosol Science*, 29, 375-386, 1998.

Draxler, R. R. Hybrid single-particle Lagrangian integrated trajectories (HY-SPLIT): model description, *Tech. Memo. ERLARL-166,* Natl. Oceanic and Atmos. Admin., Silver Spring, Md, 1988.

Gao, S., D. A. Hegg, P. V. Hobbs, T. W. Kirchstetter, B. J. Maji, and M. Sadilek, Water-soluble organic compounds in aerosols associated with savanna fires in southern Africa: identification, evolution, and distribution, *Journal of Geophysical Research*, 108, SAF 27-1 to 27-16, 2003.

Gasparini, R., R. Li, and D. R. Collins, Integration of size distributions and size resolved hygroscopicity during the Houston supersite for compositional categorization of the aerosol, *Atmospheric Environment*, 38, 3285-3303, 2004.

Gwynn, R. C.; R. T. Burnett, and G. D. Thurston, A time-series analysis of acidic particulate matter and daily mortality and morbidity in the Buffalo, New York, region, *Environmental Health Perspectives,* 108 (2): 125-133, 2000.

Hansson, H.-C., M. J. Rood, and D. S. Covert, Experimental determination of the hygroscopic properties of organically coated aerosol particles, *Journal of Aerosol Science*, 21, S241-S244, 1990.

Hansson, H.-C., A. Wiedensohler, S. Koloutsou-Vakakis, K. Hameri, and D. Orsini, NaCl aerosol particle hygroscopicity dependence on mixing with organic compounds, *Journal of Atmospheric Chemistry*, 31, 321-346, 1998.

Hegg, D. A. and P. V. Hobbs, Measurements of sulfate production in natural clouds, *Atmospheric Environment*, 16, 2663-2668, 1982.

Hegg, D. A. and P. V. Hobbs, Sulfate and nitrate chemistry in marine cumuliform clouds. *Atmospheric Environment*, 20, 901-909, 1986

Hegg, D. A. and P. V. Hobbs, Comparisons of sulfate and nitrate production in clouds on the mid-Atlantic and Pacific Northwest coasts of the United States, *Atmospheric Chemistry*, 7, 325-333, 1988.

Hegg, D. A., D. S. Covert, H. Jonsson, D. Khelif, and C. A. Friehe, Observations of the impact of cloud processing on aerosol light scattering efficiency, *Tellus*, 56B, 285-293, 2004.

Heikes, B. G., M. Lee, J. Bradshaw, S. Sandholm, D. D. Davis, J. Crawford, J. Rodriguez, S. Liu, S. McKeen, D. Thronton, A. Bandy, G. Gregory, R. Talbot, and D. Blake, Hydrogen peroxide and methylhydroperoxide distributions related and odd hydrogen over the North Pacific in the fall of 1991, *Journal of Geophysical Research*, 101, 1891-1905, 1996.

Hering, S. V. and S. K. Friedlander, Origins of aerosol sulfur size distributions in the Los Angeles basin, *Atmospheric Environment*, 16, 2647-2656, 1982.

Hoppel W. A., G. M. Frick, and R. E. Larson, Effects of non-precipitating clouds on the aerosol size distribution in the marine boundary layer, *Geophysical Research Letters*, 13, 125-128, 1986.

Jang, M. S., N. M. Czoschke, S. Lee, and R. M. Kamens, Heterogeneous atmospheric aerosol production by acid-catalyzed particle-phase reactions, *Science*, 298, 814-817, 2002.

Jennings, S. D. and C. D. O'Dowd, Volatility of aerosol at Mace Head, on the west coast of Ireland, *Journal of Geophysical Research-Atmospheres*, 95,13937-13948, 1990.

Kelly, T. J., S. E. Schwartz and P. H. Daum, Detection of acid producing reactions in natural clouds, *Atmospheric Environment*, 23, 2399-2406, 1989.

Kramer M., N. Beltz, D. Schell, L. Schultz, C. Sprengard-Eichel, and S. Wurzler, Cloud processing of continental aerosol particles: experimental investigations for different drop sizes, *Journal of Geophysical Research*, 105, 11739-11752, 2000.

Laj, P., S. Fuzzi, M. C. Facchini, G. Orsi, A. Berner, C. Kruisz, W. Wobrock, A. Hallberg, K. N. Bower, M. W. Gallagher, K. M. Beswick, R. N. Colvile, T. W. Choularton, P. Nason, and B. Jones, Experimental evidence for in-cloud production of aerosol sulfate, *Atmospheric Environment*, 31, 2503-2514,1997.

Langer, J. and H. Rodhe, A global three-dimensional model of the tropospheric sulfur cycle, *Journal of Atmospheric Chemistry*, 13, 225-263, 1991.

Lee C. T. and S. Y. Chang, A GC-TCD method for measuring liquid water mass of collected aerosols, *Atmospheric Environment*, 36, 1883-1894, 2002.

Lightstone, J. M., T. B. Onasch, D. Imre, and S. Oatis, Deliquescence, efflorescence, and water activity in ammonium nitrate and mixed ammonium nitrate/succinic acid microparticles, *Journal of Physical Chemistry A*, 104, 9337-9346, 2000.

Liu, B. Y. H., D. Y. H. Pui, K. T. Whitby, D. B. Kittelson, Y. Kousaka, and R. L. McKenzie, Aerosol mobility chromatograph - new detector for sulfuric-acid aerosols, *Atmospheric Environment*, 12, 99-104, 1978.

Martin, S. T., Phase transitions of aqueous atmospheric particles, *Chemical Reviews*, 100, 3403-3453, 2000.

Martin, S. T., J. H. Han, and H. M. Hung, The size effect of hematite and corundum inclusions on the efflorescence relative humidities of aqueous ammonium sulfate particles, *Geophysical Research Letters*, 28, 2601-2604, 2001.

Martin, S. T., H. M. Hung, R. J. Park, D. J. Jacob, R. J. D. Spurr, K. V. Chance, and M. Chin, Effects of the physical state of tropospheric ammonium-sulfate-nitrate particles on global aerosol direct radiative forcing, *Atmospheric Chemistry and Physics Discussions*, 3, 5399-5467, 2003b.

Martin, S. T., J. C. Schlenker, A. Malinowski, H. M. Hung, and Y. Rudich, Crystallization of atmospheric sulfate-nitrate-ammonium particles, *Geophysical Research Letters*, 30, 2102, 2003a.

McHenry, J. N. and R. L. Dennis, The relative importance of oxidation pathways and clouds to atmospheric ambient sulfate production as predicted by the regional acid deposition model, *Journal of Applied Meteorology*, 33, 890-905,1994.

McMurry, P. H., and M. R. Stolzenburg, On the sensitivity of particle size to relative humidity for Los Angeles aerosols, *Atmospheric Environment*, 23, 497-507,1989.

McMurry, P. H., M. Litchy, P. F. Huang, X. Cai, B. J. Turpin, W. D. Dick, and A. Hanson, Elemental composition and morphology of individual particles separated by size and hygroscopicity with the TDMA, *Atmospheric Environment*, 30, 101-108, 1996.

Nenes A., S. N. Pandis, and C. Pilinis, ISORROPIA: a new thermodynamic equilibrium model for multiphase multicomponent inorganic aerosols, *Aquatic Geochemistry*, 4, 123-152, 1998a.

Nenes A., C. Pilinis, and S. N. Pandis, Continued development and testing of a new thermodynamic aerosol module for urban and regional air quality models, *Atmospheric Environment*, 33, 1553-1560, 1998b.

O'Dowd, C. D., S. G. Jennings, M. H. Smith, and W. Cooke, A high temperature volatility technique for determination of atmospheric aerosol composition, *Journal of Aerosol Science*, 23, S905-S908, 1992.

O'Dowd, C. D., J. A. Lowe, and M. H. Smith, The effects of clouds on aerosol growth in the rural atmosphere, *Atmospheric Research*, 54, 201-221, 2000.

O'Sullivan, D. W., B. G. Heikes, M. Lee, W. Chang, G. Gregory, D. R. Blake, and G. W. Sachse, Distribution of hydrogen peroxide and methylhydroperoxide over the Pacific and South Atlantic oceans, *Journal of Geophysical Research*, 104, 5635-5646, 1999.

Peng, C. and C. K. Chan, The water cycles of water-soluble organic salts of atmospheric importance, *Atmospheric Environment*, 35, 1183-1192, 2001.

Pinnick, R. G., S. G. Jennings, and G. Fernandez, Volatility of aerosols in the arid southwestern United States, *Journal of the Atmospheric Sciences*, 44, 562-576, 1987.

Rood, M. J., T. V. Larson, and D. S. Covert, Measurement of laboratory and ambient aerosols with temperature and humidity controlled nephelometry, *Atmospheric Environment*, *19*, 1181-1190, 1985.

Rood, M. J., M. A. Shaw, T. V. Larson, and D. S. Covert, Ubiquitous nature of ambient metastable aerosol, *Nature*, 337, 537-539, 1989.

Russell M., D. T. Allen, D. R. Collins, and M. P. Fraser, Daily, seasonal and spatial trends in PM2.5 mass and composition in southeast Texas, *Aerosol Science and Technology*, 38, Suppl. 1, 14-26, 2004.

Santarpia J. L., R. Li, and D. R. Collins, Direct measurement of the hydration state of ambient aerosol populations, *Journal of Geophysical Research-Atmospheres,* 109, D18209, doi:10.1029/2004JD004653, 2004.

Sato, M., J. Hansen, D. Koch, A. Lacis, R. Ruedy, O. Dubovik, B. Holben, M. Chin, and T. Novakov, Global atmospheric black carbon inferred from AERONET, *Proceedings of the National Academy of Sciences*, 100, 6319-6324, 2003.

Saxena, P., L. M. Hildemann, P. H. McMurry, and J. H. Seinfeld, Organics alter the behavior of atmospheric particles, *Journal of Geophysical Research-Atmospheres*, 100, 18,755-18,770, 1995.

Seinfeld, J. H. and S. N. Pandis, *Atmospheric Chemistry and Physics*, Wiley, New York, 1998.

Sievering H., B. Lerner, J. Slavich, J. Anderson, M. Posfai, and J. Cainey, O_3 oxidation of SO_2 in sea-salt aerosol water: size distribution of non-sea-salt sulfate during the first aerosol characterization experiment (ACE 1), *Journal of Geophysical Research*, 104, 21707-21717, 1999.

Stolzenburg, M., N. Kreisberg, and S. Hering, Atmospheric size distributions measured by differential mobility optical particle size spectrometry, *Aerosol Science and Technology*, 29, 402-418, 1998.

Swietlicki, E., J. C. Zhou, D. S. Covert, K. Hameri, B. Busch, M. Vakeva, U. Dusek, O. H. Berg, A. Wiedensohler, P. Aalto, J. Makela, B. G. Martinsson, G. Papaspiropoulos, B. Mentes, G. Frank, and F. Stratmann, Hygroscopic properties of aerosol particles in the northeastern Atlantic during ACE-2, *Tellus Series B-Chemical and Physical Meteorology*, 52, 201-227, 2000.

Tang, I. N. and H. R. Munkelwitz, Aerosol growth studies—III ammonium bisulfate aerosols in a moist atmosphere, *Journal of Aerosol Science*, 8, 321-330, 1977.

Tang, I. N. and H. R. Munkelwitz, An investigation of solute nucleation in levitated solution droplets, *Journal of Colloid and Interface Science*, 98, 430-438, 1984.

Tang, I. N. and H. R. Munkelwitz, Composition and temperature-dependence of the deliquescence properties of hygroscopic aerosols, *Atmospheric Environment Part A-General Topics*, 27, 467-473, 1993.

Tang, I. N. and H. R. Munkelwitz, Water activities, densities, and refractive-indexes of aqueous sulfates and sodium-nitrate droplets of atmospheric importance, *Journal of Geophysical Research-Atmospheres*, 99, 18801-18808, 1994.

Tang, I. N., A. C. Tridico, and K. H. Fung, Thermodynamic and optical properties of sea salt aerosols, *Journal of Geophysical Research-Atmospheres*, 102, 23269-23275, 1997.

ten Brink, H. M., A. Khlystov, G. P. A. Kos, T. Tuch, C. Roth, and W. Kreyling, A high-flow humidograph for testing the water uptake of ambient aerosol, *Atmospheric Environment,* 34, 4291-4300, 2000.

Twomey, S., Pollution and planetary albedo, *Atmospheric Environment*, 8, 1251-1256, 1974.

Weber, R. J., D. Orsini, Y. Daun, Y. N. Lee, P. J. Klotz, and F. Brechtel, A particle-into-liquid collector for rapid measurement of aerosol bulk chemical composition, *Aerosol Science and Technology*, 35, 718-727, 2001

Wexler, A. S. and S. L. Clegg, Atmospheric aerosol models for systems including the ions H^+, NH^{4+}, Na^+, SO_4^{2-}, NO^{3-},Cl^-, Br^-, and H_2O, *Journal of Geophysical Research-Atmospheres*, 107, 4207, 2002.

Wexler, A. S. and J. H. Seinfeld, 2nd-generation inorganic aerosol model, *Atmospheric Environment Part A-General Topics*, 25, 2731-2748, 1991.

Xiong, J.Q., M. Zhong, C. Fang, L. C. Chen, and M. Lippmann, Influence of organic films on the hygroscopicity of ultrafine sulfuric acid aerosol, *Environmental Science and Technology*, 32, 3536-3541, 1998.

Yuskiewicz, B. A., F. Stratman, W. Birmili, A. Wiedensohler, E. Swietliki, O. Berg, and J. Zhou, The effects of in-cloud mass production on atmospheric light scatter, *Atmospheric Research*, 50, 265-288, 1999.

Zhang, X. Q., P. H. McMurry, S. V. Hering, and G. S. Casuccio, Mixing characteristics and water-content of submicron aerosols measured in Los Angeles and at the Grand Canyon, *Atmospheric Environment Part A-General Topics*, 27, 1593-1607, 1993.

VITA

Joshua L. Santarpia

Department of Atmospheric Sciences
Texas A&M University
3150 TAMU
O&M Eller Bldg
College Station, TX
77843

Education

Bachelor of Science – Physics. Years Attended (1994 - 1997)
New Mexico Institute of Mining and Technology Socorro, New Mexico
Graduated with honors.
Master of Science - Atmospheric Science. Years Attended (1997 - 2001)
Texas A&M University College Station, Texas
Committee Chairman: Dr. Michael Biggerstaff. Thesis titled: The Kinematic and Cloud-to-Ground Lightning Structure of a 9-10 June, 1998 Red River Mesoscale Convective System.
Doctor of Philosophy - Atmospheric Science. Years Attended (2001 - 2005)
Texas A&M University College Station, Texas
Committee Chairman: Dr. Don Collins.

Awards and Service

Silver Scholarship – New Mexico Institute of Mining and Technology 1994-1997
Graduate Regents Fellowship – Texas A&M University 1997-1998
Member of Sigma Pi Sigma, the physics honor society – 1996
President – Local chapter of the Society of Physics Students 1996-1997
Graduate Representative for Atmospheric Sciences – College Graduate Council 2002-2003

Publications

Santarpia J. L., R. Li, D. R. Collins, Direct measurement of the hydration state of ambient aerosol populations, *Journal of Geophysical Research-Atmospheres,* 109, D18209, doi:10.1029/2004JD004653, 2004.
Santarpia, J. L., R. Gasparini, R. Li, and D. R. Collins, Diurnal variations in the hygroscopic growth cycles of ambient aerosol populations, *Journal of Geophysical Research,* (accepted).